Contributions of Caspase-8 and RIPK3 to Alzheimer's Disease (AD) Pathogenesis

Sushanth Kumar

Amarillo, TX

Bachelor of Science, Biomedical Engineering

Bachelor of Science, Biochemistry

Minor: Physics

University of Arkansas, Fayetteville, 2015

A Dissertation presented to the Graduate Faculty of the University of Virginia in Candidacy for the Degree of Doctor of Philosophy

Department of Biology

Neuroscience Graduate Program

University of Virginia

May, 2023

Abstract

Alzheimer's disease (AD) is a devastating neurodegenerative condition characterized by the formation of amyloid-beta (Aβ) plaques, development of neurofibrillary tangles, neuroinflammation, and neuronal loss. While it's generally accepted that the accumulation of the protein aggregates Aβ and tau help set the stage for AD the precise molecular mediators of cell death and inflammation have yet to be fully elucidated. Identification of novel effectors that drive cell loss and inflammation would not only yield mechanistic insights, but perhaps more importantly, provide inroads into new druggable targets for disease intervention. Currently, there are two FDA-approved disease-modifying therapies for AD. Both drugs, aducanumab and lecanemab, received approval within the past two years and are monoclonal antibodies that target Aβ to facilitate its clearance from the brain parenchyma. Given their recent introductions to the therapeutic space, it remains to be seen how effective either drug will be in slowing disease progression.

In this dissertation, we set out to examine the roles of the Caspase-8 and receptor interacting protein kinase-3 (RIPK3) in AD progression. Both Caspase-8 and RIPK3 drive distinct flavors of cell death but in addition are key regulators of a number of inflammatory pathways. Moreover, the roles of either protein in AD pathogenesis have not been examined in great detail. We found that combined deletion of Caspase-8 and RIPK3, but not RIPK3 alone, led to diminished Aβ deposition and microgliosis in the 5xFAD mouse model of AD. Despite its well-known role in cell death, Caspase-8 did not appear to affect cell loss in the 5xFAD model. In contrast, we found that Caspase-8 was a critical regulator of Aβ-driven inflammasome gene expression and IL-1β release. Interestingly, loss of RIPK3 had only a modest effect on disease progression. Future work will need to address the precise cell types that Caspase-8 is operating in to promote AD along with a more thorough characterization of the signaling pathways that the Caspase-8/RIPK3 axis may be influencing.

Additional experiments in this dissertation describe our preliminary work in trying to better understand the means by which microglial cells transition from homeostatic to inflamed states using single cell mass cytometry.

In summary, our findings reiterate the growing importance of developing a more comprehensive picture of the AD inflammatory state. We hope that our observations will help arm the field with more tractable therapeutic targets for AD intervention.

Acknowledgements

I would like to thank my official mentor, Christopher Deppmann, and my unofficial co-mentor, John Lukens. Both Chris and John were invaluable to my scientific training. On the research side, they helped me frame my eventual thesis project and also offered encouragement and guidance when experiments were stalling. On the career front, they listened to my goals and offered helpful advice as I began to take the next steps in my scientific journey. Chris's knack for story-telling and his emphasis on looking at problems from a 30,000 foot view has played a massive role in how I view scientific questions. He also gave me the freedom to explore while remaining a constant pillar of support. John is one of the best advocates a student can have. He's a great scientist with an innate ability to ask the right questions. But moreover, he's an amazing person to work with. I cannot thank Chris and John enough and will deeply miss the 5-10 minutes of banter we would have at the start of our meetings before diving into the science. Thank you both for coaching me. I hope that in the future I can become a mentor as thoughtful, creative, and motivating as the two of you.

As a student I spent most of my time in Chris Deppmann's lab. One of the aspects of a lab that I have grown to appreciate during graduate school is the importance of establishing a good culture. I was fortunate to be a part of a phenomenal environment during my time in the Deppmann lab. Two of the biggest reasons why the environment was the way that it was were due to the efforts of Pamela Neff and Tony Spano. Pam was our lab manager extraordinaire and a joy to be around. She ordered our reagents, handled all of our administrative business, and kept the lab functioning. She was undoubtedly the lab MVP and the science would not have been possible without her. Much like Pam, Tony also helped keep the lab running. In addition, Tony's humor and expertise in all things molecular biology were beneficial to everyone. I will miss our brief encounters throughout the day and the chuckles you brought me. I would be remiss if I didn't also thank my lab-mates both past and present. Thank you for the

conversations, support, and intellectual input. All of you helped contribute to our amazing environment and made my time in the lab the enriching experience that it was.

It was also through this environment that I was able to work alongside three stellar undergraduates in Sakar Budhathoki, Christopher Oliveira, and August Kahle. They helped make life in the lab significantly easier and helped make the science presented in this thesis possible. By the end of their undergraduate training, all three had developed into independent thinkers. Thank you all for helping me grow as a scientist, teacher, and person. Excited to see the great things that you all will do!

I would also like to thank my committee members Barry Condron, Ali Guler, Eli Zunder, and John Lukens for asking probing questions and providing support throughout my training. After every committee meeting, I would leave feeling slightly more motivated and better about myself and my work. You are phenomenal mentors and I am grateful to have you all in my life.

Last but not least I would like to thank my immediate family for their patience and emotional support. I know I don't thank them enough but they mean the world to me and I cherish each and every one of them. I certainly would not have made it through graduate school without my family.

Table of Contents

List of Figures and Tables

Chapter 1. An introduction to Alzheimer's disease

1.1 Origins of Alzheimer's Disease

"I have, so to say, lost myself." - Auguste Deter

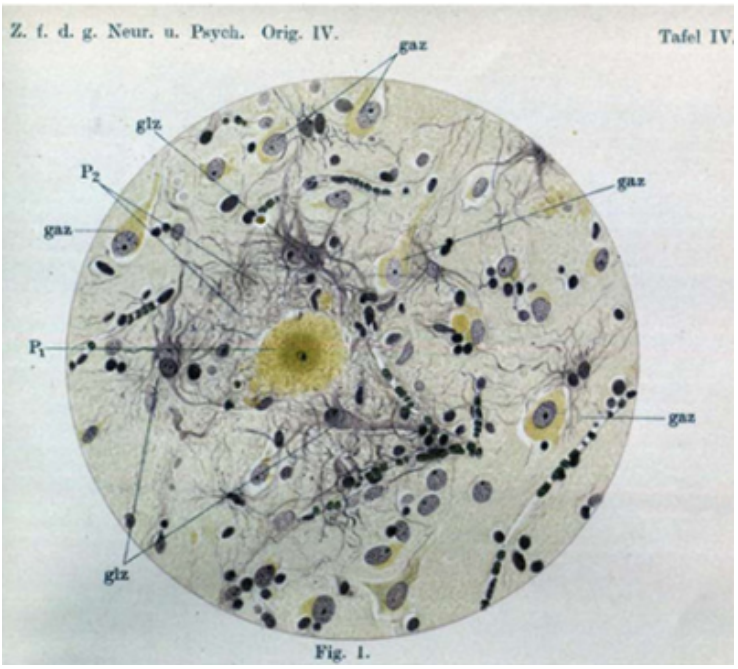

Figure 1.1. **Illustration taken from Alois Alzheimer's 1911 article describing histological brain sections from cases of Auguste Deter and Johann F**. Image denotes the presence of neurofibrillary tangles (gaz), plaques (P1), and reactive glia (glz).

In 1901, the German neurologist Alois Alzheimer began a long-term case study on a 50 year old female named Auguste Deter. Auguste had been admitted to a Frankfurt psychiatric hospital where she reportedly presented with symptoms of aggressiveness, impaired comprehension, aphasia, and a progressively failing memory. Sadly, her symptoms got worse over time and she passed away on April 8, 1906. Upon her passing, Alzheimer and colleagues began a careful examination of Auguste's brain. Histological characterization of the brains of Auguste Deter and Johann F., Alzheimer's second patient, outlined the key features that we attribute to AD: pronounced brain atrophy, intraneuronal inclusion bodies (neurofibrillary tangles), amyloid plaque deposits, and gliosis particularly occurring near plaques. Interestingly,

while Johann's clinical presentation was similar to Auguste's, his brain did not contain tangles. The tragic cases of Auguste Deter, Johann F., and others like them, along with the clinical recordings by Alois Alzheimer helped provide the foundation for what we now recognize as Alzheimer's disease (AD) (1, 2).

1.2 Beginning to understand the molecular basis of AD

Up until the early 1980s, the field of AD research was limited to crude morphological and biochemical descriptions of post-mortem brains. Lack of insight into the genetics of AD presented a wall for further research. However, a significant degree of progress was made in the field using linkage analysis of early-onset familial AD patients. These studies led to the identification of mutations in the genes *APP, PSEN1,* and *PSEN2*, which are responsible for the vast majority of the rare, early onset presentations of AD (3, 4, 5). Mutations in these genes converge on one common molecular phenotype: an increase in the ratio of $A\beta_{1-42}/A\beta_{1-40}$.

1.2.1 APP

Aptly named, the amyloid precursor protein (APP) is responsible for generating the Aβ peptide which is the predominant component of the extracellular deposits (plaques) observed in AD. APP processing can be subdivided into physiological (non-amyloidogenic) and pathophysiological (amyloidogenic) pathways. Under the non-amyloidogenic pathway, APP is first cleaved at the plasma membrane by α-secretase to yield an extracellularly released soluble APP alpha (sAPPα) peptide and a membrane-tethered C83 fragment. C83 is then processed by γ-secretase which produces non-toxic P3 and AICD fragments. However, during the amyloidogenic pathway, APP is first cleaved by β-secretase (β-APP-cleaving enzyme-1 (BACE1)) which produces a soluble APP beta (sAPPB) peptide along with a membrane-tethered C99 fragment. It should be noted that BACE1 is predominantly localized to endosomes (6). Thus, APP trafficking and subcellular localization plays an important role in its

processing with increased intracellular retention being generally associated with amyloidogenic processing. Similar to the non-amyloidogenic pathway, the C99 fragment is cleaved by γ-secretase, which can reportedly occur at either the membrane or endosomes, to yield the AICD fragment along with Aβ (7). Cleavage by γ-secretase produces a number of Aβ species. The most common is Aβ ending at position 40 ($Aβ_{1-40}$) while the pathological variant ends at position 42 ($Aβ_{1-42}$) (8). PSEN1 and PSEN2 are major subunits in the γ-secretase complex and in the context of familial AD, mutations in these proteins can lead to increased production of $Aβ_{1-42}$ (9). Owing to its toxic nature, $Aβ_{1-42}$ is more hydrophobic and thus more susceptible to aggregation. Monomer units of $Aβ_{1-42}$ can interact with one another to form soluble oligomers which can aggregate further into insoluble plaques. In general, it's believed that the soluble oligomers contribute the most to the neurotoxicity seen in AD (10). More recent studies have also uncovered new routes of APP cleavage via η-secretase and δ-secretase. Initial processing by η-secretase gives rise to a released sAPPη and CTF-η fragment. Further processing of the CTF-η by α-secretase and β-secretase can give rise to Aη-α and Aη-β products, respectively. The consequences of η-secretase processing to either AD or normal physiology remain unclear. Studies by Willem et al suggested that the Aη-α product has synaptotoxic effects. The group also showed accumulations of Aη-α in dystrophic neurites in both human and AD mouse models (11). APP cleavage by δ-secretase serves as an additional means of generating neurotoxic metabolites. Similar to that of β-secretase, δ-secretase's activity is also enhanced in acidic environments making it predominantly localized to endosomal compartments. δ-secretase acts as an asparagine endopeptidase (AEP) and cleaves APP at N373 and N585 residues. Experiments by Zhang et al, have argued that the APP_{1-373} fragment can lead to pronounced axonal fragmentation in primary cultured neurons. Initial cleavage at N585 enhances subsequent BACE1 processing giving rise to increased Aβ production. The group also showed that 5xFAD mice lacking δ-secretase appear to have reduced Aβ levels as well as ameliorated cognitive impairment (12). Finally, it is also possible for APP to be cleaved by the BACE1

homolog BACE2 (θ-secretase). BACE2 has relatively low brain expression and while it can process APP at the same site as BACE1 it does so with much less efficiency (13). However, BACE2 can also cleave APP at a novel θ-site to yield products that can no longer be processed by BACE1 to produce Aβ (14). A study by Alić et al provided further support for the anti-amyloidogenic role of BACE2. Patients with trisomy 21 oftentimes present with early-onset dementia due to an extra copy of APP. However, some individuals are spared from AD-like pathology. The group cultured cerebral organoids from patients with Down's syndrome (DS) and healthy controls. While most of the DS organoids went on to develop AD-like pathology, two did not. To examine the relevance of BACE2, the group deleted one of the three extra copies of BACE2, which is also on chromosome 21, from a pathology-free DS organoid. Interestingly, elimination of one copy of BACE2 led to early development of plaques from the organoid that had previously been free from AD-like pathology (15). BACE2 levels vary from person to person and SNP variations within the *BACE2* correlate with age of onset of dementia in DS individuals which may help account for why DS patients are not necessarily protected from AD (16).

Early genetic studies pointed to a causative role for Aβ in the development of AD. This led to the formation of the amyloid hypothesis which states that Aβ is the initiating factor behind AD and the resulting formation of neurofibrillary tangles, inflammatory response, neurotoxicity, and cognitive decline are a consequence of its accumulation (17). This view has dominated the field for the past several decades and has been the impetus for the large number of drugs designed to facilitate the removal of brain amyloid. However, is Aβ all that bad? Excess generation of $A\beta_{1\text{-}42}$ can give rise to pathology but $A\beta_{1\text{-}42}$ is also produced during homeostasis (albeit at lower levels) suggesting that it has a function beyond driving disease. The $A\beta_{1\text{-}42}$ peptide is highly conserved evolutionarily with humans sharing identical sequences with coelacanths (a 400 million year old fish taxon) (18). A compound that is purely a bad actor would likely have been selected against a long time ago. Work out of the late Robert Moir's

group provided substantial evidence for Aβ serving as an innate immune molecule. The group first noted that Aβ bears structural resemblance to known antimicrobial peptides (AMPs), many of which are also amyloids. These observations were then corroborated by functional studies showing that synthetic Aβ was capable of slowing the proliferation of several bacterial and fungal species (19). Follow-up studies using mice models, nematode models, and cell lines, would show that overexpression of Aβ afforded protection against *S. typhimurium* and *C. albicans* infection. It appeared to the group that much like other AMPs, Aβ would form fibrils trapping the invading pathogen (20). Furthermore, infection of 5xFAD mice with herpes simplex virus (HSV) leads to rapid plaque production surrounding viral particles (21). Taken together, these findings have raised the interesting hypothesis that initiation of AD could be mediated by pathogen infection. Brains of AD patients have been shown to harbor certain fungal and bacterial strains (22, 23). In addition, a number of groups have drawn a linkage between HSV and AD. Early work by Ruth Ithzaki's lab first provided definitive evidence of the presence of HSV1 in both AD and control human brains (24). In later studies, the group analyzed plaques from post-mortem AD brains and observed that 90% of them contained HSV1 DNA (25). In 2018, Readhead et al performed a large-scale meta-analysis on sequencing data from AD and healthy controls. The group noted that AD samples had a greater abundance of human herpesvirus 6A (HHV-6A), human herpesvirus 7 (HHV7), and HSV1 (26). Despite the large body of evidence, a major drawback of the studies arguing in favor of the infection hypothesis is that they mainly only show correlation. Due to declining quality of self-care and a weakened immune system, individuals with AD could just be more susceptible to infection. However, it remains plausible that infection or viral reactivation under the right environment may be the catalyst for AD pathogenesis in certain cases.

Besides mediating host defense, APP and its corresponding catabolites may also play key roles in learning and memory. Notably, APP knockout mice show impairments with passive

avoidance learning with age (27). These observations could be explained to some degree through the actions of sAPPα which others have shown to be critical in memory formation. Administration of recombinant sAPPα to aged mice has been shown to buffer against cognitive decline. Moreover, knocking in sAPPα into the APP locus of mice deficient in APP leads to potent improvements in LTP and behavioral impairments (28). The homeostatic functions of other APP proteolytic fragments remains largely unclear.

1.2.2 ApoE

Despite their utility in understanding disease origins, mutations associated with familial AD account for less than 5 % of cases. The late-onset or sporadic form of AD is far more common but also significantly more complicated. Genetic mutations tied to late-onset AD (LOAD) can play crucial roles in determining disease onset as well as severity. Polymorphisms in the *APOE* gene are viewed as the strongest risk factor for LOAD. The gene encodes for the apolipoprotein E (ApoE) protein which mediates the recycling and distribution of cholesterol throughout the body. All the cholesterol within the brain is produced locally due to the blood-brain barrier which prevents entry of lipoproteins. Cholesterol is a major constituent of myelin sheaths and thus deficits in cholesterol synthesis or transport can lead to neurological disease (29). ApoE, primarily produced by astrocytes and microglia, interacts with proteins such as ABCA1 to form lipoprotein particles which carry cholesterol to neurons via members of the low-density lipoprotein receptor (LDLR) family (30). While the transport of cholesterol is the primary function of ApoE, the protein can also facilitate Aβ clearance. There are three isoforms of ApoE: ApoE2, ApoE3, and ApoE4 which differ by only 1 or 2 amino acids. ApoE3 is the most common allele and is neutral in terms of AD risk. In contrast, individuals carrying 1 or 2 alleles of ApoE4 have a 3- or 12-fold increased risk of developing AD, respectively. ApoE2 is protective with individuals carrying 1 or 2 alleles having a 40 % less likelihood of developing AD when compared to carriers of 2 ApoE3 alleles (31). Early *in vitro* studies demonstrated that synthetic

Aβ peptides can bind to purified ApoE from plasma (32). Furthermore, post-mortem analysis of AD brains has shown that ApoE is co-deposited with Aβ in plaques (33). Given that *APOE4* carriers harbor more Aβ than non-carriers this would suggest that perhaps isoform-specific binding plays a role in Aβ clearance and that ApoE4 has the weakest affinity for Aβ. However, studies from the Holtzman group challenged this hypothesis. In their experiments, the group mixed cell-derived Aβ with reconstituted ApoE particles at physiological concentrations and detected minimal amounts of ApoE/Aβ complexes. Interestingly, when assessing the Aβ clearance capacity of cell lines producing either ApoE2, ApoE3, or ApoE4 the group found that ApoE deficient cells are the best clearers (34). In an elegant experiment, Liu et al. was able to demonstrate that overexpression of ApoE4 but not ApoE3 impedes *in vivo* Aβ clearance. The group bred APP/PS1 mice to ApoE inducible mouse lines to evaluate the contribution of ApoE isoform to pathology at different stages. To assess clearance efficacy, a gamma secretase inhibitor was added to halt Aβ production and *in vivo* microdialysis was used to measure interstitial Aβ concentration in mice aged to 3-4 months. The clearance kinetics when ApoE3 was overexpressed mirrored that of control mice whereas ApoE4 overexpression led to a pronounced increase in Aβ half-life (35). Overall, these observations suggest that instead of helping clear Aβ, ApoE may compete with natural clearance pathways during pathology.

AD transgenic mice that lack *APOE* have significantly reduced plaque deposition (36). However, the plaques that do remain are less compact due to decreased microglial plaque recruitment suggesting that ApoE plays a role in the AD innate immune response (37, 38). Indeed, in addition to influencing amyloid clearance, ApoE and its isoforms also regulate glial reactivity and cytokine release. ApoE4 in particular has been shown to prime microglia and astrocytes toward a pro-inflammatory state during AD (39, 40). Furthermore, ApoE4 expressing glial cells show increased lipid droplet accumulation which may account for their inflammatory

bias (41, 42). Thus ApoE4's status as a genetic risk factor in AD likely stems from its pleiotropic roles in mediating amyloid clearance, inflammation, and lipid homeostasis.

1.2.3 What about tau?

The accumulation of the pathological tau protein in AD was also noted by Alois Alzheimer. Normally, tau serves as a microtubule-associated-protein (MAP) where it acts to stabilize microtubule bundles. Tau is mainly found in axonal compartments and plays an essential role in fast axonal transport processes. Microtubule-bound tau act as guideposts for the motor proteins kinesin and dynein. High concentration regions of tau cause kinesin detachment and dynein to reverse its course along the microtubule (43). Thus, the railroad tracks that tau helps lay down maintains the proper distribution of cargo between neuronal compartments. Dysfunction in tau localization leads to a fundamental breakdown of neuronal integrity.

Tau is a highly regulated protein and subject to numerous post-translational modifications. The most pathologically relevant of which is phosphorylation. Many serine and threonine residues in and around the microtubule-binding-domain of tau are targets for a variety of kinases, with glycogen synthase kinase 3 beta (GSK3β) garnering perhaps the most attention in AD. GSK3β is a serine-threonine kinase that is involved in the regulation of a number of vital cellular pathways. Moreover, it is constitutively active and able to phosphorylate tau at 42 sites (44). Not surprisingly, GSK3β is often observed to be dysregulated in AD and boosting its activity leads to an exacerbation of pathology (45). Tau hyperphosphorylation by GSK3β, or other kinases, hampers tau's microtubule binding ability and ultimately promotes tau oligomer formation. As the tau oligomer grows it adopts a β-sheet rich structure forming fibrils which eventually proceed to the neurofibrillary tangles observed in AD. Similar to Aβ, soluble tau

oligomers are viewed as the neurotoxic species that are responsible for propagating disease. Stereotactic injection of tau oligomers, but not fibrils or monomers, promotes neuronal loss in WT mice (46). In some models neurodegeneration is absent even in the presence of tangles (47). Studies by Kuchibhotla et al. showed that neurons in the visual cortex that bear significant amounts of misfolded tau are still able to respond to visual stimuli and are functionally indistinguishable from non-tau bearing neighboring neurons (48). These observations suggest that much like Aβ plaques, neurofibrillary tangles may serve a protective function by reducing the pool of available oligomeric species.

1.2.4 Relationship between Aβ and tau

Soluble forms of Aβ and tau oligomers act in concert to promote the descent into AD. During the preclinical stages of AD, a rise in Aβ plaque deposition generally precedes neurofibrillary tangle formation by several years (49). Longitudinal imaging studies have also shown that accumulation of Aβ is required for the spread of tau from the medial temporal lobe to other cortical regions (50). Aβ oligomers when added to cultured neurons can promote tau hyperphosphorylation and tau missorting into somatodendritic compartments (51). Experiments by Götz et al also showed that injecting Aβ fibrils into the brains of mutant tau transgenic mice leads to a five-fold increase in tau burden at the injection site (52). Aggregation of tau is not a mere consequence of Aβ build-up but may also play a critical role in AD progression. Leroy et al. demonstrated this by showing that removal of tau from the APP/PS1 line, which doesn't exhibit pronounced tau pathology, leads to an amelioration in neuronal survival and cognition. Moreover, APP/PS1; $Tau^{-/-}$ mice exhibited reduced amyloid plaque burden indicating that tau misfolding can feedback onto amyloid production (53). How is the functional dependency of Aβ on tau misfolding mediated? One mechanism seems to be through aberrant activation of neuronal receptors. Oligomeric forms of Aβ have been shown to interact with a number of receptors such as NMDA, AMPA, and mGluR leading to aberrant ion fluxes which can result in

engagement of GSK3β, Fyn, and CamKII as well as other tau kinases (54, 55, 56). An alternative explanation could be through neuroinflammation. Glial activation is observed during preclinical disease stages concomitantly with Aβ deposition (49). IL-1β release by activated microglia can promote tau hyperphosphorylation through activation of tau kinases (57, 58). We will dive deeper into the topic of inflammation in AD in later sections. The importance of tau in human AD is also appreciated. Unlike with Aβ, the progression of tau pathology correlates with the development of cognitive impairments. Longitudinal PET imaging studies paired with structural MRI have revealed that tau-laden regions generally succumb to degeneration over time while Aβ burden is an insufficient predictor (59). Overall, these findings indicate that (1) Aβ accumulation triggers tau misfolding and (2) tau seems to be required for the clinical manifestations of AD.

1.3 Inflammation in Alzheimer's disease

Inflammation is our body's natural response to extrinsic and intrinsic distress signals. Acute inflammation serves as an excellent defense mechanism against infection. However, the presence of a sustained immune response, even in the absence of an apparent threat, can lead to deleterious outcomes. Chronic neuroinflammation is a hallmark of many neurodegenerative maladies, including AD. In the brain, inflammation is associated with a pronounced shift in glial cell morphology and function. During AD, glial cells can be seen surrounding Aβ plaques. This reactive gliosis was first noted by Alois Alzheimer in his original drawings but its importance to disease progression would not be appreciated until many decades later. In the following section, we will highlight the cellular players involved in propagating AD immune responses and end with a brief discussion of emerging therapeutic targets for mitigating AD inflammation.

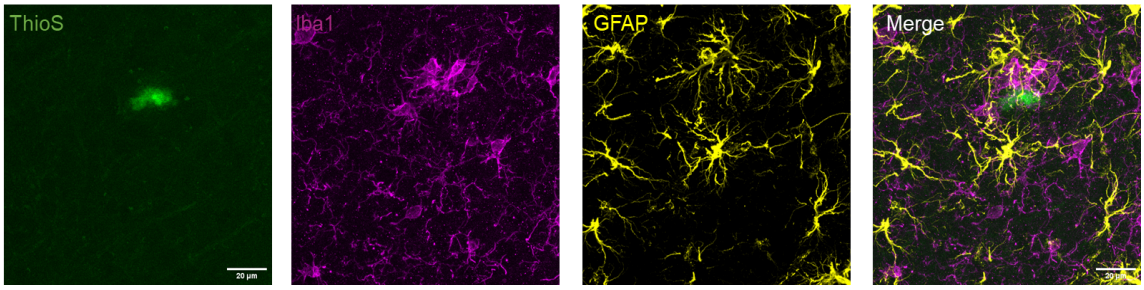

Figure 1.2. **Glial Cell Plaque Barrier**. Aβ plaque (labeled with ThioS in green) surrounded by reactive microglia (labeled with Iba1 in magenta) and astrocytes (labeled with GFAP in yellow). Image taken from a 5 month old 5xFAD mouse. Scale bar is 20 μm.

1.3.1 Microglia

Microglia serve as the brain's resident primary immune cell. The developmental origin of microglia was debated but it is now accepted that the cells arise from macrophage progenitors in the yolk sac, a membranous structure that provides nourishment to the embryo and is also the first site of hematopoiesis in rodents and humans. In mice, hematopoiesis begins in the yolk sac at E7.0. Soon after the circulatory system is fully developed, primitive macrophages from the yolk sac colonize the brain at E9.0-E10.0 where their identity is further shaped by the developing CNS environment (60). Broadly speaking, microglia can be subdivided into gray matter and white matter microglia. Gray matter microglia facilitate neuronal connectivity through engulfment of synapses and dying neurons while white matter microglia support myelination through secretion of IGF-1, and clearance of oligodendrocyte precursor cells (OPCs) and myelin debris (61, 62, 63). During aging and pathological conditions, white matter microglia exhibit an increased transcriptional diversity - moreso than gray matter microglia - as a means of coping with myelin accumulation (64). Heterogeneity in microglia can also be seen across different brain regions both in terms of morphology as well as molecular signature. For instance, cerebellar microglia are less ramified than their cortical counterparts but show an increased somal motility (65). Cerebellar microglia also have increased expression of genes important for migration and metabolism which likely contribute to their increased motility (66).

From the point of initial colonization, microglial numbers are maintained in the CNS through self-renewal and in the absence of blood-brain barrier disruption or pathology, there is no contribution of peripheral macrophages to the microglial population (67). This remarkable capacity for self-renewal is particularly evident upon administration of the colony-stimulating factor 1 receptor (CSF1R) antagonist, PLX3397, which results in elimination of ~99% of microglia. Upon removal of PLX3397, the surviving microglia divide and numbers are restored to baseline within 3 weeks (68). Despite the fact that microglia only represent 10-15% of all cells in the brain, they play vital roles in developmental synapse remodeling, CNS tissue maintenance, pathogen defense, and injury responses.

Clearance of Aβ and tau

Microglia have long been viewed as the brain's garbage collector. Granted, these small cells shape physiology in many other ways but waste build-up is a common feature in a number of CNS maladies, including AD. Microglia have a critical homeostatic function in removing Aβ and tau aggregates and do so using a number of mechanisms. Probably the most well-characterized is via phagocytosis. Phagocytosis is a receptor-mediated process by which particles > 0.5 μm are recognized and internalized by the cell. Internalized materials are associated with a specialized vesicle termed a phagosome which eventually fuses with the lysosome to degrade the ingested contents (69). The initial stage of phagocytosis is the recognition of the cargo to be engulfed. Microglial recognition of amyloid and tau aggregates is facilitated by toll-like receptors (TLRs), scavenger receptors, Fc receptors, complement receptors, Tyro3, Axl, and Mer (TAM) receptors, and TREM2 (70). Cargo recognition ultimately leads to endocytosis and lysosomal degradation. However, each of these receptors also interact with different intracellular adaptor proteins thus giving rise to a variety of potential cellular responses. For example, binding of fibrillar Aβ to either TLR2 or TLR4 triggers the robust production of NF-κB regulated cytokines (71). Microglia deficient in these receptors were found

to be unable to execute a Rac signaling cascade required for proper Aβ phagocytosis (72). Animal models of AD lacking either TLR2 or TLR4 also present with increased amyloid deposition further highlighting the roles of these receptors in proper clearance (73, 74). Scavenger receptors are a class of pattern recognition receptors that recognize polyanionic ligands. Class A scavenger receptors (SCARAs) in particular play key roles in plaque clearance, evidenced by the observation that Scara-1 knock-out microglia show a 60% reduction in their ability to uptake amyloid (75). Moreover, many scavenger receptors are intimately connected with TLR signaling pathways. The scavenger receptor CD36 has been shown to signal via Src kinases to induce the formation of a TLR4-TLR6 heterodimer which results in pro-inflammatory cytokine production (76). This cytokine production at early disease stages might be beneficial but left unchecked can exacerbate the AD neuroinflammatory signature. Thus, proper titering of CD36 levels depending on disease state is crucial (77). Overall, an improved understanding of the means by which amyloid recognition receptors coordinate to shape microglial behavior will be essential in designing novel AD interventions.

Microglia are also capable of clearing Aβ through the production of degradative enzymes. These include the matrix metalloendopeptidases insulin-degrading enzyme (IDE) and neprilysin (NEP) along with the lysosomal peptidase cathepsin B (CatB) (70). Both IDE and NEP play important roles in both the intracellular and extracellular degradation of Aβ. Furthermore, the levels of both IDE and NEP have been shown to be down-regulated in AD brains (78, 79). Mice deficient in IDE have diminished Aβ catabolism (80). Similarly, crossing APP transgenic mice to NEP deficient mice has been shown to lead to significant increases in amyloidosis (81). These findings suggest that bolstering IDE or NEP activity could be a potential strategy to diminish amyloid load. Additionally, IDE activity is also critical for the maintenance of proper brain metabolism through insulin processing. Decreased IDE levels can lead to brain hyperinsulinemia which may impede proper insulin transport across the blood-brain barrier

worsening disease severity (80). Microglia are also capable of degrading Aβ using the cysteine protease CatB. Normally, CatB functions to degrade compounds in endo-lysosomal compartments but enzymatically active forms of the protein can also be secreted through exocytosis (82). Microglia surrounding plaques upregulate their levels of CatB. Genetic ablation of CatB has also been demonstrated to lead to increased amyloid burden in APP mice (83). However, it's been shown in chronic pain models that CatB leakage from the lysosome and into the cytoplasm can promote IL-1β release which could exacerbate neuropathology (84). Whether CatB mislocalization occurs in AD remains to be seen.

Autophagy serves as an evolutionary conserved means by which organisms can recycle or remove damaged organelles and proteins (85). However, this process can also be co-opted for amyloid degradation. Impairments in autophagy, as evidenced by accumulations in autophagosomes, are commonly observed early in AD development. In line with this, down-regulation of the autophagic protein Beclin-1 enhances Aβ aggregation (86). Microglia can clear fibrillar Aβ through autophagy and dysregulation of this process can lead to inflammation via the NLRP3 inflammasome (87). Microglial loss of Atg7, an enzyme that is essential for autophagosome biogenesis, also leads to increased tau deposition and a heightened neuroinflammatory environment (88). Utilization of autophagy inducers such as statins, spermidine, and metformin have been shown to be beneficial in preclinical models for AD suggesting that boosting autophagic signaling could serve as a viable therapeutic avenue (89).

While these degradation processes are integral for preservation of brain function, there is also evidence that some of these processes can promote plaque deposition. Work from the Lemke lab has been instrumental in shaping our understanding of the role of TAM receptors in AD. TAM receptors were first recognized for their role in clearing apoptotic cells but have also been shown to be important in amyloid recognition (90). In addition, microglia surrounding plaques exhibit heightened expressions of Axl and Mer. To assess the role of these receptors in

AD pathology, Huang et al. crossed APP/PS1 mice to mice deficient in Axl and Mer (APP/PS1*Axl*$^{-/-}$*Mertk*$^{-/-}$). Intuitively, one would expect that elimination of these receptors would lead to increased plaque burden. However, the group observed the exact opposite result arguing that TAM-mediated phagocytosis of Aβ does not inhibit, but rather promotes, the formation of dense-core plaques. Levels of soluble Aβ did not differ between APP/PS1 and APP/PS1*Axl*$^{-/-}$*Mertk*$^{-/-}$ mice. Furthermore, APP/PS1*Axl*$^{-/-}$*Mertk*$^{-/-}$ mice showed worse fear acquisition than controls. These data are suggestive of a model whereby microglia may engulf oligomeric species of Aβ, condense them in the lysosome, and then release the Aβ as a dense-core plaque (91). Given that plaques are garnering increased recognition as being relatively inert and soluble oligomers promoting toxicity, these findings highlight the protective role of microglia in AD. Additional work from Kim Green's lab examining the impact of microglial depletion in the 5xFAD model also supports these conclusions (discussed later).

Microglial reactivity in AD

The activation of microglia is a consistent feature of the AD brain. But what does it mean for a microglia to be "activated"? One manner of characterization is through morphology. Microglia are highly dynamic cells that under homeostatic conditions exhibit a ramified appearance to allow for constant sampling of the CNS environment. During pathological conditions, such as AD, microglia will retract and thicken their processes adopting a "bushier" shape. The nature of this activated state has classically been viewed through the M1/M2 schema. M1 polarized microglia are generally regarded as pro-inflammatory and neurotoxic while M2 microglia are anti-inflammatory and associated with promoting tissue repair. *In vitro* studies have shown that engagement of TLR and IFN-γ signaling pathways leads to microglial production of cytokines such as TNF-α, IL-6, and IL-1β, an M1 phenotype. In contrast, *in vitro* treatments with cytokines such as IL-4 and IL-10 lead to production of TGF-β and other anti-inflammatory modulators, an M2 phenotype. While the M1/M2 paradigm is somewhat useful

in characterizing microglial activation *in vitro*, it's accepted that an activated microglia *in vivo* can rarely be placed in one of these two bins (92).

The limitations of viewing activation from the lens of either purely morphology or M1/M2 profiling is apparent. But the advent of single-cell RNA sequencing (scRNA-seq) addresses many of these concerns by enabling a more comprehensive look into activation with the added benefit of single cell resolution. The necessity for approaches such as scRNA-seq to characterize activation stems from the observation that challenges with distinct triggers can produce reactive/activated microglia that appear similar at the gross morphological level but can differ significantly at the molecular level (see M1/M2 discussion earlier). Our conception of how microglia change in the context of normal aging and disease has been significantly improved with single-cell profiling. In 2017, Keren-Shaul et al. performed scRNA-seq of CNS tissue from aged, AD, and ALS mouse models which revealed the presence of a unique subset of microglia now referred to as disease-associated-microglia (DAMs). This subset is characterized by microglia that still express canonical microglial markers such as *Iba1* and *Hexb* but downregulate homeostatic markers such as *Cx3Cr1*, *P2ry12*, and *Tmem119*. DAM upregulate genes associated with lipid metabolism and phagocytosis such as *ApoE, Trem2,* and *Cst7*. In the AD brain, DAM can be found surrounding Aβ plaques and fit the mold of a reactive microglia by morphological standards (93). We will dive deeper into DAMs and their role in AD in the following section. In contrast to DAM, microglia challenged with LPS show a pronounced downregulation of *ApoE* despite also exhibiting an activated morphological state (37). Thus, the concept of microglial activation remains nuanced but with advancements in single-cell transcriptomics and proteomics an improved understanding of the microglial activation spectrum is within reach.

Disease-associated microglia (DAM)

DAM were first discovered in the 5xFAD mouse model but have since been demonstrated in a number of other neurodegeneration paradigms as well as in normal aging. In the context of AD, DAM are present in areas containing plaques and absent in regions such as the cerebellum which shows limited amyloid load. The current model for the adoption of the DAM signature consists of two transition stages. During the first transition stage, microglia down-regulate their core homeostatic genes and begin to upregulate genes associated with AD progression such as *ApoE*, *Trem2*, and *B2m*. The mechanisms behind this first transition stage are unclear but are independent of triggering receptor expressed on myeloid cells 2 (TREM2). The second transition stage, which does require TREM2, is described as a continuation of the upregulation of genes important in lysosomal processing, phagocytosis, and lipid metabolism. Thus, TREM2 is responsible for complete DAM acquisition (93).

Given their heightened phagocytic signature, DAM are seen as a protective response towards plaque deposition. Studies that have eliminated key regulatory molecules that are essential for maintaining DAM subsets largely observe a worsening of AD pathology (94, 95). However, it is important to note that mice do not naturally develop AD so we must ask whether DAM are relevant to the human condition. Srinivasan et al. attempted to address this question by performing RNAseq on FACs purified microglia from frozen control and AD patient samples. Overall, the group noted minimal similarities in human AD microglia and the DAM signature seen in mice. While both populations showed elevated levels of *ApoE*, increased expression of genes involved in lipid metabolism, and a general accelerated aging phenotype, the specific genes involved did not bear much overlap in human AD microglia (termed HAM by the group) and DAM. The caveats to this study are that the group used a relatively small sample size (15 control and 10 AD samples) and also that RNA integrity was subpar. While a DAM signature was not seen in human AD, the group did observe a DAM-esque phenotype in microglia

harvested from MS lesions and human xenotransplanted microglia into 5xFAD brains. Why are HAM and DAM so dissimilar? The group suggests that this could be attributed to DAM being a largely protective signature while HAM being more of a defective state (96). Furthermore, the majority of the AD mouse models rely on aggressive overexpression of mutant forms of Aβ which likely does not faithfully recapitulate the majority of human AD presentations. Although mouse models have been invaluable in advancing our understanding of AD, there are clear limitations when modeling the complexity of human disease. To address some of these limitations, efforts are being made to develop chimeric models in which iPSC-derived hematopoietic progenitor cells (HPCs) are transplanted into the brain's of immunodeficient mice. These transplanted cells differentiate into microglia and interestingly bear a significant degree of transcriptomic similarity to human microglia. Crossing these chimeric mice to 5xFAD mice revealed unique microglial-plaque interactions that are potentially more similar to the human condition (97). The hope is that with continued optimization, humanized systems may serve as more robust preclinical models for AD and other neurodegenerative disorders.

TREM2

Alongside regulating DAM development, TREM2 plays an important role in mediating the AD immune response. In addition, individuals carrying the *Trem2* variant R47H are at an increased risk of developing AD with an odds ratio of 4.5 (98). TREM2 is a single-pass transmembrane receptor expressed on the surface of cells in the monocyte-macrophage lineage and is capable of binding to a wide array of ligands such as bacteria, DNA, phospholipids, and lipoproteins. Because its intracellular domain lacks signaling motifs, TREM2 engages the adaptor protein DAP12 for signal transduction. DAP12 recruits spleen tyrosine kinase (SYK) in order to stimulate pathways that promote cell survival, chemotaxis, and pro-inflammatory cytokine production (99). The R47H mutation leads to an impairment in normal TREM2 function suggesting that TREM2 plays a protective role in AD. Similar to humans, mice

bearing the R47H mutation or lacking TREM2 altogether develop greater amyloid loads at later disease stages and have a worsened pathology (95, 100). As mentioned previously, microglia form barriers around plaques. Microglial barrier formation is thought to limit plaque-associated neurotoxicity and minimize Aβ seeding. In addition to barrier formation, microglia also regulate plaque morphology by increasing plaque compactness. Plaques that are more fibrous lead to more dystrophic neurites. Loss of TREM2 significantly reduces both microglial barrier formation as well as plaque compactness (95, 101). Altogether, the data suggest that TREM2 plays a critical role in microglial Aβ sensing.

In addition to its role in amyloid recognition, TREM2 is also an important regulator of microglial fitness. Microglia deficient in TREM2 have dysregulated mTOR signaling and as a result an accumulation of autophagic vesicles in the context of AD. These metabolic deficits ultimately lead to increased microglial apoptosis which may account for why *Trem2*$^{-/-}$ AD mice have reduced microglial plaque clustering. Administration of cyclocreatine, which can provide an alternative source of ATP, was shown to improve autophagic stress in 5xFAD *Trem2*$^{-/-}$ mice (102).

Getting rid of microglia in AD

Reverse genetics approaches are a staple in the biologist's toolkit when trying to assess gene function. In a similar vein, Spangenberg et al. characterized the role of microglia to AD progression by eliminating them. The group fed 5xFAD mice with chow containing the compound PLX5622, a more selective CSF1R antagonist than PLX3397, beginning at 1.5 months of age and ending at 7 months when the mice were sacrificed. Interestingly, PLX5622 treatment led to a pronounced reduction in parenchymal plaque deposition. However, 5xFAD mice on PLX5622 still exhibited poor performance in the Morris water maze test for spatial learning and memory. Upon closer examination, it was found that A□ deposition had been

redistributed to the blood vessels akin to cerebral amyloid angiopathy. Furthermore, total amyloid levels as measured by ELISA from 5xFAD and 5xFAD PLX5622 treated animals were similar. These results demonstrate that microglia play an important role in the initiation of plaque deposition and localization during AD. It is also worth mentioning that the plaques that did persist in the PLX5622 condition had significantly higher levels of dystrophic neurites suggesting again that microglial barrier function is protective (103). In an earlier study, the group examined how microglial elimination at 10 months of age influences pathology and found a reduction in neurite dystrophy and increase in spine density with PLX3397 treatment. Furthermore, plaque load was unchanged upon microglial elimination (104). These observations touch on the double-edged nature of microglia in AD. At early stages of disease, microglial activation may be beneficial in plaque maintenance but at later stages microglia lose their protective capabilities and shift to a neurotoxic role.

1.3.2 Astrocytes

Astrocytes are the most abundant cell type in the brain outnumbering neurons by a factor of five. These star-shaped cells tile the entire CNS in a contiguous manner and have vital functions in providing neuronal support, synapse construction, and blood-brain barrier maintenance to name a few. Astrocytes originate from neural stem cells called radial glia during the second week of embryonic development in rodents (105, 106). Expansion of astrocyte numbers continues throughout early postnatal development before ultimately decaying and being restricted to neurogenic niches such as the dentate gyrus during adulthood (107). Much like microglia, astrocytes possess slightly different functions and shapes depending on whether they are located in the gray or white matter. Protoplasmic astrocytes (gray matter) are characterized by a highly branched morphology and round somas while fibrous astrocytes (white matter) are more elongated with long and thin processes that extend along nerve fibers. Given their close apposition to synapses, protoplasmic astrocytes play an important role in

neuronal information processing by modulating neurotransmitter amounts. In particular, astrocytes express a number of glutamate transporters to help maintain physiological levels of excitatory transmission. Fibrous astrocytes are not as important for information processing but do regulate myelination through the secretion of platelet-derived growth factor-alpha (PDGF) which promotes survival of OPCs. In addition, fibrous astrocytes are also gap-junction coupled to oligodendrocytes which provides metabolic support and ion buffering for partnered oligodendrocytes (108).

Alongside these gray and white matter differences, astrocyte function can be tailored depending on brain region. Chai et al reported that striatal and hippocampal astrocytes are specialized to local circuits. More specifically, the group found that striatal astrocytes were enriched in *Aldh5a1* which is involved in GABA degradation while hippocampal astrocytes were enriched in *Glu1* which is important for glutamate synthesis. Considering that the striatum consists of predominately GABAergic medium spiny neurons and the hippocampus comprises mainly excitatory glutamatergic neurons, these findings suggest that the neuronal environment plays an important role in shaping astrocyte molecular profile (109). Other transcriptomic studies have also reported differences in neurotransmitter transporter levels when comparing cortical and cerebellar astrocytes (110).

Astrocytes in AD

Similar to microglia, astrocytes during AD show a tendency to lose core homeostatic functions in favor of disease-promoting pathogenic activities. For example, astrocytes in AD display impairments in proper glutamate transport and increase their secretion of detrimental factors such as complement component C3 to exacerbate disease (111, 112). Gene expression profiling studies have provided additional insights into the complex responses of astrocytes in pathological settings. Work from the Barres lab showed that following either systemic LPS

administration or ischemia, astrocytes can be polarized to adopt either neurodegenerative or neuroprotective signatures, respectively. These two broad populations would later be termed as A1 or A2 (similar to the M1/M2 schema for microglia) (113). Liddelow et al. would demonstrate that A1 astrocytes are induced via activated microglia through the secretion of ILα, C1q, and TNFα. Elimination of any one of these three molecules (ILα, C1q, and TNFα) diminishes A1 reactivity. Owing to their neurodegenerative nature, A1 astrocytes have also been shown to be present in human AD. Studies have demonstrated that up to 60 % of GFAP-positive astrocytes are also positive for A1 markers such as C3 in the prefrontal cortex of AD brains (114). However, more recent studies from Jiwaji et al. have challenged the utility of the A1/A2 classification in AD. The group utilized TRAP-sequencing to determine astrocyte specific gene expression profiles from both APP/PS1 and $Mapt^{P301S}$ mice. They found that the astrocyte transcriptional changes seen in either AD model did not mirror what had previously been reported following LPS or ischemia. Instead, most astrocytes seemed to exhibit properties of both the described A1 and A2 signatures suggestive of a more complex heterogeneous response (115). It is worth noting that the A1 and A2 classifiers were derived from acute challenges and thus may not be reflective of chronic disorders such as AD.

Additional sc-RNA-Seq and single-nucleus RNA-seq (snRNA-seq) studies have shed light on the heterogeneity seen with astrocytes in AD. Lau et al. harvested nuclei from the prefrontal cortex of 21 individuals(12 with AD and 9 without). Subcluster analysis indicated the presence of 9 transcriptomically unique populations (a1-a9). Clusters a2, a4, a5, a7, a8, and a9 were similar in proportion between AD and non-AD samples. However, clusters a1 and a6 were larger in AD samples while that of a3 was smaller. Examination of differentially expressed genes showed that clusters a1 and a6 were upregulated in stress-response markers such as *CRYAB* (a heat shock protein) and the alarmin *HMGB1*. Cluster a3 showed a largely homeostatic gene signature and was enriched in markers associated with neurotransmitter metabolism (116).

Habib et al. performed similar snRNA-seq experiments from 5xFAD and WT mice. The cells fell into 6 clusters which ranged from *Gfap*^{lo} to *Gfap*^{hi}. In 5xFAD mice, a unique *Gfap*^{hi} population emerged which was termed disease associated astrocytes (DAAs). Both *Gfap*^{hi} astrocytes and DAAs upregulated genes involved in inflammatory signaling and lipid metabolism pathways. DAAs also showed an upregulation of genes associated with amyloid metabolism and clearance such as *Ctsb* (Cathepsin B). Consistent with the human studies of Lau et al, *Gfap*^{lo} astrocytes, which represented homeostatic states, were present in larger numbers in WT vs 5xFAD mice. Moreover, pseudotime analysis showed that over the course of both AD and normal aging that *Gfap*^{lo} astrocytes shift into DAAs and *Gfap*^{hi} subsets (117). The studies put forth by Lau et al. and Habib et al. have revealed that astrocyte activation in AD is both complex and dynamic. Furthermore, understanding the relevance of these different subpopulations to disease as well as how they interact with other neural cell types will be particularly insightful.

Glymphatic System

Astrocytes also play a central role in the clearance of waste from the CNS. The elimination of excess interstitial fluid and solutes is critical for tissue homeostasis. For the majority of tissues in the body this waste removal is achieved through lymphatic vasculature. However to date there is no evidence that the brain parenchyma possesses lymphatic vessels which begs the question of how the brain handles this important function. In 2012, Maiken Nedergaard's group provided an elegant framework for how fluid washes through the brain to remove waste products. This framework was termed the glymphatic system, with the 'g' referencing the glia limitans which is composed of astrocyte foot processes that line perivascular spaces. According to the model, para-arterial cerebrospinal fluid (CSF) is pushed by arterial pulsation through the brain parenchyma creating a convective flow which carries interstitial materials to the para-venule space before ultimately being drained to the cervical lymph system (118). At the time it was unclear how dirty CSF drained to the cervical lymphatics

but this would be addressed by experiments from the Kipnis group and Alitalo group who would demonstrate the existence of lymphatic vessels in the meninges which are capable of draining CSF (119, 120). The expression of the water channel AQP4 on the astrocyte endfeet is critical for the exchange of CSF-ISF between perivascular spaces and brain parenchyma. Iliff et al. demonstrated that mice deficient in AQP4 exhibit significantly suppressed influx of perivascularly injected CSF or clearance of injected Aβ or mannitol (118). Interestingly, it has been shown that a redistribution of AQP4 from astrocytic endfeet to more parenchymal processes occurs in AD (121). Moreover, polymorphisms in human *AQP4* are a genetic risk factor for LOAD and APP/PS1 mice lacking AQP4 have aggravated pathology (122, 123).

1.3.3 Efforts to target AD associated inflammation

A growing body of work suggests that AD is driven by a self-perpetuating inflammatory cycle. It stems that efforts to curb this inflammation using anti-inflammatory therapies may provide beneficial outcomes. Unfortunately to date there has not been much convincing success in this realm. Many of us have likely used non-steroidal anti-inflammatory drugs (NSAIDs) to alleviate fever, but there was evidence suggesting their potential in treating AD as well. NSAIDs work by inhibiting the cyclooxygenase (COX) enzymes which generate lipid mediators called prostaglandins that are capable of promoting inflammation. Previous studies have shown that inhibition of prostaglandin signaling can restore microglial homeostatic functioning as well as rescue memory impairments in APP/PS1 mice (124). Moreover, there are a number of epidemiological studies that have suggested that long-term usage of NSAIDs reduces the risk of succumbing to AD (125, 126). However, randomized clinical trials have failed to show efficacy in NSAID usage as an AD therapeutic. The most recent study, INTREPAD, examined the effects of naproxen on presymptomatic high AD risk patients in their 60s. Twice daily administration of naproxen over a span of two years yielded no signs of reducing progression of presymptomatic AD patients. Naproxen-treated individuals did however exhibit increased adverse events (127).

Separate trials investigating other NSAIDs such as ibuprofen, celecoxib, and rofecoxib have also demonstrated that NSAIDs offer no significant benefit to AD progression (128).

Minocycline is a tetracycline antibiotic that also possesses anti-inflammatory activity. Previous animal studies had indicated that minocycline can dampen AD-associated inflammation (129). In 2019, Howard et al. published their findings on a randomized clinical trial in which participants with mild AD were given either placebo, 200 mg/day, or 400 mg/d of minocycline over the course of 24 months. However, no significant differences in cognitive performance or a patient's general well-being as measured by the Bristol Activities Daily Living Scale (BADLS) were seen between placebo and minocycline-treated groups (130).

Despite these setbacks, there are still potential benefits of targeting neuroinflammation as a means of AD prevention. If anything, the failed NSAID and minocycline studies point to a necessity in identifying and targeting relevant inflammatory pathways. In the case of minocycline, its exact target and mode of action in an AD setting is unclear. Additionally, there is also a possibility that minocycline could be interfering with support functions of microglia that facilitate plaque clearance. In summary, identification and development of drugs that are able to selectively target detrimental inflammatory pathways while preserving homeostatic glial function is needed.

Upregulation of pro-inflammatory cytokines such as TNF-α and IL-1β have been pinned as key contributors to pathophysiology in AD. As such, clinical efforts to design inhibitors against these molecules are currently underway. One such drug , XPro1595, was developed by INmune and is a brain-permeant TNF-α inhibitor that specifically targets soluble TNF-α preventing its interactions with TNFR1 which can exacerbate neuroinflammation. XPro1595 is currently in Phase 2 clinical trials to determine its efficacy in treating MCI and AD (131). Canakinumab is an anti-IL-1β monoclonal antibody developed by Novartis for the treatment of immune disorders.

Currently, Canakinumab (brand name Ilaris) is used to treat arthritis but given the body of work implicating dysregulated IL-1 signaling in AD, it is also being tested for its efficacy in the treatment of neurological disorders. Phase 2 clinical trials testing Canakinumab as a therapeutic for MCI and AD are in progress and expected to complete in 2026 (132). As discussed previously, microglia have nuanced roles in AD. Ideally, one would want to be able to limit microglial inflammatory signaling while bolstering phagocytic capacity. TREM2 is essential in proper microglial plaque recognition and clearance. Administration of the TREM2 agonizing antibody, AL002c, into 5xFAD mice expressing either the common variant or R47H mutation led to decreases in plaque load, neurite dystrophy, and microglial inflammation (133). AL002 is currently in Phase 2 clinical trials (134). Alongside TREM2, the microglial receptor CD33 has also emerged as a therapeutic target for AD. CD33 (also known as Siglec-3), is a pattern recognition receptor that recognizes sialic acid residues that coat the surfaces of various pathogens as well as amyloid plaques. Signaling through CD33 leads to inhibition of TREM2 mediated Aβ clearance pathways. As such, AD transgenic mice that lack CD33 show reduced plaque burden (135). Moreover, *CD33* risk alleles that lead to increased CD33 expression correlate with more advanced cognitive decline and AD (136). To blunt CD33 pathways, Alector developed AL003, a monoclonal antibody that blocks CD33. AL003 is still in Phase 1 studies (137). While it's still early to say whether or not these interventions will serve as disease-modifying therapies they all share a common theme of targeting specific molecules or pathways that are known to be dysfunctional in human AD - this is in stark contrast to minocycline. These efforts, along with a continued interest in anti-inflammatory compounds, will hopefully give rise to viable AD treatments.

1.4 Cell death pathways implicated in Alzheimer's disease

Cell death is a fundamental biological phenomenon. Everyday we lose billions of cells during homeostatic processes. Abnormalities in cell death can have wide-reaching implications

from developmental defects that lead to premature lethality to maladies such as cancer. Cell death was initially described in the 19th century as an accidental phenomenon. This “coagulative necrosis” as it was called was viewed as a passive wasting away of the cell that occurred upon exposure to a noxious stimuli. However, morphological observations in the 1960s hinted that there might be a programmed form of cell death that occurs during embryogenesis (138, 139). In 1972 a seminal paper by Kerr, Wyllie, and Curry coined this form of cell death as apoptosis. Using electron microscopy, Kerr et al delineated the structural changes that an apoptotic cell undergoes along with its subsequent phagocytosis (140). We would later learn largely through experiments done using the nematode worm *Caenorhabditis elegans* that apoptosis is carried out by members of the caspase family (141). Additional regulators of apoptotic cell death would be uncovered about a decade later (142, 143). Thus, up until the mid-1990s, our view of cell death was viewed as a dichotomy between necrosis and apoptosis which marked un-regulated and regulated forms of loss, respectively. What has happened since then is a rapid expansion in the discovery of additional regulated death mechanisms. While each of these pathways has their own set of protein machinery there is a significant degree of cross-talk between different modes of cell death (i.e. interactions between Caspase-8 and RIPK3 demonstrated in this study). Understanding when, where, why, and how a particular type of cell death is favored over another is an active area of research.

Gradual neuronal loss is one of the clinical hallmarks of AD. The hippocampus and entorhinal cortex are among the first regions to show degeneration and display neurofibrillary tangles in AD. Pathology later spreads to neocortical regions coinciding with the emergence of cognitive decline (144, 145). While we appreciate the role of cell death in AD, the molecular mediators driving cell loss remain unclear. One of the challenges stems from the observation that many rodent models of AD fail to show the extensive degree of neuronal loss seen in the human condition. Another consideration is that postmortem assessment of human tissue

provides a limited amount of information. Cell death in AD occurs progressively over a span of several decades and histopathological examination only provides a picture of the end. Furthermore, it's likely that multiple modes of cell death are involved in the neuronal loss seen in AD and at possibly different disease stages which clouds the picture further. In this section, we highlight some of these regulated cell death pathways and their contributions to AD progression.

1.4.1 Necroptosis

Necroptosis is a form of regulated necrosis that is mediated by receptor interacting protein kinases 1 and 3 (RIPK1, RIPK3), and the substrate mixed-lineage kinase domain-like protein (MLKL). Necroptosis is executed by sequential phosphorylation of RIPK1, RIPK3, and MLKL following activation of TNFR family members, TLRs, or intracellular sensors like ZBP1. In the cases of TLR or ZBP1-induced necroptosis RIPK1 is dispensable. Activation of RIPK3 is driven by homotypic interactions of rip homotypic interaction motifs (RHIMs) domains within its C-terminus region. In addition to RIPK3, RIPK1, TRIF (a TLR adaptor protein), and ZBP1 contain RHIM domains which can facilitate RIPK3 activation and autophosphorylation via RHIM-RHIM interactions. The execution of necroptosis is carried out once phosphorylated MLKL translocates to the plasma membrane and forms pores that lead to release of damage associated molecular patterns (DAMPs) and ultimately cell lysis (146). Due to its lytic nature, necroptosis is largely viewed as an immunogenic form of cell death in stark contrast to apoptosis.

Why do we need a regulated form of inflammatory cell death? In the 1970s, evolutionary biologist Leigh Van Valen proposed the 'Red Queen Hypothesis' which states that antagonistic species have a need to constantly evolve in order to avoid extinction (147). This principle can also be applied to our understanding of host-pathogen interactions. Therefore, inflammatory modes of cell death like necroptosis may have evolved as a mechanism to control infection as

part of an evolutionary arms race against pathogens that are consistently developing means of evading the host immune system. Elimination of a host cell can be useful in innate immune responses during times when the host cell has been reprogrammed to act in the pathogen's best interests. Thus in conditions where apoptosis is inhibited, such as in the case of murine CMV which expresses viral inhibitor of Casp8 activation (vICA), an alternative mode of cell suicide is needed (148). This is achieved by necroptosis which is unlocked with Caspase-8 inhibition.

Aside from pathogen clearance, necroptosis has also been shown to be engaged in neurodegenerative conditions like AD. Several groups have shown increased levels of phospho-RIPK3 and phospho-MLKL in the brains of AD patients (149-151). Up-regulation of these markers, generally correlated with poorer cognitive performance (149). In addition to inducing cell death, necroptosis is an inflammatory pathway. Recent research has demonstrated that RIPK1-RIPK3 can signal through NF-κB to drive pro-inflammatory cytokine production prior to inducing cell death (152, 153). In AD, up-regulation of pro-inflammatory cytokines such as IL-6, IL-1, and TNFα are observed concurrently with the emergence of plaques (154-156). Interestingly, blocking RIPK1 activity reduces inflammation and Aβ burden in the APP/PS1 model (157). However, RIPK1 in addition to promoting necroptosis, can also promote inflammatory cytokine production as well as apoptosis. Collectively, these studies are suggestive that necroptosis is engaged during AD. Whether necroptosis drives pathology in AD represents a significant gap in our knowledge.

1.4.2 Apoptosis

As discussed earlier, apoptosis was the first discovered regulated cell death pathway. Apoptosis is carried out by caspase proteases which are responsible for cleaving thousands of targets during the progression of apoptosis (158). Due to the actions of caspases, apoptotic

cells display membrane blebbing, nuclear fragmentation, cell shrinkage, and are eventually rapidly phagocytosed. The efficient clearance and preservation of an intact membrane makes apoptosis a non-inflammatory process. Other groups have also demonstrated that apoptotic cells release molecules such as adenosine monophosphate (AMP) through Pannexin-1 channels which promote an anti-inflammatory gene expression profile in the phagocyte (159). The observation that apoptosis is non-inflammatory may help explain why it appears to be the predominant form of cell death during development. To illustrate, mice deficient in pro-apoptotic proteins such as Bax, Bak, Bok, Apaf1, or Caspase-3 often present with gross morphological defects and/or perinatal lethality (160-162). Apoptosis can be subdivided into two pathways: an extrinsic pathway in which the apoptotic signal is sensed by death receptors at the plasma membrane or an intrinsic pathway in which the signal is perceived within the cell resulting in mitochondrial outer membrane permeabilization (MOMP). We will discuss both pathways in the sections below as well as their implications in AD.

Extrinsic Apoptosis

Extrinsic apoptosis is a distinct form of programmed cell death mediated through death receptor-ligand interactions (i.e. TNFR family members). Extracellular signals are conveyed through adaptor proteins and the initiator caspase, Caspase-8. Subsequent dimerization and auto-processing of caspase 8 leads to activation of caspase-3 which executes apoptosis. Up-regulation of death receptors has been observed in AD patient models (163, 164). Furthermore, death receptor 6 (DR6) has been reported to form a complex with p75NTR, another death receptor, which has been demonstrated to be essential for mediating the toxic effects of Aβ on cultured neurons (163). Early studies have also demonstrated the presence of cleaved caspase 3 in both neurons and astrocytes in aged AD brains (165). Thus, the up-regulation of death receptors and downstream activation of caspase 3 suggest that extrinsic apoptosis may be involved in AD progression.

Intrinsic Apoptosis

The intrinsic apoptotic pathway is activated when stresses emanating from within the cell lead to mitochondrial dismantling. Permeabilization of the mitochondrial membrane via pro-apoptotic BCL-2 proteins results in release of cytochrome c and cleavage of caspase-9 and and caspase-3. Two stresses that can lead to MOMP that are particularly relevant in AD are ER and genotoxic stress. Intraneuronal accumulation of Aβ and tau has been shown to induce the unfolded protein response (UPR) in neurons (166, 167). Prolonged activation of UPR can lead to transcriptional upregulation of a number of proapoptotic factors including the BCL-2 family of proteins. Elevated levels of Bax have been observed in human AD samples (168, 169). In addition, inhibition of Bax was found to diminish Aβ-induced toxicity in hippocampal slice cultures (170). On the flip side, overexpression of the anti-apoptotic protein Bcl-2 was shown to be protective in the 3xTg AD mice (171). Excessive genotoxic stress can also converge on Bax/Bak mediated MOMP. Maintenance of genomic integrity is vital for cell function. Due to their postmitotic nature, neurons are particularly vulnerable to amassing genomic stress. Several groups have shown evidence of accumulation of double strand breaks in neurons during early stages of AD (172, 173). Studies by Misiak et al also showed that impairing DNA repair mechanisms can worsen AD pathology. DNA polymerase-β (Polβ) helps facilitate base excision repair (BER). Compared to 3xTg littermates, 3xTg/Polβ$^{+/-}$ were found to have increased amounts of double strand breaks and also significantly more cleaved caspase-3^{+} cells (174).

Work by Zhang et al provided additional compelling evidence for the role of intrinsic apoptosis in AD. The group studied the contributions of the pro-apoptotic protein BAD to AD progression. When BAD is hypophosphorylated, it moves to the mitochondrial membrane and blocks BCL-2 and BCL-XL, ultimately promoting apoptosis. Zhang et al not only demonstrated that BAD is upregulated in neurons from both AD patients and 5xFAD mice but also that BAD knockout protected against cortical layer V neuron loss in 5xFAD mice. Interestingly, BAD loss

did not completely prevent neurodegeneration suggesting that other modes of death are perhaps contributing (175).

1.4.3 Pyroptosis

Pyroptosis (‘fiery death’) is a regulated form of inflammatory cell death. In many respects, pyroptosis bears a great deal of similarity to necroptosis. Execution of pyroptosis is carried out via the actions of Gasdermin-D which when cleaved, translocates to the plasma membrane to induce cell lysis. In the process of pyroptotic death, a number of DAMPs and other inflammatory molecules such as IL-1β and IL-18 are released to alert the immune system (176). Therefore, much like necroptosis, pyroptosis is designed to protect us against infection and can be triggered by a range of pathogen molecules. The pathway was initially discovered by Zychlinsky et al who showed that infection by *Shigella flexneri* leads to macrophage suicide (177). The group first characterized the death as apoptosis due to its caspase-dependency but later examination revealed it to be pyroptosis. Canonically, pyroptosis is mediated through the assembly of multi-protein complexes termed inflammasomes which are capable of sensing a diverse array of cell stresses. Inflammasomes consist of three main components: a sensor, the adaptor protein apoptosis-associated speck-like protein containing CARD (ASC), and pro-caspase-1. The most well-studied inflammasome sensors are absent in melanoma 2 (AIM2), which responds to cytosolic double-stranded DNA, and the NOD-like receptor (NLR) family members, NLRP1, NLRP3, and NLRC4, which respond to stimuli such as ATP, reactive oxygen species (ROS), and DAMPs (178). Inflammasome sensing triggers the recruitment of ASC which subsequently oligomerizes, forming large protein complexes termed specks which reach around 1 μm in size. Via its CARD domain, ASC proceeds to recruit pro-caspase-1 to the inflammasome complex. Caspase-1 undergoes an autoproteolytic event in the inflammasome complex leading to its activation and cleavage of inflammatory mediators pro-IL1β, pro-IL 18, and the ultimate executioner of pyroptosis, Gasdermin-D. Interestingly, in the absence of

Gasdermin-D, caspase-1 is capable of cleaving BID which results in mitochondria, triggering outer membrane permeabilization (MOMP) and subsequent apoptosis (179).

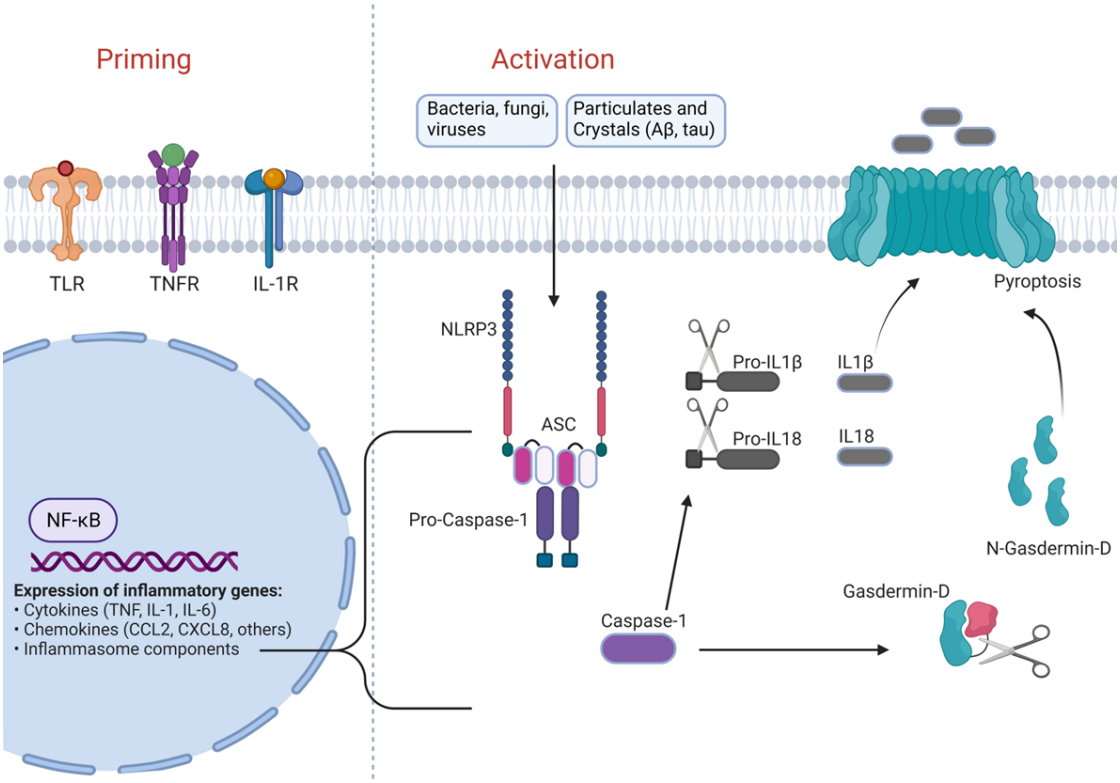

Figure 1.3. NLRP3 inflammasome signaling. Schematic of NLRP3 signaling. There are two main steps to inflammasome signaling (1) an initial priming stage which involves transcriptional upregulation of inflammasome components as well as expression of numerous cytokines and chemokines (2) actual assembly of the inflammasome complex which consists of the NLRP3 inflammasome sensor protein, adaptor protein ASC, and pro-Caspase-1. This event leads to the activation of Caspase-1, subsequent processing of precursor cytokines pro-IL1 and pro-IL18 to their active forms, and in many cases, execution of a form of cell death called pyroptosis which is governed by the pore forming protein Gasdermin-D.

It is also worth mentioning that in addition to the canonical pyroptosis pathway there is also a non-canonical pathway. Work out of Visva Dixit's lab discovered that LPS-primed macrophages are capable of undergoing pyroptosis following treatment with cholera toxin B (CTB). Furthermore, this death was dependent on caspase-11 and Gasdermin-D but not NLRP3, ASC, or caspase-1 (180). Later studies would go on to show that CTB was merely acting as a carrier to facilitate LPS delivery into the cell. To illustrate, LPS transfection is sufficient to stimulate caspase-11 dependent pyroptosis (181). These studies led to the

somewhat surprising finding that caspase-11 can directly bind to LPS (182). The non-canonical pathway seems to primarily serve as a safety net to destroy gram negative bacteria that have escaped the phagosome and entered the cytosol of the cell (183).

There is strong evidence that pyroptosis may play a role in AD progression. Several AD mouse models have shown rescue of pathological hallmarks through either genetic or pharmacological targeting of NLRP3, Caspase-1, and ASC (154; 184-188). The majority of these studies suggest that NLRP3 inflammasome engagement in glial cells by aggregates such as Aβ and tau lead to increased neuroinflammation and neuronal loss. Despite the fact that neurons have the capacity to undergo pyroptosis, it is unclear if neuronal pyroptosis is the main mechanism by which neurons are lost in AD. Work by Tan et al showed increased colocalization of NLRP1 and NeuN in aged APP/PS1 mice. Primary cortical neurons challenged with Aβ underwent death but were protected with siRNA knockdown of NLRP1. The group also demonstrated that NLRP1 silencing reduced cortical neuron loss and cognitive impairment in APP/PS1 mice (189). However, the study by Tan et al did not examine Gasdermin-D cleavage in either their *in vitro* or *in vivo* experiments. A later study by Kashual et al also showed that AD insults lead to elevations in NLRP1 in primary neurons. Instead of leading to pyroptosis, Kashual et al suggested that NLRP1 activation led to cleavage of caspase-6 which is associated with axon degeneration. Caspase-6 cleavage was found to be dependent on caspase-1 (190). The lack of *in vivo* data clouds the relevance of the NLRP1-caspase-1-caspase-6 axis to AD.

1.4.4 Ferroptosis

Pioneering work out of Brent Stockwell's lab added ferroptosis to the growing list of cell death modalities. As its name suggests, ferroptosis is an iron-dependent form of cell death that is driven by excess lipid peroxidation. Much like necroptosis and pyroptosis, ferroptosis is inflammatory. The pathway emerged during a study to identify small-molecules that were selectively lethal to RAS mutant tumor cells. From the screen, the compounds RSL3 and erastin were found to induce a non-apoptotic, caspase-independent form of death in these tumor cells (191). Notably, both compounds were shown to increase intracellular levels of ROS and death was prevented with iron chelation or prevention of iron uptake (192). In later studies, erastin was found to inhibit system X_c^-, an amino acid antiporter that mediates the exchange of extracellular l-cystine for intracellular l-glutamate across the plasma membrane. Imported cystine is reduced to cysteine which is a key substrate in glutathione biosynthesis. A sustained supply of glutathione is required to support the activity of the cellular lipid peroxide, GPX4 (which is directly inhibited by RSL3). Lethality in ferroptosis occurs as a result of peroxidation of poly-unsaturated fatty acids (PUFAs) which leads to disruptions in membrane integrity (193). What role does iron have in ferroptosis? Iron is an essential element and is found in two forms within the cell: Fe^{2+} and Fe^{3+}. Fe^{3+} is more stable than Fe^{2+} and is the form that iron is preferentially stored and transported as. On the other hand, free Fe^{2+} is capable of reacting with hydrogen peroxide (natural by-product of mitochondrial activity) to produce hydroxyl radicals in the Fenton reaction which can lead to lipid peroxidation. Thus, ferroptosis is intricately linked to iron metabolism, uptake, and storage.

As we age our brain iron levels increase and this is believed to lead to cognitive decline. Moreover, high concentrations of iron are oftentimes found within insoluble plaques and neurofibrillary tangles (194). Given the capacity of excess iron to promote oxidative stress, this has led some to hypothesize that ferroptosis may be a key driver in AD-associated neuronal

loss. Studies by Chen et al, demonstrated that 5xFAD mice display increased levels of lipid peroxidation and that overexpression of GPX4 can help mitigate neurodegeneration and memory impairments (195). Along similar lines, other groups have demonstrated that administration of selenium, a trace element required by GPX4, reduced neuroinflammation, reduced tau pathology, and spatial memory deficits in 3xTg-AD mice (196). While these preliminary studies are promising, there is still a great deal that needs to be done in terms of establishing the role of ferroptosis in AD as well as determining whether targeting the pathway is a viable long-term strategy for reducing AD pathogenesis.

1.5 Conclusion

Considering the many failures of anti-amyloid therapies, there is a pressing need for alternative AD treatment approaches. Genome-wide association studies (GWAS) have identified many AD risk genes in innate immunity and microglial signaling. Although our understanding of the AD immune response has improved substantially, there are still gaps in our knowledge of the inflammatory and death processes underlying the disease. In the following chapter, we outline our findings on the contributions of Caspase-8 and RIPK3 in A amyloidosis. Our results show that the combined loss of Caspase-8 and RIPK3, but not RIPK3 alone, protected against excessive amyloid deposition and microgliosis in 5xFAD mice. These findings present Caspase-8 as a novel regulator of AD pathogenesis and argue that Caspase-8 inhibition could serve as a therapeutic strategy.

Chapter 2. Role of the Caspase-8/RIPK3 axis in Alzheimer's disease pathogenesis and Aβ-induced NLRP3 inflammasome activation

Sushanth Kumar[1, 2], Sakar Budhathoki[1], Christopher B. Oliveira[1], August D. Kahle[1], Osman Y. Calhan[1] John R. Lukens[2, 3*], and Christopher D. Deppmann[1, 2*]

[1]Department of Biology, University of Virginia, Charlottesville, VA 22908, USA. [2]Neuroscience Graduate Program, School of Medicine, University of Virginia, Charlottesville, VA 22908, USA. [3]Center for Brain Immunology and Glia (BIG), Department of Neuroscience, School of Medicine, University of Virginia, Charlottesville, VA 22908, USA.

2023, JCI insight, 8(3): e157433, https://doi.org/10.1172/jci.insight.157433

2.1 Abstract

The molecular mediators of cell death and inflammation in Alzheimer's disease (AD) have yet to be fully elucidated. Caspase-8 is a critical regulator of several cell death and inflammatory pathways; however, its role in AD pathogenesis has not yet been examined in detail. In the absence of Caspase-8, mice are embryonic lethal due to excessive RIPK3-dependent necroptosis. Compound RIPK3 and Caspase-8 mutants rescue embryonic lethality, which we leveraged to examine the roles of these pathways in an amyloid beta (Aβ)-mediated mouse model of AD. We find that combined deletion of Caspase-8 and RIPK3, but not RIPK3 alone, leads to diminished Aβ deposition and microgliosis in the 5xFAD mouse model of AD. Despite its well-known role in cell death, Caspase-8 does not appear to impact cell loss in the 5xFAD model. In contrast, we found that Caspase-8 is a critical regulator of Aβ-driven inflammasome gene expression and IL-1β release. Interestingly, loss of RIPK3 had only a modest effect on disease progression suggesting that inhibition of necroptosis or RIPK3-mediated cytokine pathways are not critical during mid stages of Aβ amyloidosis. These findings suggest that therapeutics targeting Caspase-8 may represent a novel strategy to limit A□ amyloidosis and neuroinflammation in AD.

2.2 Introduction

Alzheimer's disease (AD) is a progressive neurodegenerative disease that is characterized by the accumulation of amyloid beta (A□) and tau. The build-up of these species and other neurotoxic factors is associated with an up-regulation of pro-inflammatory cytokine production and cell death signaling (197). Initially these responses are thought to be beneficial and aid in the clearance of harmful aggregates (198, 199). However in AD these physiologic responses shift to chronic activation which can give rise to deleterious neuroinflammation, neuronal loss, and cognitive decline. While recent single-cell transcriptomic studies have provided some insights into how cells transition from a healthy to diseased state during AD as well as pathways that may drive pathology, we still lack full knowledge of the molecular mediators responsible for propagating inflammation and cell death in AD (93, 111, 200).

Caspase-8 serves as an essential regulator of a number of cell death and inflammatory pathways. Caspase-8 was first described as a key component of the extrinsic apoptotic pathway, which is mediated through death receptor-ligand interactions (e.g. tumor necrosis factor receptor superfamily (TNFRSF) members). Upon death receptor activation, adaptor proteins and procaspase-8 are recruited, promoting the dimerization and autoprocessing of procaspase-8 to its active form Caspase-8 which then proceeds to execute apoptosis via Caspase-3 activation (201). Up-regulation of death receptors has been observed in AD patients (163, 164). Early studies have also demonstrated the presence of active forms of Caspase-3 and Caspase-8 in the brains of AD patients (165, 202). However, whether extrinsic apoptotic programs are required for the cell death associated with AD has not been fully examined to date.

In addition to promoting apoptosis, Caspase-8 serves as an important negative regulator of RIPK1-RIPK3-mediated necroptosis, which is an inflammatory form of cell death. The role

that Caspase-8 plays in curbing necroptosis is especially important during development where the deletion of Caspase-8 alone results in excessive RIPK1-RIPK3-driven necroptosis and leads to embryonic lethality in Caspase-8-deficient mice (12-14). Interestingly, various components of the necroptotic signaling pathway including RIPK1 and RIPK3 have been implicated in several neurodegenerative conditions (203-205). Therefore, the possibility exists that RIPK3 deletion alone or in combination with Caspase-8 deletion also affects Alzheimer's-related disease pathogenesis (206). *Casp8*$^{-/-}$*Ripk3*$^{-/-}$ mice are deficient in both extrinsic apoptosis and necroptosis and are viable which provides us with an opportunity to study the contributions of these two cell death/signaling pathways in AD (207-209).

Beyond regulating cell death, Caspase-8 also acts as a key mediator of inflammatory cytokine production. Following death receptor or toll-like receptor (TLR) activation, Caspase-8 can promote NF-κB-mediated cytokine production (e.g. TNFα and IL-6) (210, 211). Caspase-8 can also promote inflammation through its regulation of NLRP3 inflammasome signaling (212-214). The NLRP3 inflammasome is a multi-protein complex that plays an essential role in innate immunity. Activation of the inflammasome leads to release of the pro-inflammatory cytokines IL-1β and IL-18 as well as the execution of a Gasdermin-D-driven form of cell death known as pyroptosis (176). An additional component of inflammasome activation is the formation and release of the adaptor protein ASC (apoptosis-associated speck-like protein containing a CARD). Previous reports have shown that released ASC specks are capable of binding to A□ and accelerating its aggregation and increasing its toxicity to bystander cells. Moreover, inhibition of ASC speck formation either genetically or pharmacologically has been shown to blunt pathology in multiple AD mouse models (154, 184-187). To date, the role of Caspase-8 in AD-associated inflammasome function has not been investigated.

In this study, we set out to determine the contributions of Caspase-8 and RIPK3 in A□ amyloidosis. We demonstrate here that combined loss of Caspase-8 and RIPK3 in mice

carrying human presenilin 1 (PSEN1) and amyloid precursor protein (APP) with 5 familial AD mutations (5xFAD mice), decreases overall AD pathology. More specifically, we observe that combined loss of Caspase-8 and RIPK3 reduced A□ deposition and microgliosis in the 5xFAD mouse model of AD. While we did not observe a role for Caspase-8 and/or RIPK3 in regulating neuronal loss, we did find that the Caspase-8/RIPK3 signaling axis regulates NLRP3 inflammasome signaling and IL-1□ secretion in response to A□ amyloidosis.

2.3 Results

2.3.1 Induction of Caspase-8 and RIPK3 expression in AD

To examine whether Caspase-8 and/or RIPK3 are altered in AD, we performed RNAscope to evaluate mRNA expression in 5-month-old WT and 5xFAD mice. Ripk3 expression was increased in both the subiculum and thalamus, whereas Casp8 expression was only significantly elevated in the thalamus of 5xFAD mice relative to WT controls. In the cortex, no significant differences were observed in Casp8 or Ripk3 between 5xFAD and WT mice (Figure 2.1, A–D). In addition, we also analyzed a published transcriptomic data set (NCBI Gene Expression Omnibus accession number GSE33000) from human prefrontal cortex samples, which revealed increased expression of both CASP8 and RIPK3 in patients with AD (Figure 2.1, E and F). Overall, these findings suggest there may be a role for extrinsic apoptotic and necroptotic pathways in both the 5xFAD mouse model and human AD brain.

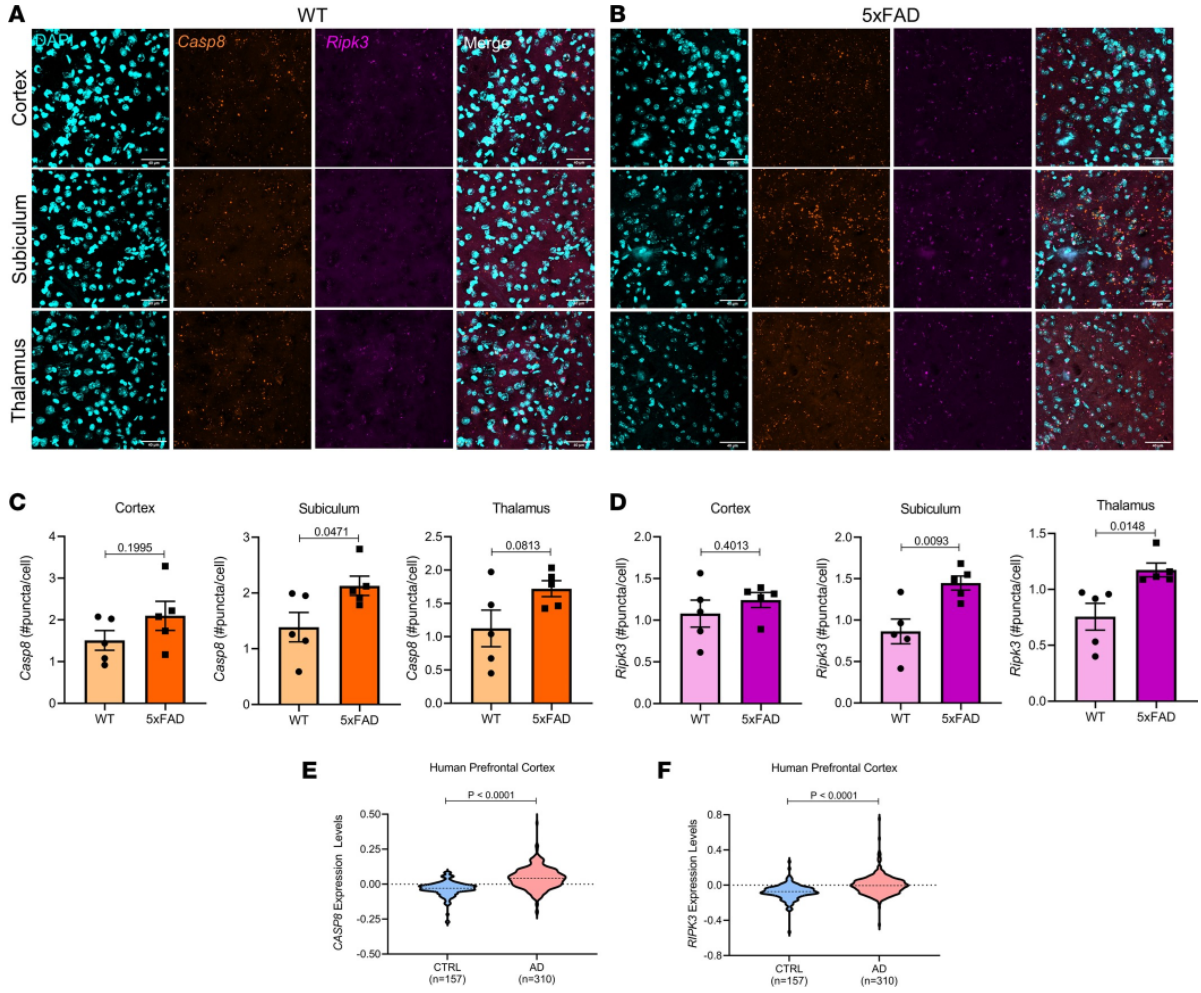

Figure 2.1. **Induction of Caspase-8 and RIPK3 expression in AD**. (A and B) Representative images of the cortex, subiculum, and thalamus from 5-month-old WT and 5xFAD mice stained with *Casp8* (orange) and *Ripk3* (magenta) RNAscope probes. Scale bars: 40 μm. (C) Quantification of *Casp8* staining. (D) Quantification of *Ripk3* staining (*n* = 5 5xFAD mice, *n* = 5 WT mice). (E and F) *CASP8* and *RIPK3* expression data obtained from a human transcriptomic data set (GSE33000) of dorsolateral prefrontal cortex tissue from 157 patients without dementia and 310 patients with AD. (C–F) Data were analyzed by Student's *t* test. Data reported as mean ± SEM (C and D) or as violin plots (E and F). Ctrl, control.

2.3.2 Combined loss of Caspase-8 and RIPK3 reduces Aβ amyloidosis in 5xFAD mice.

To investigate a role for Caspase-8 and RIPK3 in AD-related pathogenesis, we generated compound mutants between 5xFAD mice and *Caspase8*$^{-/-}$ and/or *Ripk3*$^{-/-}$ mice. Because of the early lethality of Caspase-8 single-KO mice, 5xFAD *Casp8*$^{-/-}$ *Ripk3*$^{-/-}$ (i.e., double KO [DKO]) mice were compared with age- and sex-matched 5xFAD and 5xFAD *Ripk3*$^{-/-}$ littermate controls to evaluate the role of Caspase-8 in AD pathogenesis.

Before tissue collection, 5xFAD, 5xFAD *Ripk3*$^{-/-}$, and 5xFAD DKO mice were aged to 5 months. We first assessed deposition of Aβ by staining with thioflavin S (ThioS), which marks plaques. In 5xFAD mice, deposition begins in the subiculum before spreading to overlying cortical regions. One of the first cortical regions affected in the 5xFAD line is the retrosplenial cortex (RS). Interestingly, we found that combined deletion of Caspase-8 and RIPK3 led to a marked reduction in the number of Aβ plaque deposits in the RS. In contrast, loss of RIPK3 alone did not significantly reduce Aβ, as measured by ThioS staining (Figure 2.2, A and B). We observed a similar degree of Aβ reduction in 5xFAD-DKO mice when quantifying ThioS^{+} puncta in the subiculum of the hippocampus at 3 and 5 months. Consistent with findings of previous studies, we did not yet observe appreciable levels of Aβ deposition in the cortex of 3-month-old 5xFAD mice (215).

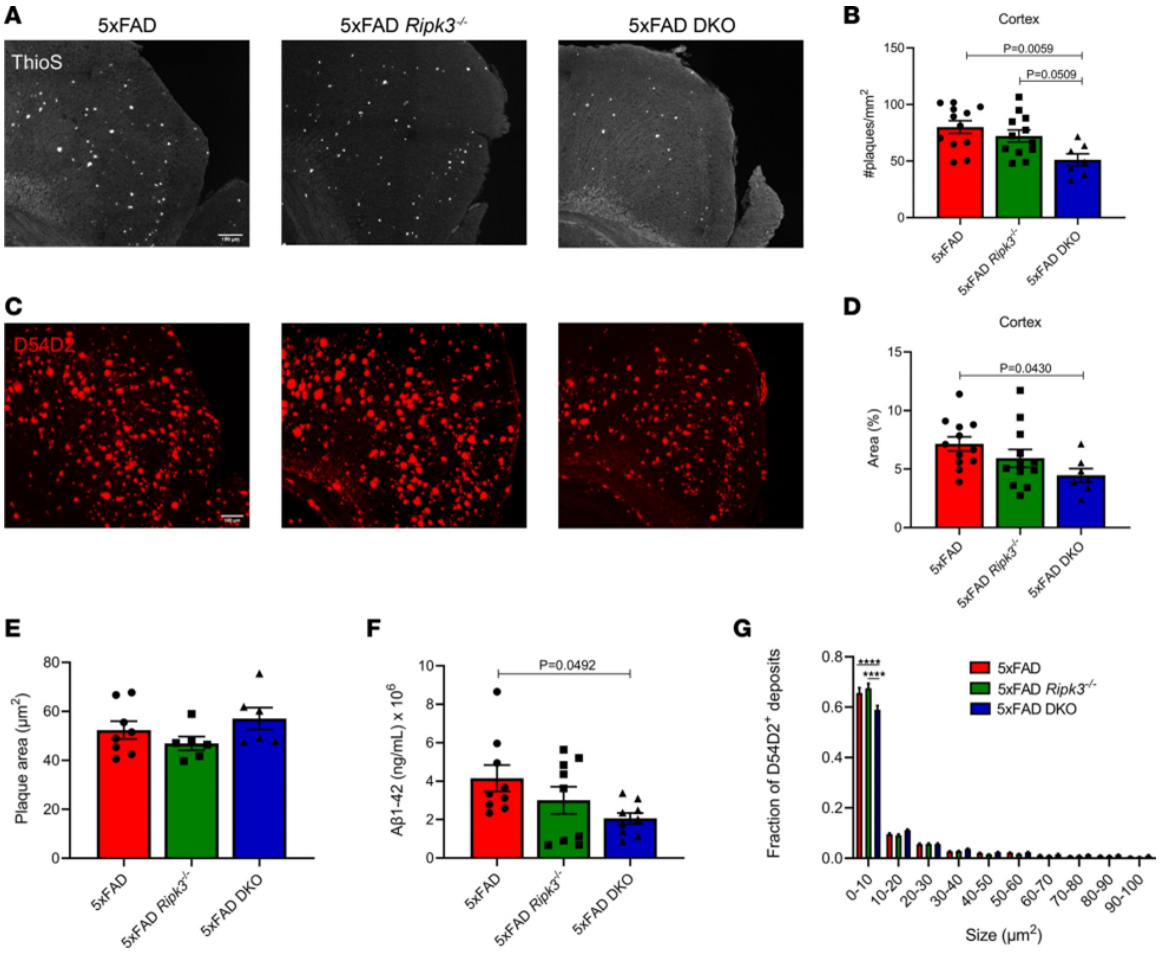

Figure 2.2. The Caspase-8/RIPK3 axis promotes Aβ amyloidosis in 5xFAD mice. (A and C) Representative IHC images of the RS taken at ×20 original magnification (*n* = 12 5xFAD mice, *n* = 12 5xFAD *Ripk3*$^{-/-}$ mice, and *n* = 7 5xFAD-DKO mice). Scale bar: 100 μm. (A) ThioS staining in the RS. (B) Quantification of ThioS staining. Each data point is an average of 2–3 different sections per mouse. (C) D54D2 staining in the RS. (D) Quantification of D54D2 staining. Each data point is an average of 2–3 different sections per mouse. (E) Aβ1-42 ELISA for guanidine-soluble fraction from cortices of 5-month-old mice (*n* = 9 5xFAD mice, *n* = 9 5xFAD *Ripk3*$^{-/-}$ mice, *n* = 9 5xFAD-DKO mice). (F) Quantification of the mean plaque size from D54D2 staining in RS (*n* = 8 5xFAD mice, *n* = 6 5xFAD *Ripk3*$^{-/-}$ mice, and *n* = 6 5xFAD-DKO mice). (G) Fraction of D54D2 deposits falling within designated bins. Analysis was carried out in the RS for deposits less than 100 μm^2 (*n* = 8 5xFAD mice, *n* = 6 5xFAD *Ripk3*$^{-/-}$ mice, and *n* = 6 5xFAD-DKO mice). (A–F) Data were analyzed by 1-way ANOVA followed by Tukey's post hoc test. (G) Data were analyzed by 2-way ANOVA followed by Tukey's post hoc test. All *n* values refer to the number of mice used, and error bars indicate SEM. ****$P < 0.0001$.

In addition to ThioS, we stained with the D54D2 Ab, which captures both dense, core Aβ plaques in addition to smaller, oligomeric species. Loss of Caspase-8 along with RIPK3 mitigated D54D2 deposition in the RS compared with the RS of 5xFAD mice (Figure 2.2, C and D). In contrast, depletion of RIPK3 alone on the 5xFAD background only resulted in a slight

trend toward decreased D54D2 staining in the RS; however, this did not reach statistical significance (Figure 2.2, C and D). Interestingly, we did not observe significant changes to subicular D54D2 deposition at either 3 or 5 months (Figure 2.4, B, D, F, and H). Consistent with our cortical D54D2 data, we also observed that the levels of cortical guanidine-soluble Aβ1-42 were markedly reduced in 5xFAD DKO versus 5xFAD mice via ELISA (Figure 2.2E). Plaque parameters such as area, volume, intensity, and sphericity (a measure of plaque compactness) were unchanged between genotypes (Figure 2.2E and Figure 2.3). D54D2 staining revealed much more heterogeneity in plaque sizes. Although average plaque size was similar between genotypes, combined loss of Caspase-8 and RIPK3 led to a significant reduction in the number of smaller (0–10 μm^2) $D54D2^+$ deposits (Figure 2.2G). Overall, these data suggest that Caspase-8 contributes to amyloid deposition in the 5xFAD model.

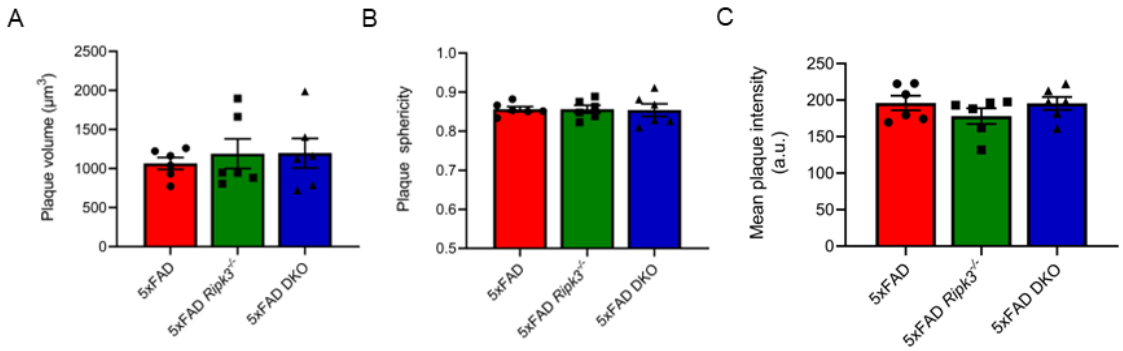

Figure 2.3. Genetic ablation of Caspase-8 and/or RIPK3 in 5xFAD mice does not alter A plaque sphericity, intensity, or volume. Cortical $Thios^+$ plaques were imaged at 40x magnification and labelled using the Surfaces feature in Imaris 9.7.2 and evaluated for (A) sphericity, (B) mean intensity, and (C) volume. (A-C) Results from 6-10 plaques were averaged per data point (n=6 for 5xFAD, n=6 for 5xFAD *Ripk3*$^{-/-}$, and n=6 for 5xFAD DKO). Data were analyzed by one-way ANOVA followed by Tukey post hoc test. All n values refer to the number of mice used and error bars indicate s.e.m.

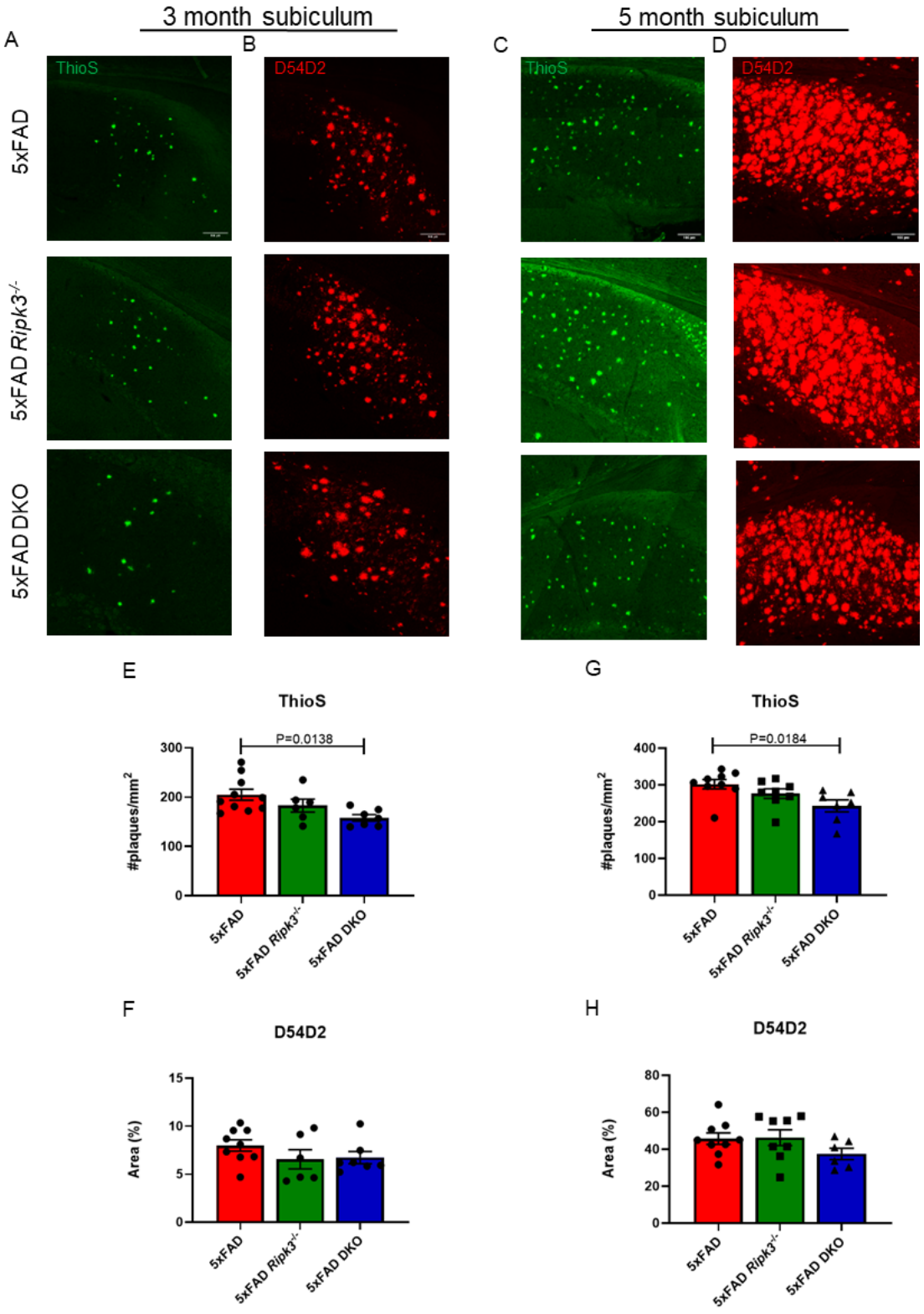

Figure 2.4. The Caspase-8/RIPK3 axis regulates subicular amyloid deposition. Representative IHC images of the subiculum taken at 40x magnification (n=10 for 5xFAD, n=6

for 5xFAD *Ripk3*$^{-/-}$, and n=7 for 5xFAD DKO). (**A**) Representative ThioS staining at 3 months. (**B**) Representative D54D2 staining at 3 months. (**C**) Representative ThioS staining at 5 months. (**D**) Representative D54D2 staining at 5 months. (**E**-**H**) Quantification for (**A**-**D**). Data were analyzed by one-way ANOVA followed by Tukey post hoc test. All n values refer to the number of mice used and error bars indicate s.e.m.

2.3.3 Reduced microgliosis with loss of Caspase-8 and RIPK3 in 5xFAD mice.

Chronic deposition of Aβ leads to a persistent glial response that promotes neuroinflammation. Moreover, excessive microglial and astrocyte engagement is thought to promote further Aβ deposition (216). Consistent with findings of previous studies, 5xFAD mice had elevated ionized calcium-binding adapter molecule 1 (Iba1) immunoreactivity compared with that of non-transgenic littermates (Figure 2.6, A and C, and Figure 2.7, A and B) (104). We found that 5xFAD DKO mice had significantly reduced cortical Iba1 staining compared with both 5xFAD and 5xFAD *Ripk3*$^{-/-}$ mice. A similar reduction was also seen in the subiculum of 3-month-old mice (Figure 2.5). Microgliosis was largely absent in the cortex of 3-month-old mice, likely because of lack of cortical amyloid pathology at this early time point (data not shown).

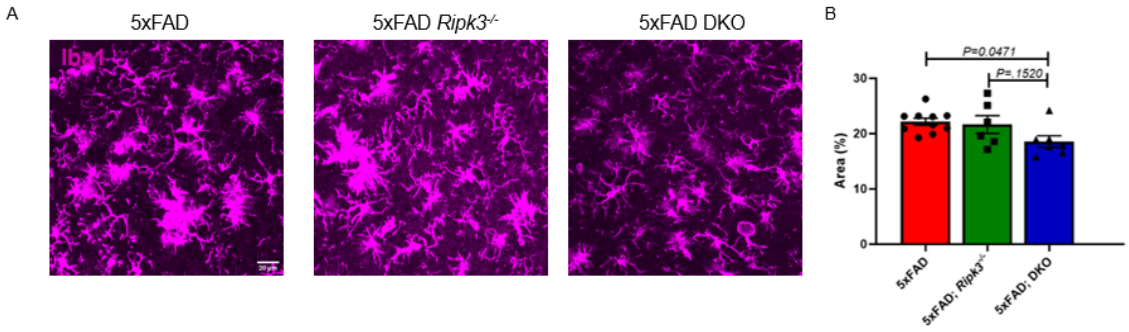

Figure 2.5. Reduced subicular microgliosis with loss of Caspase-8 and RIPK3 in 5xFAD mice. Representative IHC images of the subiculum taken at 40x magnification for 3-month-old mice (n=10 for 5xFAD, n=6 for 5xFAD *Ripk3*$^{-/-}$, and n=7 for 5xFAD DKO). (**A**) Representative Iba1 staining. (**B**) Quantification of Iba1 staining. Each data point is an average of 2-3 different fields of view taken throughout the subiculum over 3 sections per mouse. Data were analyzed by one-way ANOVA followed by Tukey post hoc test. All n values refer to the number of mice used and error bars indicate s.e.m.

To rule out the possibility of DKO microglia undergoing increased cell death, we performed TUNEL staining and observed negligible microglial TUNEL positivity across our different genotypes (Figure 2.8). We also investigated astrocyte reactivity but did not observe any significant differences in glial fibrillary acidic protein (GFAP) staining across genotypes (Figure 2.7, C and D). It should be noted that outside of the 5xFAD background, loss of Caspase-8 and/or RIPK3 did not alter baseline Iba1 or GFAP staining (Figure 2.6, A–D).

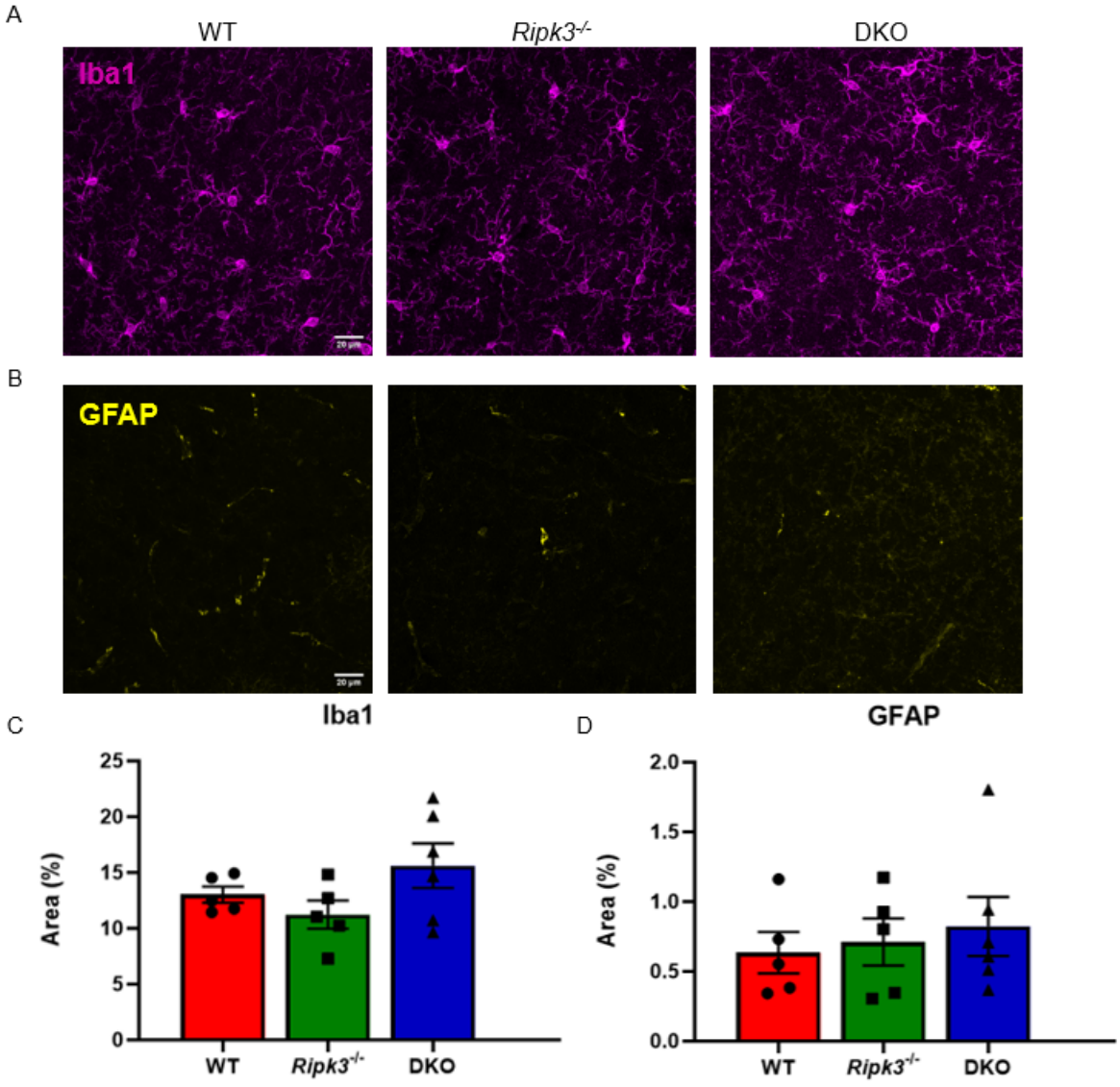

Figure 2.6. Genetic deletion of Caspase-8 and/or RIPK3 does not affect Iba1 or GFAP staining in the absence of A amyloidosis. Representative IHC images of the cortex from 5-month-old mice taken at 40x magnification (n=5 for WT, n=5 for *Ripk3*$^{-/-}$, and n=6 for DKO). (**A**) Representative Iba1 staining. (**B**) Representative GFAP staining. (**C**) Quantification of Iba1

staining. (**D**) Quantification of GFAP staining. (**C**-**D**) Each data point is an average of 8 different fields of view taken throughout the cortex over 2 sections per mouse. Data were analyzed by one-way ANOVA followed by Tukey post hoc test. All n values refer to the number of mice used and error bars indicate s.e.m.

In AD, microglia form barriers around plaques, and this is critical for minimizing neuronal damage but may also contribute to overall gliosis (101, 217, 218). We analyzed cortical microglia within 15 μm of ThioS$^+$ plaques and found that combined loss of Caspase-8 and RIPK3 decreased both the total number of Iba1$^+$ cells and overall Iba1 staining in periplaque regions (Figure 2.7, E–G). Because we observed an overall decrease in Aβ amyloid load in 5xFAD DKO mice (Figure 2.2, A–E), we next wanted to determine if the Caspase-8/RIPK3 axis regulates microglial phagocytosis of Aβ. To this end, we stained for CD68, a phagolysosomal marker, and focused our attention on plaque-associated microglia. We observed that periplaque microglia in all genotypes had a similar degree of CD68 expression (Figure 2.7, H and I). This finding suggests that microglial phagocytic capacity in 5-month-old 5xFAD mice is not likely significantly altered by deletion of RIPK3 alone or in combination with Caspase-8.

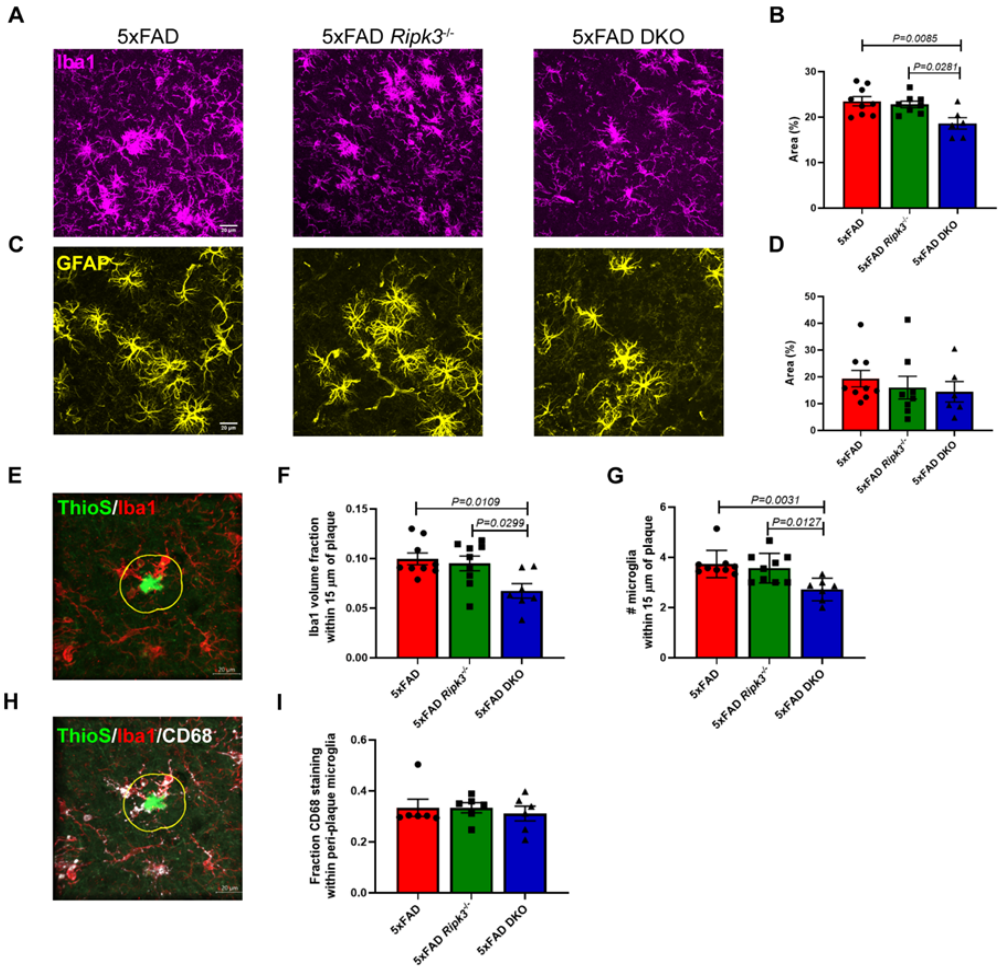

Figure 2.7. Reduced microgliosis with loss of Caspase-8 and RIPK3 in 5xFAD mice. (A and C) Representative IHC images of the cortex taken at ×40 original magnification (n = 9 5xFAD mice, n = 8 5xFAD *Ripk3*$^{-/-}$ mice, and n = 6 5xFAD-DKO mice). (A) Iba1 staining. (B) Quantification of Iba1 staining. Each data point is an average of 10 different fields of view taken throughout the cortex spanning 2 different sections per mouse. (C) GFAP staining. (D) Quantification of GFAP staining. Each data point is an average of 10 different fields of view taken throughout the cortex spanning 2 different sections per mouse. (E) Image of cortical Iba1^{+} microglia (red) surrounding ThioS^{+} plaque (green) within a 15 µm barrier (yellow) measured from plaque surface taken at ×40 original magnification. (F) Volume of Iba1 staining within the 15 µm barrier was quantified and divided by total barrier volume. (G) Number of microglia as identified by Spots function on Imaris 9.7.2 were counted within the barrier. (F and G) Results from 6–10 plaques were averaged per data point (n = 9 5xFAD mice, n = 9 5xFAD Ripk3$^{-/-}$ mice, and n = 7 5xFAD-DKO mice). (H) Image of microglia (red) costained with CD68 (white) surrounding ThioS^{+} plaque (green) within a 15 µm barrier (yellow) measured from plaque surface taken at ×40 original magnification. (I) Quantification of cortical microglial CD68 staining within a 15 µm periplaque barrier. Results from 6–10 plaques were averaged per data point. Data were analyzed by 1-way ANOVA followed by Tukey's post hoc test. All n values refer to the number of mice used, and error bars indicate SEM. Scale bars: 20 µm.

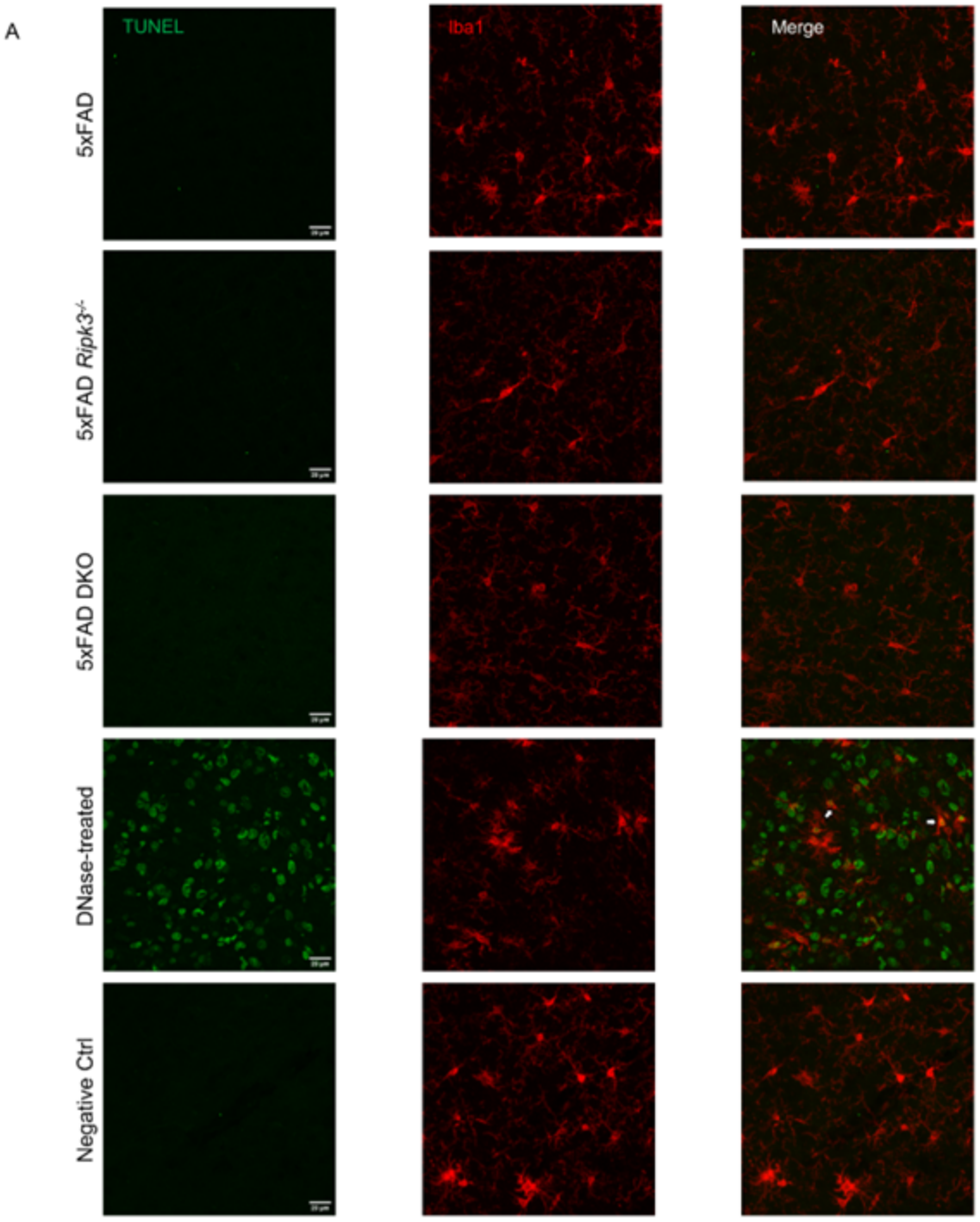

Figure 2.8. Absence of TUNEL$^+$ microglia in 5xFAD mice. (A) Representative cortical sections from 5xFAD, 5xFAD *Ripk3*$^{-/-}$, and 5xFAD DKO mice. DNase-treated and negative control cortical sections also included. White arrowheads indicate examples of TUNEL$^+$ microglia in DNase-treated cortical sections.

2.3.4 Reduction of microglial activation with loss of Caspase-8 and RIPK3 in 5xFAD mice.

To evaluate if combined loss of Caspase-8 and RIPK3 influences microglial morphology, we next performed Sholl analysis. We did not observe any differences in overall microglial branch complexity in the cortex across the genotypes (Figure 2.9, A–D). We did, however, find that the combined loss of Caspase-8 and RIPK3 in 5xFAD mice led to a decrease in the ratio of soma to branch volume (Figure 2.9D). As AD progresses, microglia undergo a shift in their transcriptome, which is often referred to as a disease-associated microglial (DAM) signature (93, 111). One of the genes that shows a marked upregulation in the DAM population is the pattern recognition receptor Clec7A, which is largely absent in homeostatic microglia. We stained for Clec7A and observed that 5xFAD DKO microglia exhibit significantly reduced Clec7A staining (Figure 2.9, E–H). Overall, these data suggest that combined loss of Caspase-8 and RIPK3 leads to an overall decrease in microgliosis in response to Aβ amyloidosis.

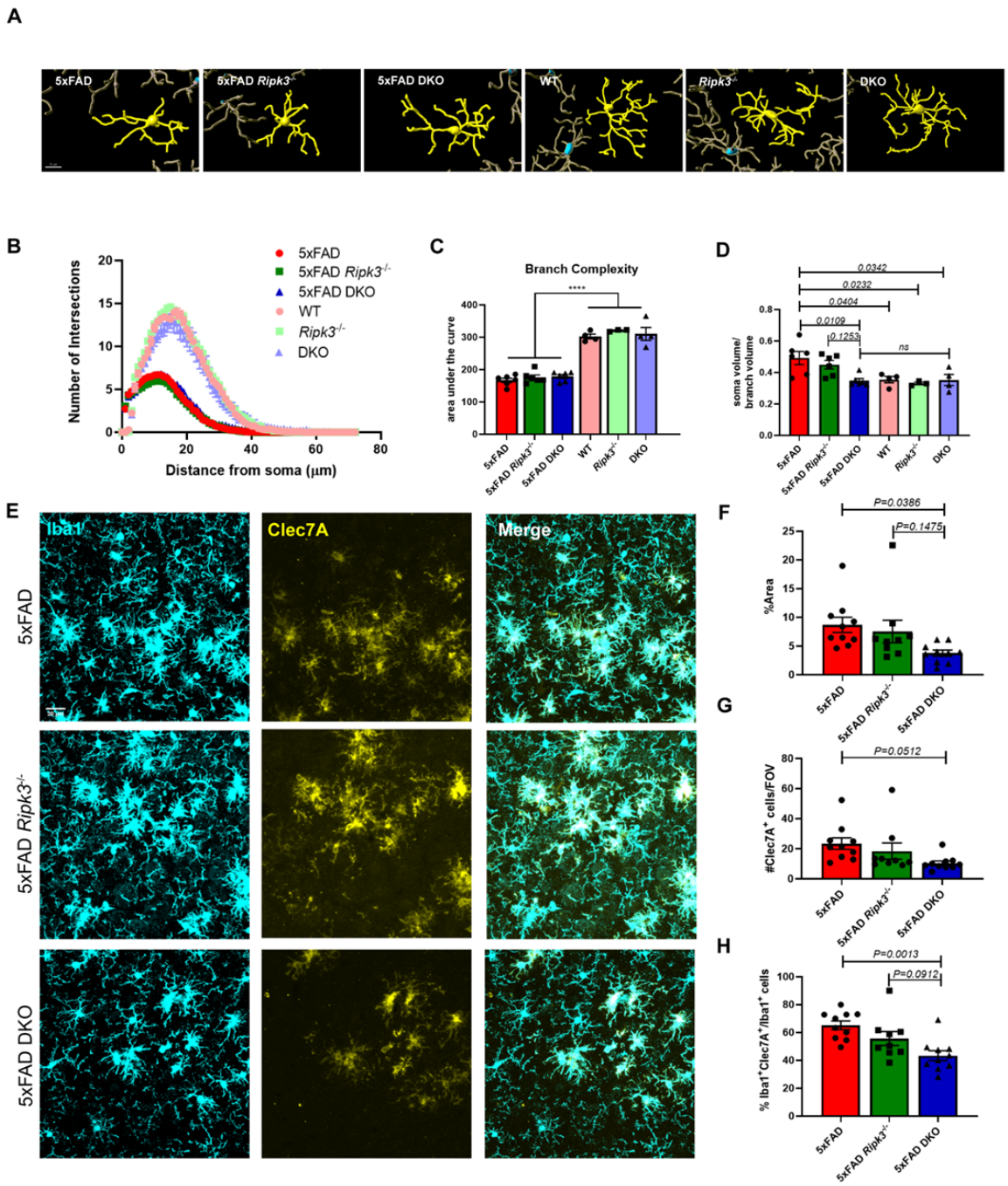

Figure 2.9. Reduction of microglial activation with loss of Caspase-8 and RIPK3 in 5xFAD mice. (A) Representative reconstructions of Iba1$^+$ cells. Scale bar: 10 μm. (B) Sholl analysis for non plaque–associated microglia. Each data point represents the number of Iba1$^+$ branches intersecting with a radius of 0–80 μm from the soma, calculated by the average of 70–80 microglia per group (*n* = 6 mice/group). (C) Quantification of the area under the curve for the microglial Sholl analysis data. Each data point represents a single mouse. ****$P <$ 0.0001. (D) Ratio of the microglia soma volume (measured using Surfaces feature in Imaris 9.7.2) to the branch volume. (A–D) (*n* = 6 5xFAD mice, *n* = 6 5xFAD *Ripk3*$^{-/-}$ mice, *n* = 6 5xFAD-DKO mice, *n* = 4 WT mice, *n* = 3 *Ripk3*$^{-/-}$ mice, *n* = 4 DKO mice). (E) Representative IHC images of cortex taken at ×40 original magnification stained for Iba1 (cyan) and Clec7A (yellow) (*n* = 10 5xFAD mice, *n* = 9 5xFAD *Ripk3*$^{-/-}$ mice, and *n* = 10 5xFAD-DKO mice). (F) Quantification of percent area coverage of Clec7A staining. (G) Quantification of the number of

Clec7A$^+$ cells per field of view (FOV). (H) Percentage of Iba1$^+$Clec7A$^+$ double-positive cells per FOV. Data were analyzed by 1-way ANOVA followed by Tukey's post hoc test. All *n* values refer to the number of mice used, and error bars indicate SEM.

2.3.5 Loss of Caspase-8 and/or RIPK3 does not affect attrition of cortical layer V neurons in 5xFAD mice.

Cell death is a key driver of neurodegenerative disease. Therefore, it is possible that changes in the amount of cell death upon elimination of Caspase-8 and/or RIPK3 could account for some of the phenotypes we observed. Various groups have demonstrated that 5xFAD mice display age-dependent neuronal loss, especially in cortical layer V (219, 220). To evaluate neuronal loss, we counted NeuN$^+$ cells in layer V of the cortex. Layer V neurons were identified using the layer V/VI marker chicken ovalbumin upstream promoter transcription factor interacting protein 2 (Ctip2) (Figure 2.11A). Significant reductions in NeuN cell density were observed in 5xFAD mice relative to nontransgenic WT controls. However, we did not observe significant differences in neuronal counts across 5-month-old 5xFAD, 5xFAD *Ripk3*$^{-/-}$, and 5xFAD DKO mice. Corresponding non-5xFAD control mice also showed no differences in NeuN density (Figure 2.10). Quantification of Ctip2 density revealed a similar pattern to the analysis from NeuN staining (Figure 2.11, A and B). These data suggest that deletion of RIPK3 alone or combination with Caspase-8 does not appreciably affect neuronal cell death in cortical layer V.

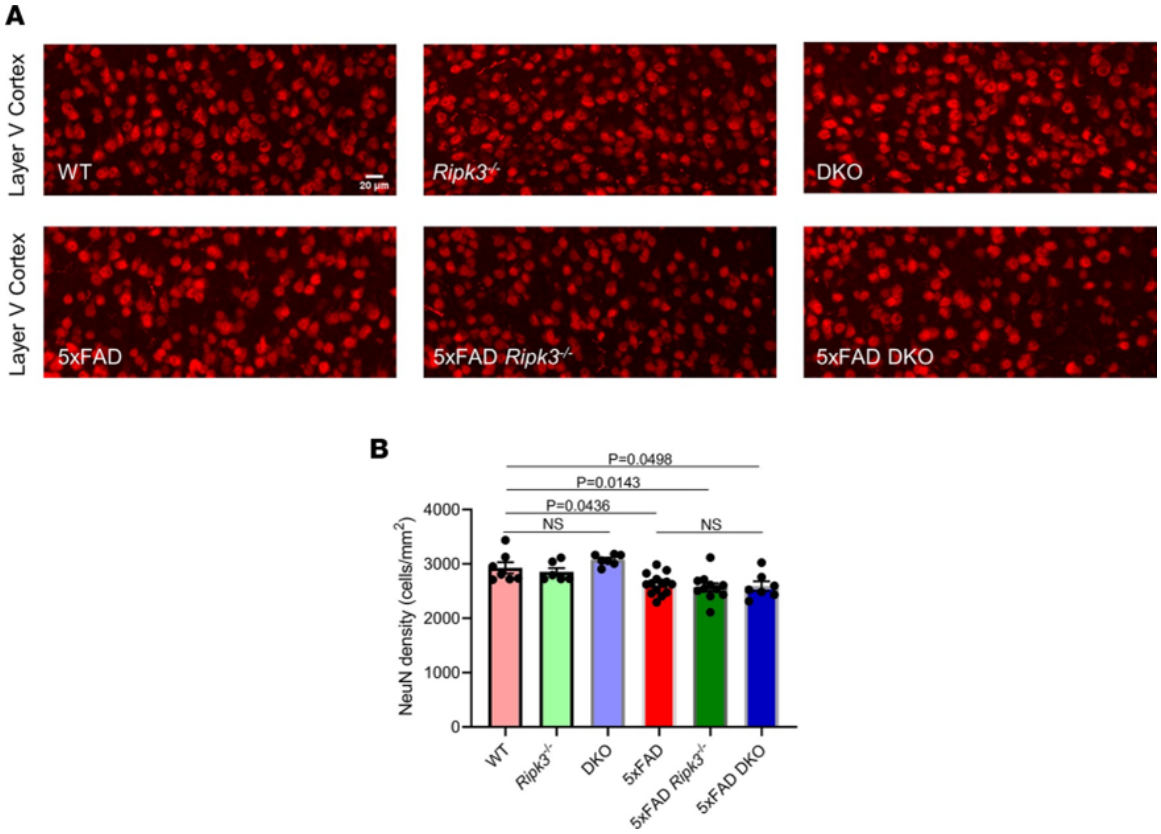

Figure 2.10. Loss of Caspase-8 and/or RIPK3 does not alter cortical layer V neuron density in 5xFAD mice. (A) Representative IHC images of cortical layer V stained for NeuN taken at ×20 original magnification (n = 7 WT mice, n = 6 Ripk3$^{-/-}$ mice, n = 7 DKO mice, n = 14 5xFAD mice, n = 11 5xFAD Ripk3$^{-/-}$ mice, and n = 7 5xFAD-DKO mice). (B) Quantification of NeuN staining. Data were analyzed by 1-way ANOVA followed by Tukey's post hoc test. Data expressed as mean ± SEM.

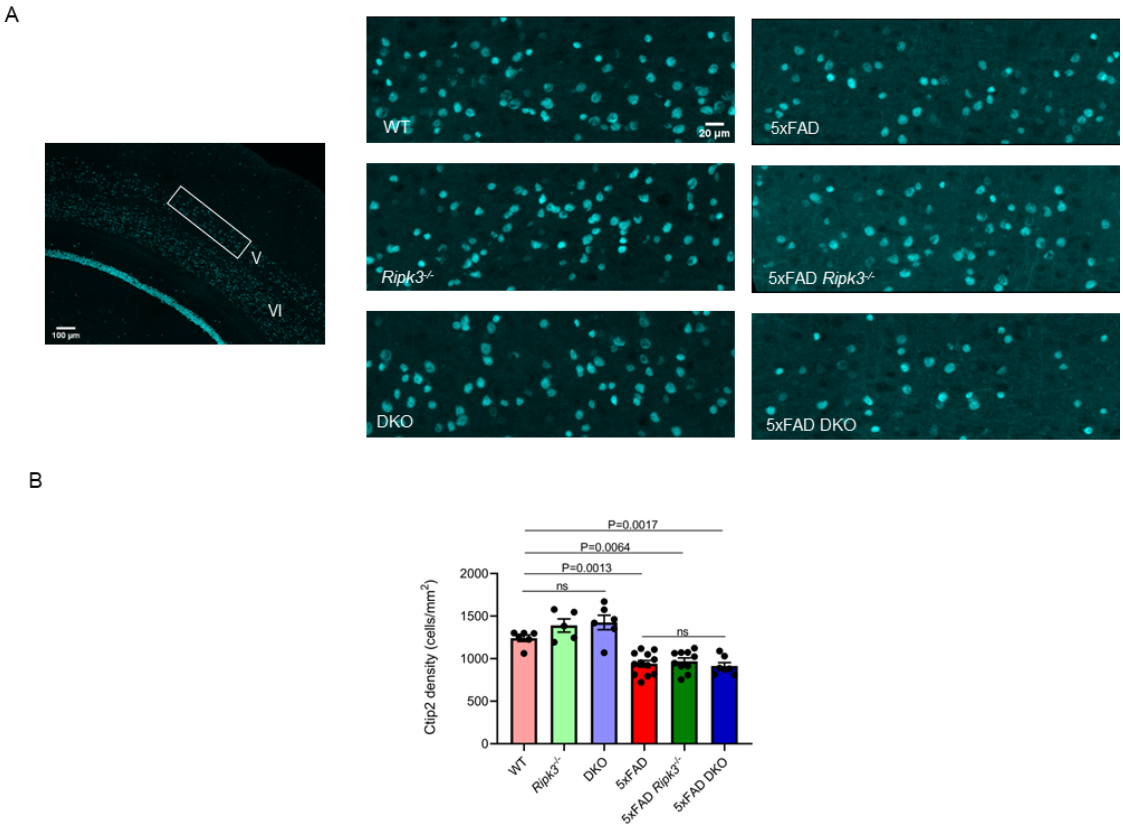

Figure 2.11. Layer V identification via Ctip2. (A) Coronal sections were stained to mark cortical layers V and VI with white rectangle marking region of NeuN quantification (left). Representative IHC images of cortical layer V stained with Ctip2 taken at 20x magnification (right) (n=6 for WT, n=5 for *Ripk3*$^{-/-}$, n=6 for DKO, n=12 for 5xFAD, n=10 for 5xFAD *Ripk3*$^{-/-}$, and n=7 for 5xFAD DKO). (B) Quantification of Ctip2 staining. Data were analyzed by one-way ANOVA followed by Tukey post hoc test. Data expressed as mean ± s.e.m.

2.3.6 The Caspase-8/RIPK3 axis regulates NLRP3 inflammasome priming and activation in response to Aβ.

If not by cell death, how does Caspase-8 affect AD progression? We speculated that Caspase-8 may regulate inflammatory cytokine production in response to Aβ. Indeed, authors of recent reports in other models of disease have identified Caspase-8 as a key regulator of the NLRP3 inflammasome, where Caspase-8 has been shown to influence both the priming and activation steps of inflammasome signaling (212, 213, 221). Our results suggest a role for

Caspase-8 in regulating AD-associated gliosis; however, the question remains whether this is through inflammasome activation or an alternative mechanism.

We first sought to probe this question in an in vitro setting. To investigate AD-associated inflammasome signaling and IL-1β production, we generated mixed astrocyte–microglia cultures from P0 to P2 and challenged them with synthetic Aβ oligomer preparations (Figure 2.12A). Consistent with findings of prior studies, we observed that Aβ can activate the NLRP3 inflammasome, resulting in IL-1β release (Figure 2.12, B and C) (154, 185, 222). Inhibiting either NLRP3 (MCC950) or caspase-1 (Ac-YVAD-cmk) led to a reduction in the secretion of IL-1β by mixed glial cultures that were stimulated with Aβ oligomers (Figure 2.12C). IL-1β release was also significantly dampened in DKO mixed glial cultures that were treated with Aβ oligomers (Figure 2.12B). Similarly, pretreatment with a Caspase-8 enzymatic inhibitor (zIETD-fmk) resulted in significant reductions to IL-1β release in response to Aβ oligomers (Figure 2.12C). To facilitate IL-1β release, cultures were pretreated with LPS for 3 hours (Figure 2.12A). Previous work has implicated Caspase-8 as important in the transcriptional upregulation of inflammasome components (212). After LPS priming, we observed significant increases in *Nlrp3*, *Il1b*, and *Casp1* transcripts in both WT and *Ripk3*$^{-/-}$ mixed glial cultures. DKO cultures, however, showed a marked blunting. Levels of *Pycard* (a gene encoding for ASC) did not show increases after LPS priming, but we did observe that primed DKO cultures exhibited a downregulation of *Pycard* expression after LPS stimulation (Figure 2.12, D–G).

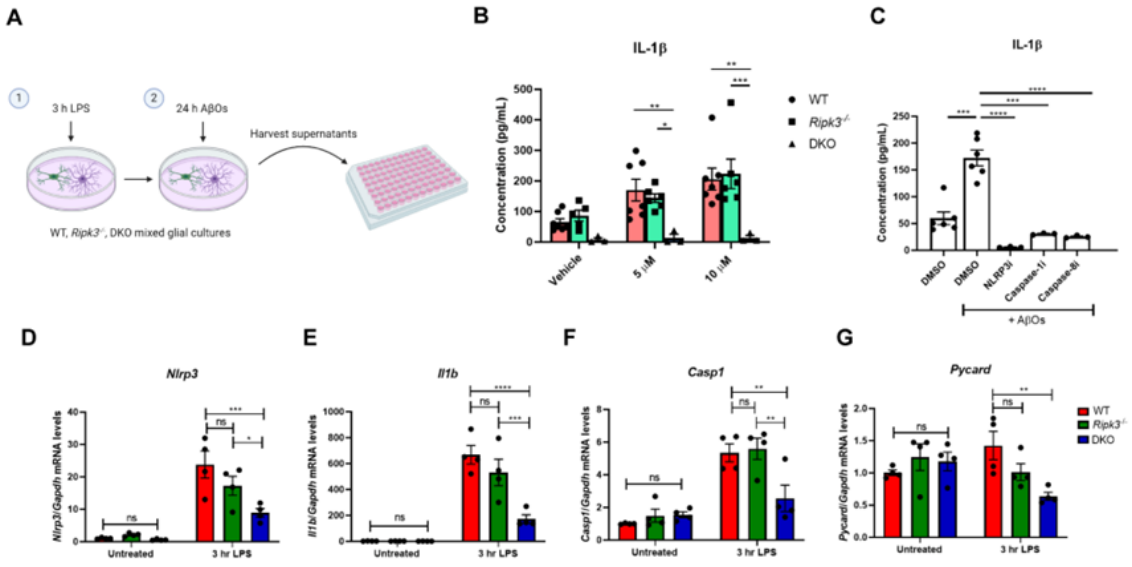

Figure 2.12. Caspase-8 promotes Aβ-induced IL-1β release from mixed astrocyte–microglia cultures. (A) Schematic for treatment paradigm. Mixed astrocyte–microglia cultures were primed for 3 hours with 500 ng/mL LPS, then treated for 24 hours with oAβs. Supernatants were then harvested and evaluated for IL-1β release. (B) Supernatants were collected from WT, *Ripk3*$^{-/-}$, and DKO mixed glial cultures after 24 hours of treatment with either vehicle, 5 μM, or 10 μM oAβs, and evaluated for IL-1β release via ELISA. 5 μM: WT versus DKO $^{**}P = 0.0087$, and *Ripk3*$^{-/-}$ versus DKO $^{*}P = 0.0381$; 10 μM: WT versus DKO $^{**}P = 0.0012$, and *Ripk3*$^{-/-}$ versus DKO $^{***}P = 0.006$. (C) WT mixed glial cultures were treated with oAβs either in the presence of an NLRP3 inhibitor (NLRP3i) (MCC950, used at 1 μM), a caspase-1 inhibitor (caspase-1i) (Ac-YVAD-cmk, used at 10 μM), or a Caspase-8 inhibitor (Caspase-8i) (zIETD-fmk, used at 10 μM). DMSO versus DMSO (+ oAβs), $^{***}P < 0.001$; DMSO (+ oAβs) versus NLRP3i, $^{****}P < 0.0001$; DMSO (+ oAβs) versus caspase-1i, $^{***}P < 0.001$; DMSO (+ oAβs) versus Caspase-8i, $^{****}P < 0.0001$. (D–G) Mixed-culture gene transcript levels for *Nlrp3*, *Il1b*, *Casp1*, and *Pycard* before and after 3-hour LPS priming ($n = 4$ WT mice, $n = 4$ *Ripk3*$^{-/-}$ mice, and $n = 4$ DKO mice). $^{*}P < 0.05$, $^{**}P < 0.01$, $^{***}P < 0.001$, $^{****}P < 0.0001$. (B) Data were analyzed by 2-way ANOVA followed by Tukey's post hoc test. (C–G) Data were analyzed by 1-way ANOVA followed by Tukey's post hoc test. Data are from at least 3 independent experiments and expressed as mean ± SEM.

The above in vitro studies pointed to a potential role for Caspase-8 in regulating NLRP3 inflammasome priming after Aβ challenge. To validate our findings in vivo, we assessed transcript levels for *Nlrp3*, *Il1b*, *Casp1*, and *Pycard* in hippocampal lysates. We observed that Aβ deposition in 5xFAD mice led to elevated levels of *Nlrp3* and *Il1b*, in comparison with levels in WT controls (Figure 2.13, A and B). Moreover, we found that combined deletion of Caspase-8

and RIPK3, but not RIPK3 alone, in 5xFAD mice reduced *Nlrp3* and *Il1b* transcript expression to WT levels (Figure 2.13, A and B). In contrast, no changes in *Nlrp3* and *Il1b* expression were detected with targeted deletion of the Caspase-8/RIPK3 axis in non-5xFAD mice (Figure 2.13, A and B). We also did not observe any changes to the *Casp1* transcript (Figure 2.13C). Interestingly, *Pycard* expression was upregulated in 5xFAD transgenic mice, but loss of Caspase-8 and/or RIPK3 did not alter its levels (Figure 2.13D). Overall, these results point to a role for Caspase-8 in regulating transcription of inflammasome components in the 5xFAD model.

During inflammasome assembly, ASC forms fibril-like structures that can be released into the extracellular space. It is thought that ASC speck release is important for sustaining an ongoing immune response (223, 224). More recently, it has been demonstrated that extracellular ASC specks can promote both the seeding and spread of Aβ in a prion-like fashion (186, 225). We were interested in examining ASC speck numbers across our genotypes. Upon staining for ASC, we observed ASC fibrils near plaques and rarely in non–plaque-containing regions. Interestingly, we found that loss of RIPK3 or combined loss of Caspase-8 and RIPK3 in 5xFAD mice both led to a significant reduction in the number of ASC specks surrounding plaques (Figure 2.13, E and F).

To further characterize the role of the Caspase-8/RIPK3 axis in regulating IL-1β secretion, we leveraged a previously described assay to measure IL-1β release from isolated brain cells ex vivo (226). Single-cell suspensions derived from cortical homogenates from WT,

5xFAD, 5xFAD *Ripk3*$^{-/-}$, and 5xFAD DKO mice were plated for 48 hours, and supernatants were collected for IL-1β ELISAs. We found that suspensions generated from 5xFAD and 5xFAD *Ripk3*$^{-/-}$ cortices released appreciable amounts of IL-1β. Consistent with our data in Figure 5B, combined loss of Caspase-8 and RIPK3 led to a significant inhibition of IL-1β release (Figure 2.13G). Taken together, these data suggest that Caspase-8 plays a central role in NLRP3 inflammasome signaling.

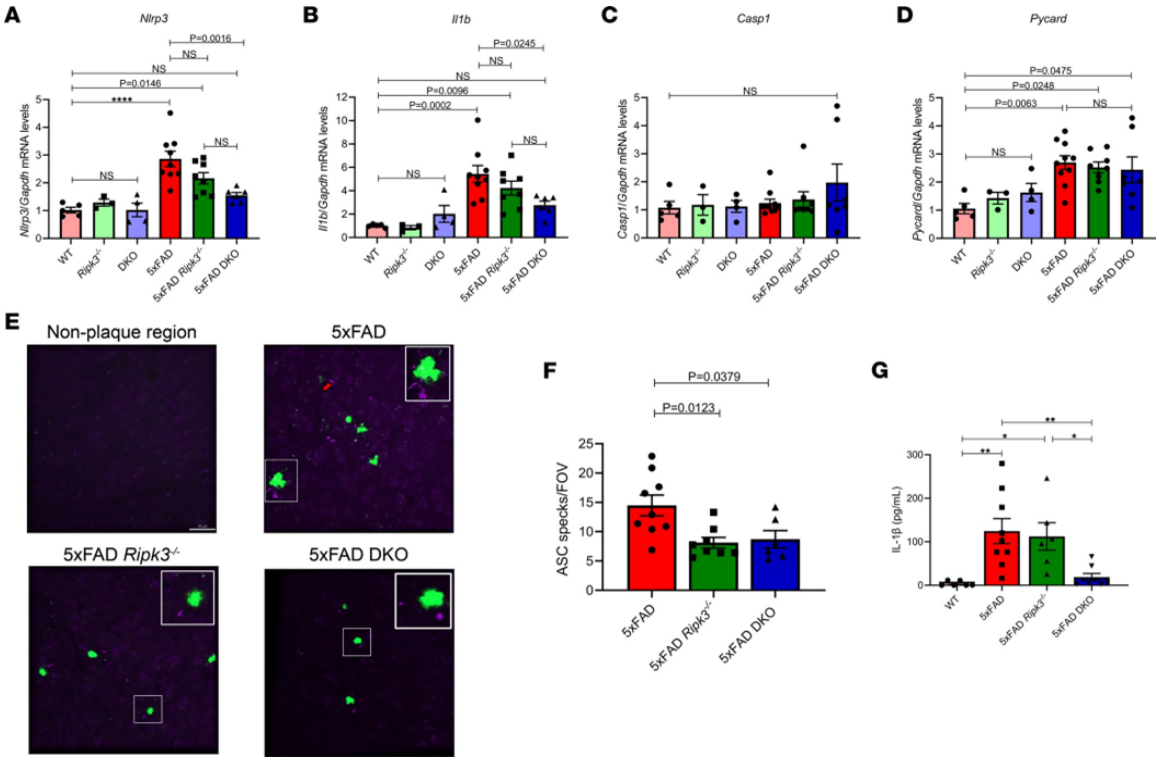

Figure 2.13. The Caspase-8/RIPK3 axis regulates inflammasome signaling in 5xFAD mice. (A–D) *Nlrp3* gene transcript levels (A), *Il1b* gene transcript levels (B), *Casp1* gene transcript levels (C), and *Pycard* gene transcript levels (D) from the hippocampi of 5-month-old mice (n = 5 WT mice, n = 3 *Ripk3*$^{-/-}$ mice, n = 4 DKO mice, n = 9 5xFAD mice, n = 8 5xFAD *Ripk3*$^{-/-}$ mice, and n = 6 5xFAD-DKO mice). ****P < 0.0001. (E) Representative IHC images of the cortex of 5-month-old mice, stained for ThioS (green) and ASC (purple), taken at ×40 original magnification (scale bar: 30 μm; n = 9 5xFAD mice, n = 8 5xFAD *Ripk3*$^{-/-}$ mice, and n = 6 5xFAD-DKO mice). Red arrow denotes ASC speck. (F) Quantification of the number of ASC specks per field of view (FOV) from E. (G) Supernatants were collected from ex vivo brain suspensions from 5-month-old mice after a 48-hour incubation and evaluated for IL-1β release via ELISA: WT versus 5xFAD, **P = 0.0050; WT versus 5xFAD *Ripk3*$^{-/-}$, *P = 0.0247; 5xFAD versus 5xFAD DKO, **P = 0.0077; 5xFAD *Ripk3*$^{-/-}$ versus 5xFAD DKO, *P = 0.0418 (n = 6 WT mice, n = 9 5xFAD mice, n = 6 5xFAD *Ripk3*$^{-/-}$ mice, and n = 8 5xFAD-DKO mice). Data were analyzed by 1-way ANOVA followed by Tukey's post hoc test. Data are expressed as mean ± SEM.

2.4 Discussion

Cell death and inflammatory pathways play central roles in the pathogenesis and spread of AD. Protein aggregates such as Aβ and tau can act as damage-associated molecular patterns, giving rise to an immune response (197). Although acute inflammation is beneficial and can aid in Aβ phagocytosis, the chronic nature of the AD immune response is thought to incite further Aβ deposition, generating a pathological positive feedback loop. Identification of the molecular players responsible for driving AD-associated neuroinflammatory responses versus those that facilitate beneficial clearance of neurotoxic material, therefore, is vital.

Here, we show that combined deletion of Caspase-8 and RIPK3 limited AD pathology. In contrast, we found that RIPK3 deletion alone did not appear to have an appreciable effect on pathology in the 5xFAD model, suggesting that many of the phenotypes observed in our 5xFAD DKO mice are likely driven by Caspase-8. Overall, these data suggest that the Caspase-8/RIPK3 axis, and Caspase-8 in particular, is critically involved in AD-related disease progression as measured by amyloid deposition and microgliosis in the 5xFAD model. Deposition in the 5xFAD model begins in the subiculum before spreading throughout the hippocampus and overlying cortex. Interestingly, we found that D54D2 deposition was unchanged in the subiculum at both 3 and 5 months, whereas ThioS^{+} plaques were significantly reduced in 5xFAD DKO mice (Figure 2.4). On the basis of this finding, it is tempting to speculate that Caspase-8 may be more important for disease spread as opposed to initiation. In our analysis of D54D2^{+} Aβ plaques, we observed that 5xFAD DKO mice had significantly fewer Aβ deposits that were small (0–10 μm^2) in comparison with those of 5xFAD or 5xFAD *Ripk3*$^{-/-}$ mice (Figure 2.2G). Amyloid deposits become larger over time, with smaller plaques serving as seeds for larger deposits (227, 228). Therefore, our observations in 5xFAD DKO mice point toward a potential role for Caspase-8 in promoting plaque seeding and overall Aβ spread.

Caspase-8 is critical in mediating cell death and inflammatory responses in macrophage populations (212, 213, 229). Here, we demonstrate that combined deletion of Caspase-8 and RIPK3 led to a significant dampening of the microglial response in the 5xFAD model. Both overall cortical microglial coverage and the microglial plaque response were reduced in 5xFAD DKO mice. Given that 5xFAD DKO mice also exhibited diminished plaque burden, it would appear that the reduced microglial activation/plaque interaction may be beneficial in this setting in contrast to other cases, such as with TREM2 loss, which leads to increased plaque load and worsening of cognitive function (101, 218). We suspect that Caspase-8 plays a key role in regulating microglial responses to Aβ. Indeed, our morphological analysis revealed that 5xFAD DKO mice have soma-to-branch volume ratios that are similar to those of their nontransgenic counterparts. This reduction in microglial activation likely contributes to the reductions in Aβ aggregates that we observed in our 5xFAD DKO mice. Although it is likely that the smaller number of Aβ aggregates contributes to the diminished microglial reactivity in 5xFAD DKO mice, we believe that changes in overall amyloid burden are probably driven by intrinsic changes in microglial function. This reasoning is supported by our findings that loss of Caspase-8 and RIPK3 led to reductions in the number of microglia surrounding individual plaques, our morphological analysis showing diminished activation in 5xFAD DKO microglia, and work from Spangenberg et al. in which they demonstrated that depletion of microglia in the 5xFAD model leads to marked reductions in parenchymal plaque deposition (103). Overall, our work positions Caspase-8 as a key regulator of amyloidosis and Aβ-mediated microgliosis.

We observed that loss of RIPK3 did not significantly alter amyloid deposition and gliosis in 5xFAD mice, which, despite components of the necroptotic signaling pathway being reportedly activated in AD (149-151), argues for RIPK3 not appearing to appreciably affect Aβ amyloidosis in 5xFAD mice. However, in many of our studies, we were only able to detect significant changes when comparing 5xFAD mice with their 5xFAD-DKO counterparts and not between 5xFAD *Ripk3*$^{-/-}$ and 5xFAD-DKO mice. This finding may point to a partial protective

effect of RIPK3 deletion in the 5xFAD model. A number of groups have demonstrated a role for RIPK3 in ERK- and NF-κB–mediated cytokine production that occurs either prior to or independent of cell death (152, 153). Although we largely observed significant protection against amyloid deposition and microgliosis with combined deletion of both Caspase-8 and RIPK3, it is still possible that RIPK3 affects other aspects of disease pathogenesis that were not specifically explored in our studies.

Moreover, it should be noted that the possibility still exists that RIPK3 and necroptosis could still play more significant roles during the later stages of AD, as other groups have suggested (149). Many previous studies relied on the targeting of RIPK1, which is best known as an upstream regulator of RIPK3 but can also initiate noncanonical inflammatory pathways and other forms of cell death that are independent of RIPK3 and necroptosis (157, 214, 230-232). In these previously published studies, it was shown that inhibiting RIPK1 limits neurodegenerative disease (157, 231, 232). Coupling these published RIPK1 findings with those of our studies demonstrating that RIPK3 deletion does not significantly affect Aβ amyloidosis suggests that RIPK1 likely contributes to neurodegenerative disease through its regulation of noncanonical inflammatory cytokine production and not via induction of RIPK3-dependent events. Consistent with this idea, a recent study revealed a cell death–independent role for RIPK1 in the regulation of microglial responses in the APP/PS1 mouse model of AD (157). More specifically, the authors showed that RIPK1 coordinates the acquisition of the DAM phenotype in APP/PS1 mice.

Caspase-8 is an initiator caspase in the extrinsic apoptotic pathway. It is possible that alterations in cell death execution resulting from loss of Caspase-8 and/or RIPK3 could be contributing to the observed phenotypes. Consistent with previous reports, we also observed a reduction in cortical layer V neuron density when comparing 5xFAD and WT mice (220, 233). However, we observed no differences in $NeuN^+$ density between 5xFAD, 5xFAD *Ripk3*$^{-/-}$, and 5xFAD DKO mice. Taken together, these data suggest that Caspase-8 is required for AD

progression; however, to our surprise, it does not appear that Caspase-8 appreciably affects neuronal cell death in 5xFAD mice, despite playing a substantial role in promoting amyloidosis and microgliosis. This observation suggests that the cell loss that occurs in response to Aβ amyloidosis in 5xFAD mice is possibly mediated by Caspase-8–independent death pathways, such as intrinsic apoptosis, pyroptosis, and ferroptosis, as others have illustrated (195, 233, 234).

AD pathology spreads across the brain over the course of decades. Deposition of tau and Aβ follows a fairly stereotyped pattern of progression, with initial signs emerging in the transentorhinal cortex before proceeding to higher order cortical regions (235, 236). Oligomeric forms of Aβ, when harvested from patient samples, can act as seeds and promote pathology when injected into the hippocampus of presymptomatic mice (237). In a similar prion-like fashion, pathogenic tau harvested from patients can seed endogenous mouse tau and propagate spread (238). Several studies have demonstrated evidence for both transsynaptic and nonsynaptic modes of disease progression (238-241). For example, microglia can release extracellular vesicles containing tau aggregates, which contribute significantly to nonsynaptic spread of pathology (239). In addition, several studies have implicated members of both the TNFRSF and TLR family in driving neuronal loss, inflammation, and disease spread in AD. Interestingly, Caspase-8 serves as a common downstream signaling mediator for many of these TNFRSF and TLR receptors (207).

How precisely might Caspase-8 influence the spread of AD pathology? Protein aggregates such as Aβ and tau can activate the NLRP3 inflammasome (154, 184, 186), the components of which are predominantly expressed by astrocytes and microglia in the CNS (242, 243). We observed in 5xFAD mice elevated hippocampal transcript levels of both *Nlrp3* and *Il1b*, which were significantly dampened with co-deletion of Caspase-8 and RIPK3 but not RIPK3 alone. A by-product of inflammasome activation is the release of ASC to the extracellular

space. A number of studies have shown that ASC specks can seed Aβ and tau deposits (184, 186, 225). Thus, inhibition of ASC or upstream inflammasome components can dampen both amyloid and tau aggregation. Indeed, 5xFAD-DKO mice had significantly fewer ASC specks in plaque regions than did their 5xFAD counterparts. Interestingly, loss of RIPK3 also led to a significant reduction in ASC specks (Figure 2.13, E and F). Our findings that loss of RIPK3 was insufficient to significantly diminish amyloid load suggest that ASC specks may only be part of the equation. IL-1β has been documented as being a critical regulator of microglial proliferation and activation (244). Our ex vivo assay revealed that cortical single-cell suspensions from 5xFAD-DKO mice produced significantly less IL-1β than suspensions from 5xFAD and 5xFAD *Ripk3*$^{-/-}$ mice (Figure 2.13G). Previous reports have suggested that events downstream of NLRP3 inflammasome activation, such as IL-1β release and speck generation, are not necessarily coupled (245). It is possible Caspase-8's combined regulation of gliosis, NLRP3 inflammasome component expression, IL-1β release, and ASC speck generation are collectively required to delay amyloid spread in 5xFAD mice. Moreover, it is likely that Caspase-8 is governing other aspects of AD progression that we did not explore here. Several studies have demonstrated that Caspase-8 is a key regulator of inflammatory gene expression in large part through NF-κB signaling (207, 210). We examined phospho–NF-κB levels from hippocampal lysates but observed no differences across our transgenic mice. We also compared transcript levels of *Nfkb1* and *Nfkbia* from hippocampal lysates from WT and 5xFAD mice but again saw no differences (Figure 2.14). However, it is possible that there are subtle changes to NF-κB that are occurring in specific cell populations (e.g., microglia) that we did not capture in our bulk analysis. Therefore, it will be interesting to fully examine the scope of how Caspase-8 regulates the AD inflammatory profile by performing transcriptomics or proteomics on isolated microglia.

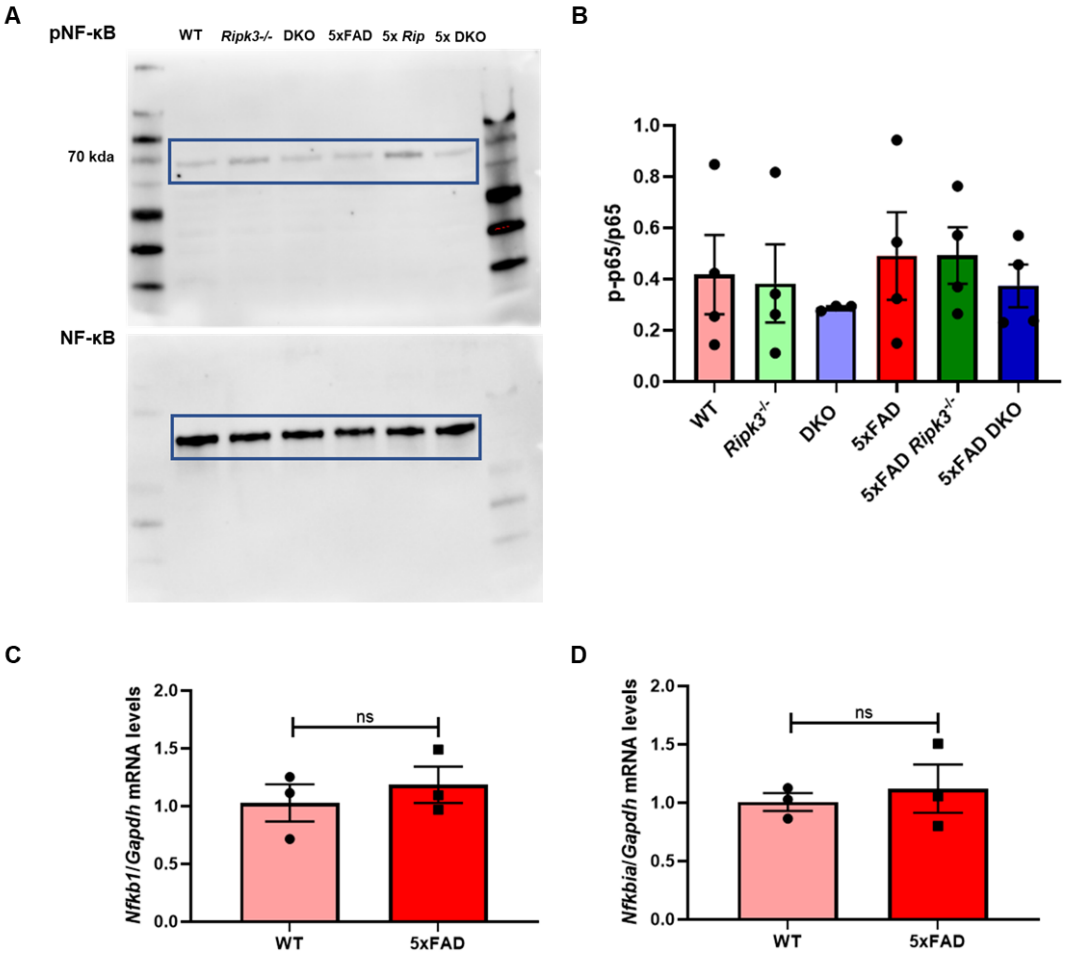

Figure 2.14. Loss of Caspase-8 and/or RIPK3 does not alter NFκB activation in 5xFAD mice. (A) Western blots of phospho–NF-κB (pNF-κB) and NF-κB from hippocampi of 5-month-old mice (*n* = 4 WT mice, *n* = 4 *Ripk3*$^{-/-}$ mice, *n* = 3 DKO mice, *n* = 4 5xFAD mice, *n* = 4 5xFAD *Ripk3*$^{-/-}$ mice, and *n* = 4 5xFAD-DKO mice) (B) Quantification of (A) with p-p65 signal normalized to p65. (C) *Nfkb1* gene transcript levels. (D) *Nfkbia* gene transcript levels from hippocampi of 5-month-old WT (n=3) and 5xFAD (n=3) mice.

In this study, we show that targeting Caspase-8 mediated inflammatory pathways may prove to be a viable strategy in AD treatment. Of course, there is still a great deal of work to be done. It is worth mentioning that the 5xFAD model is a particularly aggressive form of pathology. It is possible that the accelerated nature of the model may partially mask the effects that Caspase-8 would have in a more physiologic setting. Probing the role of Caspase-8 in other AD models and tauopathies would be very interesting in this regard. Caspase-8 can serve as either

a scaffolding protein, enzyme, or both during inflammatory signaling. While our *in vitro* studies demonstrate that Caspase-8 enzymatic function is important for promoting IL-1β release following Aβ challenge it is still unclear whether or not this is important *in vivo*. Future efforts that attempt to tease apart the scaffolding versus enzymatic function of Caspase-8 will be vital. In our studies we were able to characterize amyloidosis and microgliosis in 5xFAD mice aged to 3 and 5 months of age. In order to more thoroughly characterize how Caspase-8 and/or RIPK3 influence disease kinetics it would be valuable to evaluate mice at later time-points. Unfortunately, DKO mice develop a well-characterized lymphomegaly phenotype as they age due to the accumulation of peripheral immune cells in their lymphoid organs (204, 229). By about 6 months of age, the lymph nodes get so large around the neck that it makes it challenging for the DKO mice to breathe and eat. Below we present some images of WT and DKO 5-month-old male mice to highlight this observation. As a result of the lymphomegaly, we are asked to euthanize DKO mice at 6 months of age as a humane endpoint making analysis of later time-points difficult (Figure 2.15, A-D).

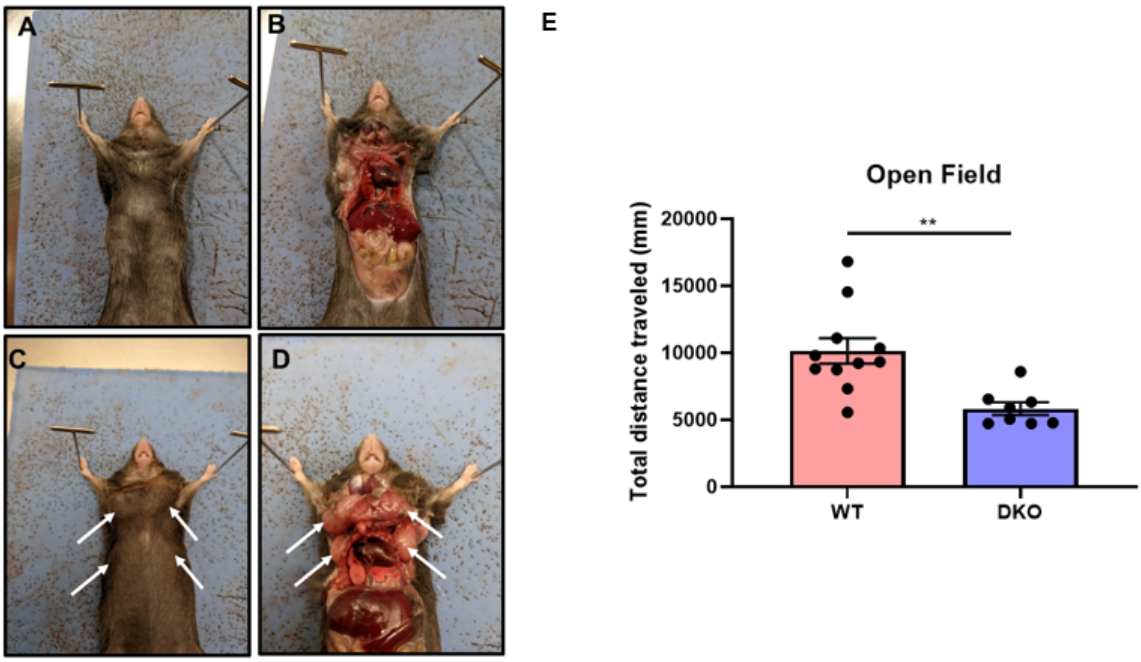

Figure 2.15. Development of lymphomegaly in DKO mice. (**A**-**B**) Picture of five month old male WT and (**C**-**D**) DKO mouse with white arrows to indicate enlarged lymph nodes. (**E**) Open field test reveals deficits in total distance traveled in DKO mice.

Other groups have demonstrated that 5xFAD mice develop learning and memory impairments with age. Performing behavioral tests would therefore be valuable in determining whether or not 5xFAD DKO mice exhibit functional improvement. But due to the aforementioned lymphomegaly, we have observed that DKO mice show reduced physical performance compared to WT littermate controls (Figure 2.15E). This presents a confound when attempting to evaluate results given that most behavioral tasks involve a physical element. On an additional note, it's tempting to speculate that the lymphadenopathy in DKO mice may have a modulatory effect on AD progression. DKO mice accumulate $CD3^{+}B220^{+}$ cells in lymphoid tissues which is reminiscent of autoimmune lymphoproliferative syndrome (ALPS) seen in humans (229). Patients with ALPs have dysregulated immune responses and elevated levels of serum IL-10 (246). Whether DKO mice also possess increased IL-10 in either peripheral or brain compartments remains to be seen. Based on our observations that 5xFAD DKO mice exhibit dampened microgliosis, we suspect that Caspase-8 activity in microglia is particularly important

for AD progression. Thus, to circumvent the confounds associated with DKO mice, we plan to generate 5xFAD mice in which Caspase-8 has been specifically deleted in microglia.

Overall, the work presented here provides insights into mechanisms governing AD progression. We demonstrate that the Caspase-8/RIPK3 axis is critical for promoting both Aβ deposition and gliosis in the 5xFAD mouse model of AD. Furthermore, we show that combined deletion of Caspase-8 and RIPK3 limits both the priming of the NLRP3 inflammasome and IL-1β secretion in response to Aβ. This work helps establish Caspase-8 as a novel mediator of AD spread and suggests that Caspase-8 may be a potential target to mitigate AD pathology.

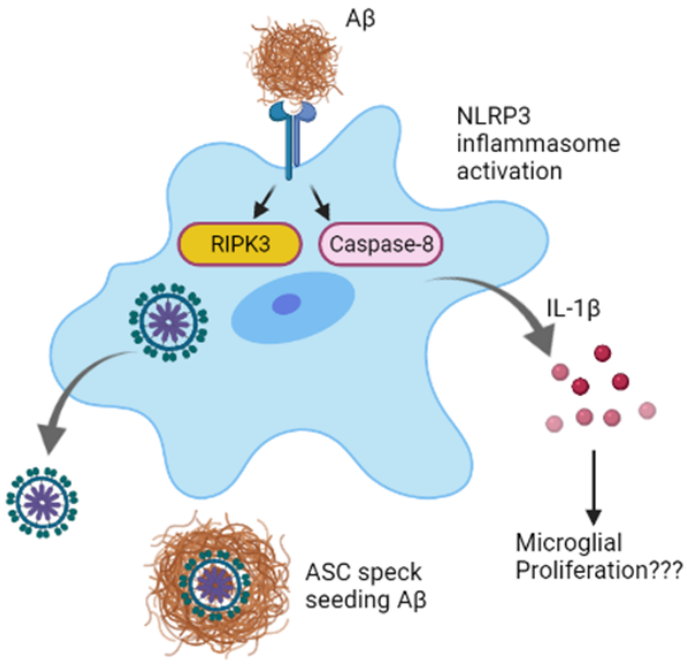

Figure 2.16. Summary of findings. Schematic depicting how Caspase-8 and RIPK3 may contribute to AD progression. Aβ internalization by a putative receptor triggers the engagement of Caspase-8 and RIPK3. Caspase-8 regulates IL-1β release which can promote microglial proliferation while RIPK3 drives ASC speck production.

Acknowledgements

The authors thank members of the Deppmann lab for helpful discussions and Pam Neff for technical assistance. We also thank George Bloom and his lab for their technical assistance in making Aβ oligomers. We thank Ammasi Periasamy and acknowledge the Keck Center for Cellular Imaging for the usage of the Zeiss 880/980 multiphoton Airy scan microscopy system (PI- AP; NIH-OD025156).

Funding

This work was supported by NIH-NINDS grant R01NS091617 (awarded to C.D.D.), NIH-NINDS grant R01NS106383 (awarded to J.R.L.), NIH-NIA grant 1RF1AG071996-01 (awarded to J.R.L.), the Alzheimer's Association grant AARG-18-566113 (awarded to J.R.L.), the Owens Family Foundation (awarded to C.D.D. and J.R.L.), the UVA Brain Institute's Presidential Neuroscience Graduate Fellowship (awarded to S.K., C.D.D., and J.R.L), and the Commonwealth of Virginia's Alzheimer's and Related Diseases Research Award Fund (awarded to C.D.D. and J.R.L.).

Author Contributions

S.K., C.D.D., and J.R.L. designed all experiments. S.K. conducted all experiments with assistance from S.B., C.O., and A.D.K., for mouse genotyping, tissue harvesting, preparation of glial cultures, and image analysis. O.Y.C carried out the RNAscope staining. S.K acquired and interpreted all data. S.K., C.D.D., and J.R.L. prepared figures and wrote the manuscript with input from all the authors.

Chapter 3. Single-cell mass cytometry analysis of microglial inflammation

3.1 Introduction

The advent of single-cell analysis techniques has significantly improved our understanding of the cellular changes that occur in both development and disease. During AD, microglia undergo a pronounced morphological shift.

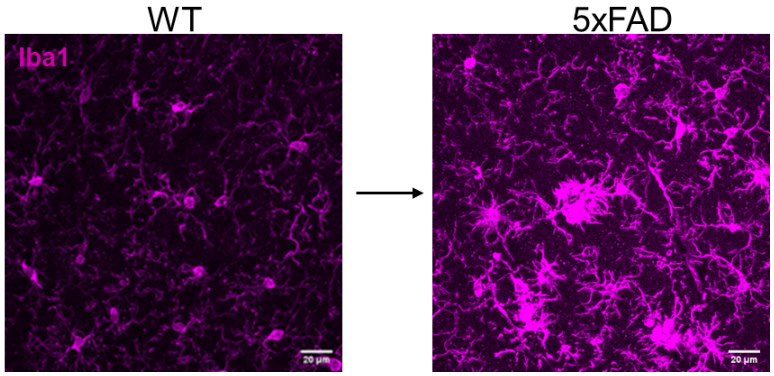

Figure 3.1. Microglia in WT and AD settings. Image of cortical microglia from 5-month-old WT and 5xFAD mice. Scale bar: 20 µm.

It's amazing that the same cell type can look so different depending on context. These changes immediately grabbed my attention while I was initially characterizing my 5xFAD mice (Figure 3.1). Behind these obvious morphological differences are more hidden effects at the gene expression and protein level. In the case of AD, many of the transcriptional changes that occur in microglia have been described (93, 111). But, not nearly as much is known at the protein level. What are the signaling programs responsible for driving a microglia from a homeostatic to an inflamed state? How do different signaling pathways coordinate to form a signaling network? How does network output ultimately influence microglial function? Largely due to technical limitations, these questions have been challenging to address in a high-throughput, comprehensive manner. However, the development of single cell mass cytometry has made it possible to unravel some of these mysteries.

3.1.1 Single cell mass cytometry

While transcriptomics has yielded innumerable biological insights, it only provides a partial picture. Our group, as well as others, have recognized that RNA and protein oftentimes show poor correspondence (247, 248). A thorough functional characterization of a cell or cell type requires some form of proteomics analysis. Mass cytometry, also known as CyTOF (Cytometry by Time-Of-Flight), is a flow cytometry variant which utilizes antibodies conjugated to isotopically pure rare earth metals to quantify proteins of interest at the single cell level (247). Current reagents allow for the simultaneous measure of 40-45 markers. For CyTOF, single cell suspensions are fixed, stained with a metal-label antibody cocktail, nebulized into droplets, ionized in an argon flame, then passed to a time of flight mass spectrometry which reads out the metal labels. If multiple samples are to be analyzed together they can be barcoded with unique combinations of palladium isotopes then pooled to minimize staining variability (Figure 3.2).

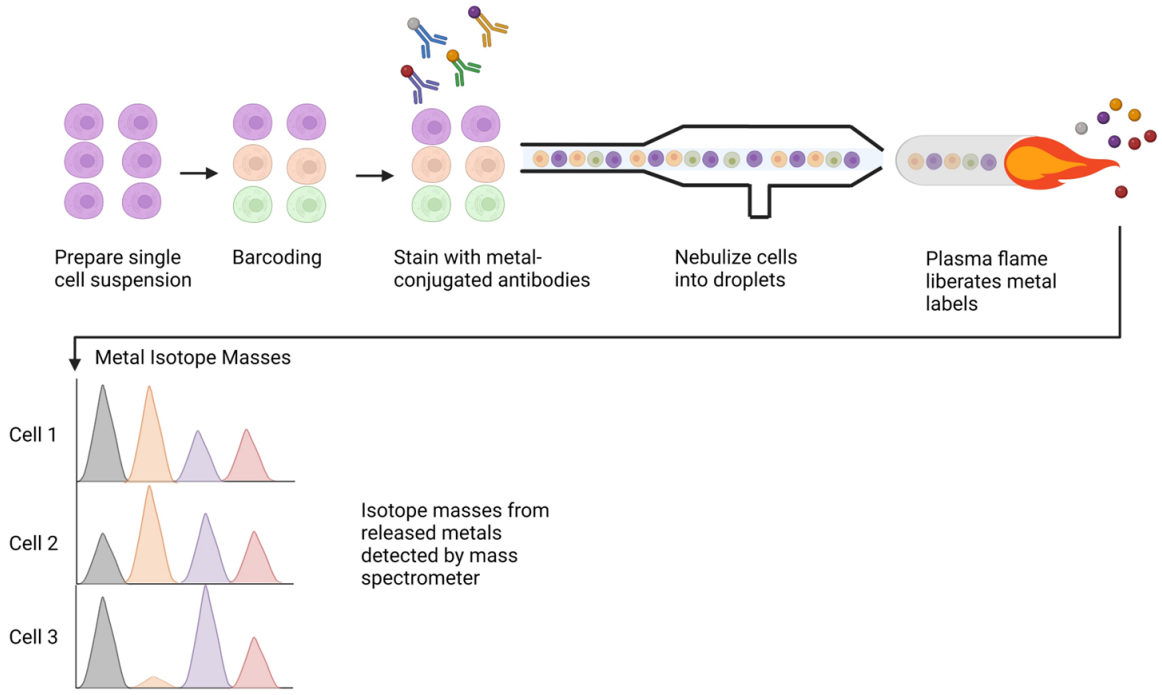

Figure 3.2. Mass cytometry workflow. Schematic for mass cytometry workflow. Briefly, single cell suspensions are fixed to preserve cell state. Multiple samples can be barcoded with unique metal combinations then combined. Samples are then stained with metal-label antibodies targeting proteins of interest. If intracellular markers are to be analyzed cells can be permeabilized following extracellular staining. Prior to introduction to the mass cytometer, cells

are passed through a nebulizer to generate single-cell droplets. Cells are then incinerated via an inductively coupled argon plasma (ICP) flame and the liberated metal labels are read-out using time-of-flight mass spectrometry.

3.1.2 Utilizing mass cytometry to study AD

Previous groups have made attempts to better understand the dynamics of AD using single cell mass cytometry. The bulk of this analysis thus far has focused on changes to myeloid cells. Similar to previously described scRNA-seq datasets, Mrdjen et al. also described the emergence of reactive microglial subsets during both aging and AD (93, 111, 249). In their study, Mrdjen et al. developed a panel consisting of 43 metal-isotope tagged antibodies targeting leukocyte lineage and activation markers. Upon staining samples from young APP/PS1 mice the group identified a microglial subset with a heightened phagocytic signature and elevated expression of the activation markers CD11c and CD14. Notably, $CD11c^{+}$ microglia can be found surrounding Aβ plaques and CD11c has previously been described as a DAM marker (93, 249). Peripheral blood mononuclear cells (PBMCs) are relatively easy to process and can offer insights into disease mechanisms. To this aim, Phongpreecha et al. isolated PBMCs from healthy, AD, and Parkinson's disease (PD) patients and used single cell mass cytometry to not only assess changes in PBMC identity but also differences in response to various immune stimulants. While the group did not note any differences in PBMC subsets, they did find an overall muted pPLCγ2 response in AD PBMCs upon treatment with IFN-a, IL-7, IL-10, IL-21, LPS, or PMA/ionomycin (250). Given their ease of isolation, monitoring pPLCγ2 responses in PBMC could serve as an attractive pharmacodynamic AD biomarker. Neuronal dysfunction and degeneration are hallmarks in AD. Characterizing the features of vulnerable as well as resilient neurons could be valuable for AD intervention. Processing adult neural tissue for mass cytometry necessitates removal of myelin. However, our group has noted that many myelin removal procedures lead to substantial neuronal losses making downstream mass cytometry analysis challenging. More recent work has attempted to bridge this gap by studying

changes in synaptic profiles in AD using synaptosome preparations. Synaptosomes are isolated synaptic terminals with proteomes that reflect native synapses. Phongpreecha et al utilized mass cytometry to characterize synaptic profiles from healthy control, AD, and lewy-body dementia (LBD) patients. One of the more notable findings from the study was the observation that CD47 was enriched in presynaptic terminals of high-tau-bearing hippocampal neurons from AD patients. Given that CD47 is a canonical “don’t eat me” signal, increased expression of CD47 might serve as a mechanism for sparing certain synapses from degradation. Additionally, the group also found that very few synapses in human AD contained Aβ. This is in stark contrast to synapses from APP/PS1 mice which were loaded with Aβ. The observations highlight important disparities in mouse and human pathology, with mice lacking significant tau pathology, which could be a critical factor contributing to synaptic dysfunction in human AD (251).

Microglial-mediated inflammation is a critical driver of AD pathogenesis. While mass cytometry has provided some insights into the different microglial populations that emerge during AD, we still lack an understanding into how homeostatic populations morph into reactive ones. In the following section, we describe our findings on the signaling dynamics of microglia during inflammation. We hope that the presented methodology can be leveraged to probe treatment-specific responses in a variety of cell types.

3.2 Results

To analyze the signaling dynamics of microglia when faced with pro-inflammatory insults we developed an antibody panel comprising 33 markers that encompass various signaling pathways in addition to cell identity markers (Table 3.1). For our initial studies, we chose to treat primary microglial cultures with LPS or polyinosinic-polycytidylic acid (poly(I:C)) for varying time. LPS and Poly(I:C) act on TLR4 and TLR3, respectively, to elicit pro-inflammatory responses. Despite the observation that these triggers produce distinct transcriptional and cytokine release

profiles, there is a poor understanding of the downstream signaling pathways involved (252, 253). We observed that treatment with LPS or poly(I:C) led to a general increase in markers associated with inflammation, growth/survival, and microglial activation. While some markers such as Cx3CR1 and pSTAT1 showed comparable time- and magnitude responses, others such as pS6 showed a markedly different temporal pattern. Moreover, while both TLR3 and TLR4 signaling can lead to activation of the MAPK pathway we found that LPS led to significantly more robust expression of pERK and pp38 within minutes of treatment [LPS: 19-fold and 11-fold; poly(I:C): 2.8-fold and 2-fold change over t=0 for pERK and pp38]. Ki67, a marker of cell proliferation, is exclusively upregulated in LPS-treated microglia, consistent with previous work demonstrating that LPS, but not poly(I:C), induces microglial proliferation (252).

Metal	Antigen	Type	Metal	Antigen	Type
In113	Olig2	Identity -	Gd158	pSTAT3	Signaling
Cd114	CD11b	Identity – microglia/macrophage	Tb159	pATM	Signaling
In115	Fibronectin	Identity – endothelial cells	Gd160	Sox2	Identity – neural stem cells
La139	pGSK3β	Signaling	Dy161	CD40	Identity – microglia/macrophage
Pr141	GFAP	Identity - astrocyte	Dy162	Galectin-1	Identity – reactive glia
Nd143	CD68	Identity – microglia (phagocytosing)	Dy164	Cx3CR1	Identity – microglia/macrophage
Nd144	pPLCγ2	Signaling	Ho165	p-γH2AX	Signaling
Nd145	pRSK	Signaling	Er166	pNFκB	Signaling
Nd146	F480	Identity – microglia/macrophage	Er168	pAkt	Signaling
Sm147	pSTAT5	Signaling	Tm169	pcJun	Signaling
Sm149	CD45	Identity – microglia/macrophage	Er170	β-Catenin	Signaling
Nd150	Ly6C	Identity – microglia/macrophage	Yb171	pERK1/2	Signaling
Sm152	Ki67	Signaling	Yb173	CC3	Signaling
Eu153	pSTAT1	Signaling	Yb174	pSTAT4	Signaling
Sm154	pSrc	Signaling	Lu175	pS6	Signaling
Gd156	p-p38	Signaling	Yb176	pCreb	Signaling

Table 3.1. Markers used for analysis of microglial signaling dynamics.

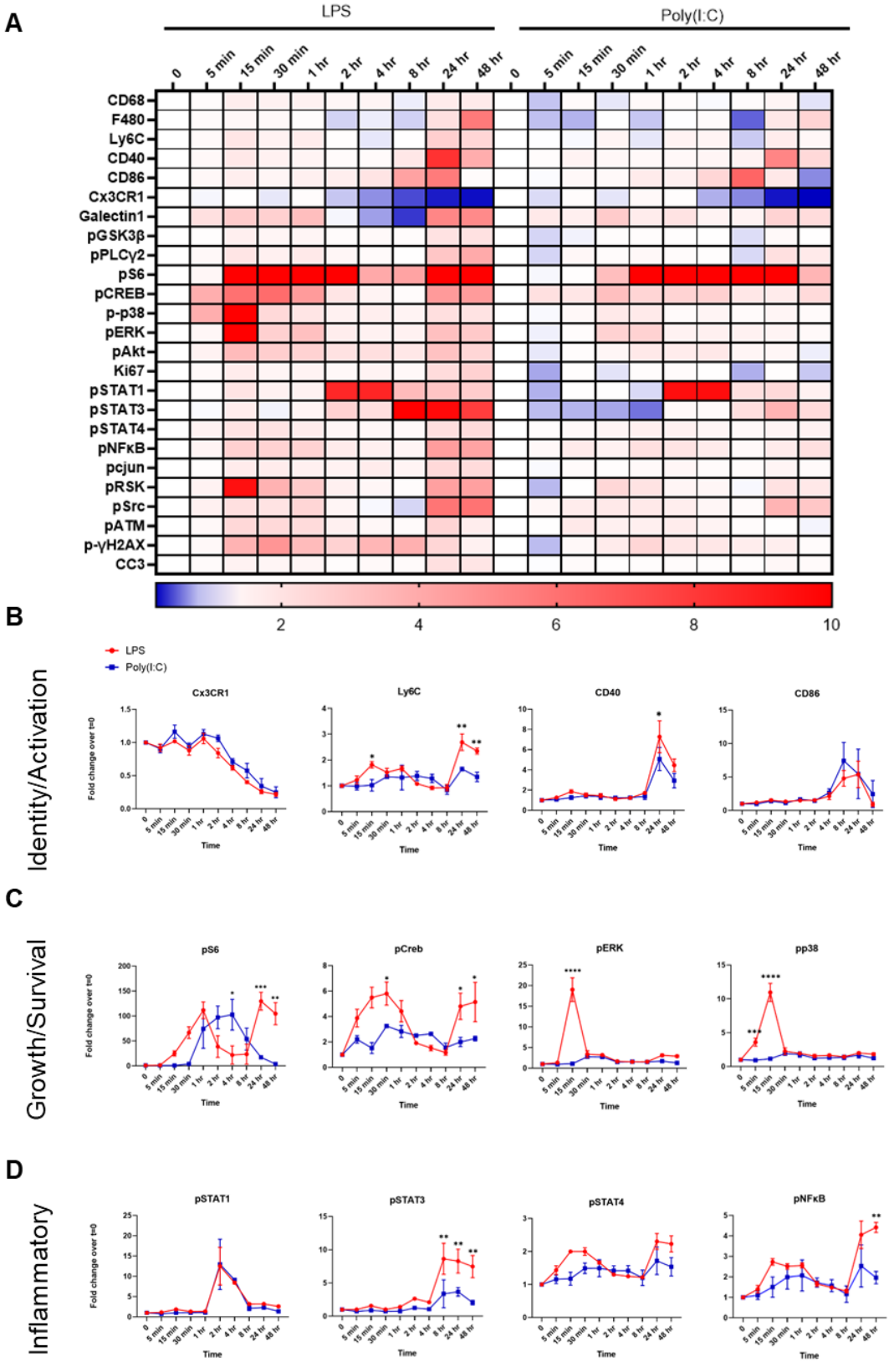
A
LPS
Poly(I:C)
0
5 min
15 min
30 min
1 hr
2 hr
4 hr
8 hr
24 hr
48 hr
CD68
F480
Ly6C
CD40
CD86
Cx3CR1
Galectin1
pGSK3β
pPLCγ2
pS6
pCREB
p-p38
pERK
pAkt
Ki67
pSTAT1
pSTAT3
pSTAT4
pNFκB
pcjun
pRSK
pSrc
pATM
p-γH2AX
CC3
2
4
6
8
10
B
Identity/Activation
LPS
Poly(I:C)
Cx3CR1
Ly6C
CD40
CD86
Fold change over t=0
Time
C
Growth/Survival
pS6
pCreb
pERK
pp38
D
Inflammatory
pSTAT1
pSTAT3
pSTAT4
pNFκB

Figure 3.3. Single-cell mass cytometry identifies population level time- and treatment-dependent alterations in microglial signaling. (**A**) Heatmap of expression of activation and signaling markers in microglia ($CD11b^{+}CD45^{+}$ cells) from microglial cultures treated with LPS or poly(I:C) for 0, 5 min, 15 min, 30 min, 1 hr, 2 hr, 4 hr, 8 hr, 24 hr, and 48 hr. Expression is represented as fold change over 0hr control. All values represent an average of 3 replicates for each time point in each condition. **(B**) Candidate markers in microglial identity/activation (**C**) growth/survival pathways and (**D**) inflammation are highlighted. Data were analyzed by 2-way ANOVA with Sidak's multiple comparisons testing. Data reported as mean ± SEM. (* = <0.05, ** = <0.01, *** = <0.001, **** = <0.0001).

Given that microglia do not exist in isolation when responding to challenges *in vivo*, we were interested in examining how other glial cells influence microglial signaling. Interestingly, when we performed these same experiments in mixed cultures we observed a striking blunting in microglial response across many markers. Notably, CD40 which peaked with a 5-7 fold increase in our pure cultures was only increased by 1.5-2 fold in mixed cultures at the 24 hr time-point. Similar decreases were seen with pS6, pCreb, pSTAT1, and pSTAT3. Our mixed cultures consist predominantly of astrocytes and microglia so we hypothesize that astrocyte secretion of anti-inflammatory factors such as IL-10 and TGF-β are serving to decrease microglial pro-inflammatory responses but this remains to be seen.

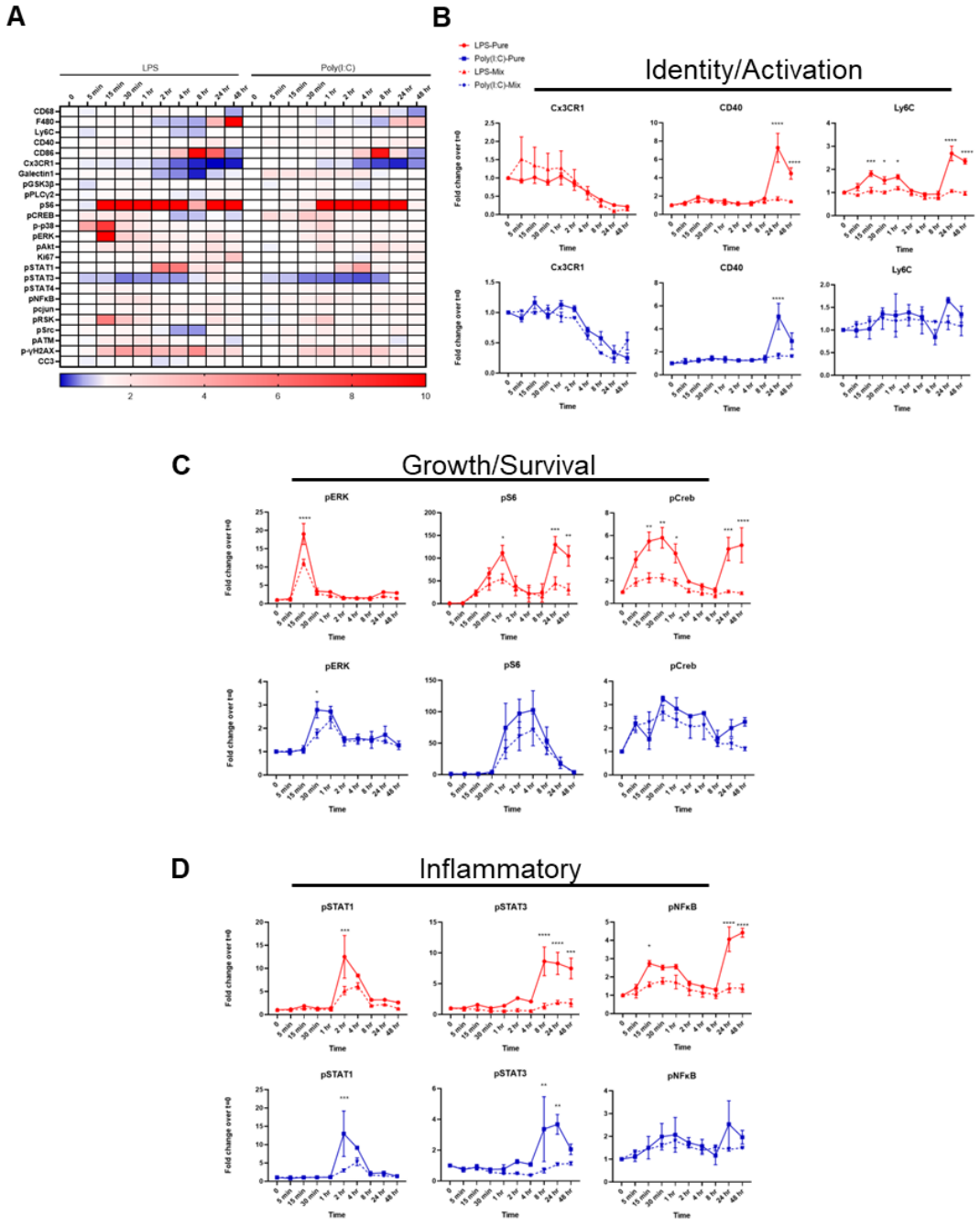

Figure 3.4. Presence of astrocytes selectively blunts microglial response to inflammatory stimuli. (**A**) Heatmap of expression of activation and signaling markers in microglia ($CD11b^{+}CD45^{+}$ cells) from mixed cultures treated with LPS or poly(I:C) for 0, 5 min, 15 min, 30 min, 1 hr, 2 hr, 4 hr, 8 hr, 24 hr, and 48 hr. Expression is represented as fold change over 0hr control. All values represent an average of 3 replicates for each time point in each condition. **(B**) Candidate markers in microglial identity/activation (**C**) growth/survival pathways and (**D**) inflammation are highlighted. Data were analyzed by 2-way ANOVA with Sidak's multiple

comparisons testing. Data reported as mean ± SEM. (* = <0.05, ** = <0.01, *** = <0.001, **** = <0.0001).

To further investigate how microglia shift in the presence of inflammatory insults, we performed clustering analysis using all of our identity and signaling markers and visualized the resulting clusters on a two-dimensional (2D) uniform manifold approximation and projection (UMAP) layout. At baseline, our cultures were dominated by homeostatic microglia that were differentiated based on Galectin expression ($Cx3CR1^{hi}Galectin^{lo}$ vs $Cx3CR1^{hi}Galectin^{med\text{-}hi}$). Notably, the $Galectin^{med\text{-}hi}$ populations had slightly higher levels of pSTAT1, pCREB, and pS6 perhaps reflecting a more activated class of homeostatic microglia. Over time, we observed a general decrease in homeostatic microglia and increases in activated subsets marked by elevated levels of signaling markers such as pSTAT1, pERK, and pp38. LPS-treated microglia exhibited a striking shift in cluster composition by 15 min, while poly(I:C)-treated microglia were delayed until 30 min. This shift was characterized by the emergence of Cluster 5, a cluster high in pp38 and pERK expression, corresponding to our previous observations of a peak in these markers at 15 minutes for LPS and 30 minutes for poly(I:C). Other key differences were noted near the end of the time course with $CD40^{hi}$ Cluster 8 making up 57.6% and 61.8% of LPS-treated microglia at 24hr and 48hr, respectively, while only making up 39.4 and 5.1% of poly(I:C)-treated microglia at the same time points.

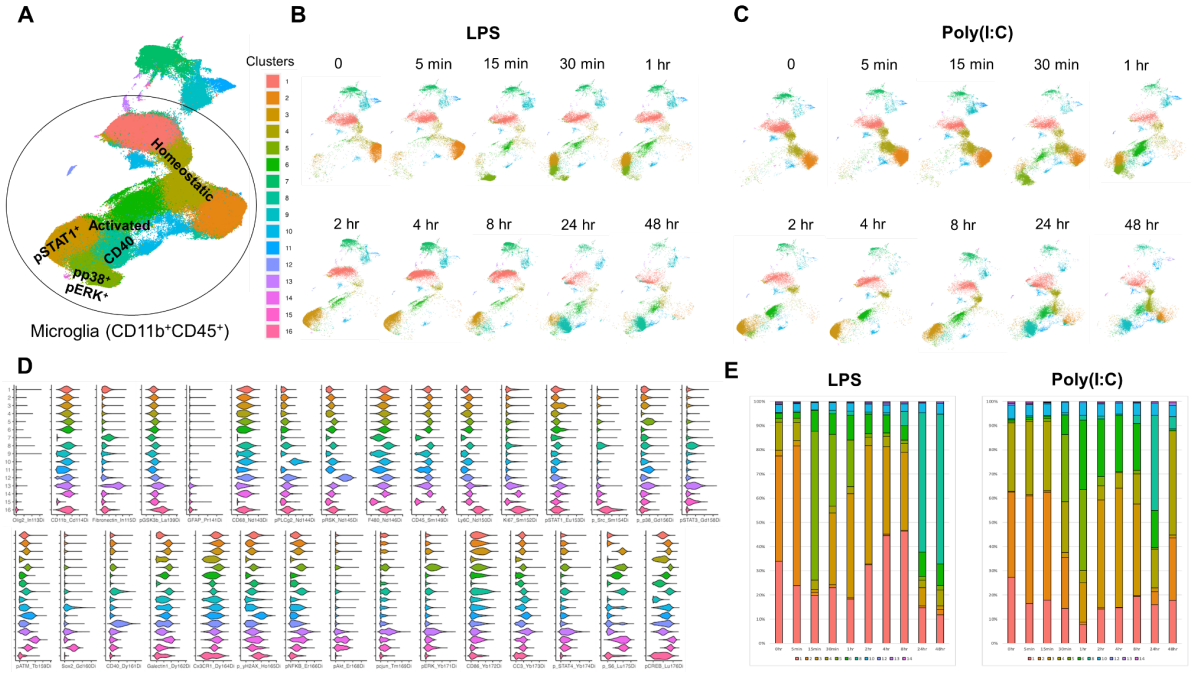

Figure 3.5. High-dimensional analysis of LPS- and poly(I:C)-treated microglia reveals distinct signaling profiles. (**A**) UMAP of LPS- and poly(I:C)-treated microglia clustered on all markers. Data generated from 3 full time courses for each treatment condition. Microglia are identified as $CD11b^{+}CD45^{+}$ events and indicated by black oval. Homeostatic and activated microglia are labeled, with additional labels for distinct signaling states **(B)** UMAPs for LPS-treated microglia broken apart by time-point (**C**) UMAPs for poly(I:C)-treated microglia broken apart by time-point. UMAP in (**A**) is a fusion of UMAPs in (**B**) and (**C**). (**D**) Violin plots of marker expression across all markers in each cluster (**E**) Proportion of total cells per cluster at each time point in microglial clusters from LPS- and poly(I:C)-treated microglia.

These findings underscore the valuable insights that single-cell mass cytometry can provide in unraveling cell signaling mechanisms. While it's possible that many of these same markers show similar dynamic changes in AD there are likely key differences in signaling programs in microglia treated with A□ or tau. We hope to perform similar experiments using more AD-relevant stimuli in future studies.

Chapter 4. Concluding remarks

Uncovering the mechanisms by which AD spreads will be necessary to devise appropriate therapeutic interventions. A growing body of research suggests that proteins

involved in cell death and inflammation contribute significantly to the deposition and spread of Aβ and tau aggregates. In this examination, we have shed light on two of these proteins: Caspase-8 and RIPK3 and their roles in the 5xFAD mouse model of AD. By eliminating both Caspase-8 and RIPK3 we found that we were able to significantly diminish both amyloid load and microgliosis. Moreover, we found that many of these effects are mediated by the NLRP3 inflammasome. As with any study, a number of critical questions remain to be answered.

First, despite the significant decreases to amyloidosis and microgliosis, we still observed death in layer V neurons. If not through extrinsic apoptotic or necroptotic means, how are these neurons dying? A likely answer is that another pathway, one independent of Caspase-8 or RIPK3, is precipitating death in this model at the time-point we evaluated. In the Introduction, we have outlined some of these candidate pathways. Unfortunately, there are many modes of cell death and the number of options is likely growing. Neurodegeneration is viewed as a hallmark of AD. The visuals of gray matter loss comparing non-demented vs AD brains are indeed striking and are a reflection of the decades-long progression of the disease. Thus, it's likely that a neuron fated to die in AD has already undergone noticeable signaling changes that may warrant removal from the circuit. In other words, once a cell has reached a 'point of no return' elimination may be favored over salvaging.

We have studied the roles of Caspase-8 and RIPK3 in disease but it's important to consider that these proteins are expressed during normal development (Caspase-8 probably ubiquitously). We have an appreciation for the importance of intrinsic apoptosis during development given the phenotypes of mice lacking effectors such as Apaf and Bax (160, 162). However, we do not yet know the contributions of intrinsic vs extrinsic apoptosis towards developmental death. On a related note, mice lacking RIPK3 and/or MLKL seem to develop just fine. The potential for compensatory pathways to emerge upon loss of RIPK3/MLKL certainly clouds the picture. Given their presence in the developing organism, if not necroptosis what are

these proteins doing? Apart from its role in cell death and inflammatory signaling, MLKL has also been shown to be critical for endosomal trafficking and in the generation of intraluminal vesicles (ILVs). Work from David Wallach's lab has shown that mice deficient in *Mlkl* exhibit a slowed degradation of ligands such as TNFα and EGF upon binding to their cognate receptors. These constitutive functions of MLKL seem to be independent of RIPK3 but can be enhanced by RIPK3 phosphorylation of MLKL (254). It remains to be seen whether these non-deadly roles of MLKL are influential during development.

What is the role of IL-1 signaling in AD? Our findings point to Caspase-8 having a central role in regulating A□-induced IL-1□ secretion using both synthetic A□ preparations as well as in *ex vivo* glial preparations from 5xFAD transgenic mice. Based on our observations that loss of Caspase-8 is partially protective, it seems that IL-1□ may have a net negative effect on AD progression. Polymorphisms in the *IL1B* have been reported to increase risk for developing LOAD (255). Furthermore, blocking IL-1 signaling using an IL-1R blocking antibody has been shown to ameliorate cognition in AD mouse models (256). There are a number of mechanisms by which IL-1□ could be fostering disease in our system. It's possible that IL-1 could be acting in an autocrine manner to promote microglial proliferation which could exacerbate neuropathology by increasing the neuroinflammatory load. We are actively exploring this hypothesis by labeling plaque-associated microglia with the proliferation marker Ki67 and quantifying differences between 5xFAD, 5xFAD *Ripk3*$^{-/-}$, and 5xFAD DKO mice. Additionally, given that Caspase-8 and RIPK3 are upstream of IL-1□ release and ASC speck generation respectively, we are interested in performing experiments in which we inject exogenous ASC specks and/or IL-1□ into 5xFAD DKO mice to determine if these manipulations are sufficient to restore pathology to 5xFAD levels.

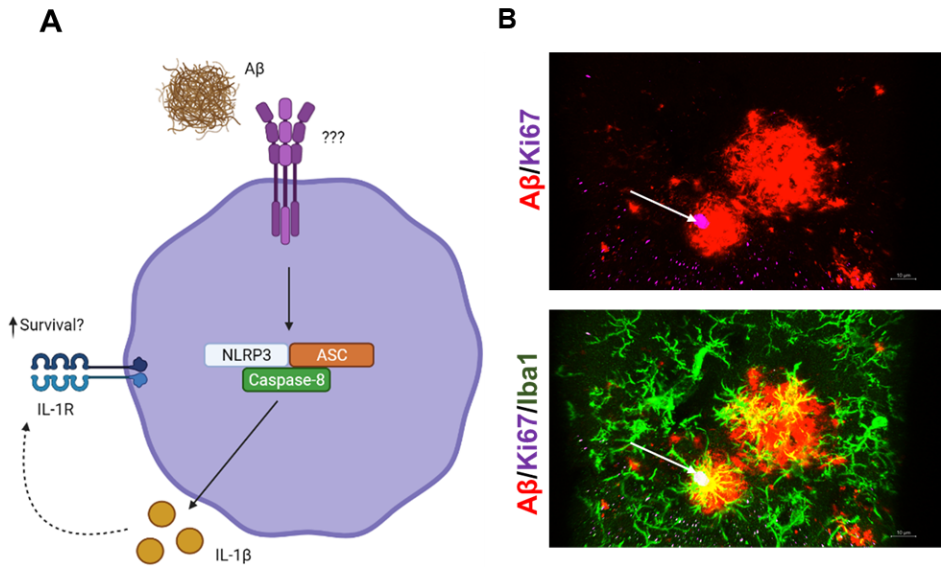

Figure 4.1. Identification of proliferating microglia. (A) Schematic depicting hypothesis for how IL-1β can sustain microglial proliferation. **(B)** Staining for proliferating microglia surrounding Aβ using Ki67 (magenta). Scale bar: 10 μm.

Conventional wisdom in the AD field has centered on the amyloid cascade hypothesis which proposes that gradually rising levels of the Aβ peptide – more specifically the $A\beta_{1\text{-}42}$ form – drives synapse loss, altered neuronal homeostasis, reactive gliosis, and subsequent neuronal loss and cognitive decline. Despite the massive investment in AD drugs that rely on Aβ removal and many clinical trials there have been significantly more treatment setbacks than successes. Efforts to remove Aβ are still being improved upon but we believe that arming the field with alternative approaches is key. Moreover, it's possible that amyloid interventions for patients that are already showing symptoms will be futile. In these circumstances, attempting to halt neuroinflammation may be the only option for preserving quality of life.

The importance of Aβ in AD is clear but it is only part of the story. While early deposition of Aβ generally marks the beginning of AD there are a number of cases of patients who possessed significant Aβ load but no signs of dementia. These “resilient” patients present clinicians and researchers with a unique opportunity to identify AD-modifying factors. Unlike

patients who succumb to AD, resilient individuals have an overall preserved brain integrity and spine density despite a comparable degree of Aβ pathology. Resilient patients can also harbor large amounts of hyperphosphorylated tau although this is rarer given that tau is more directly linked to cognitive decline. Speaking to the role of neuroinflammation in driving AD, resilient brains present with a dampened immune response. Markers such as GFAP and CD68 are reduced and resilient individuals also have distinct cytokine profiles which may confer protection (257). Other groups have also argued that lifestyle factors such as fasting and exercise could promote resilience through BDNF (258). In support of these findings, overexpression of BDNF in tau transgenic mice leads to an attenuation of neuronal loss (259). Together, these studies and observations highlight the importance of understanding the molecular mechanisms behind cognitive resilience as a means of developing novel therapeutic inroads to delay the onset of dementia.

An improved understanding of how microglia respond to pathological aggregates such as Aβ and tau will be invaluable. As a proof of principle, we attempted to characterize how microglia respond to LPS and poly(I:C) using single cell mass cytometry. Our studies revealed a number of key differences between the two treatments. For example, LPS treated microglia showed elevated Ki67 levels while poly(I:C) treated microglia did not. In addition to understanding which signaling pathways are affected by a particular stimuli we are also very interested in probing how different pathways/markers are related. For instance, does CD40 upregulation depend on previous upregulation of pSTAT1? These answers can be addressed through pharmacological experiments as well as computationally via correlational analysis such as DREMI (260). Furthermore, it's known that LPS and poly(I:C) secrete a number of cytokines that can subsequently influence microglial behavior. Understanding the differences in signaling responses between the primary insult (initial treatment with LPS v poly(I:C) and secondary insult (secreted factors) will also be informative.

Our experiments to examine microglial signaling responses were all conducted *in vitro*. It's likely that signaling *in vivo* has some key differences given the tissue environment. In order to preserve native signaling states we aimed to generate single cell suspensions from our cultures and get our samples into fixative as soon as possible. We were able to accomplish this task in 1-2 minutes for our *in vitro* samples. However when working with *in vivo* samples, dissociation takes several minutes and myelin removal (if needed) can take 30-60 minutes depending on the protocol. All of this elapsed time leaves opportunities for artifacts to be introduced and for post-translational marks to be modified. But recent advances in spatial proteomics allows us to circumvent many of these confounding factors. Imaging mass cytometry (IMC) is a technology developed by the Bodenmiller group and allows for the simultaneous detection of 40-45 markers at the protein level. The approach utilizes antibodies conjugated to isotopically pure rare earth metals and precise UV laser ablation to detect antigens of interest, enabling subcellular imaging with high resolution (261). Our group has been able to take advantage of IMC to profile the composition of neural tissue as well as examine signaling changes. In preliminary studies, we found that kainic acid treated mice upregulate pCREB in the cortex. We hope to also utilize IMC to probe signaling responses in brains from mice injected with LPS, poly(I:C), as well as in our various AD transgenics.

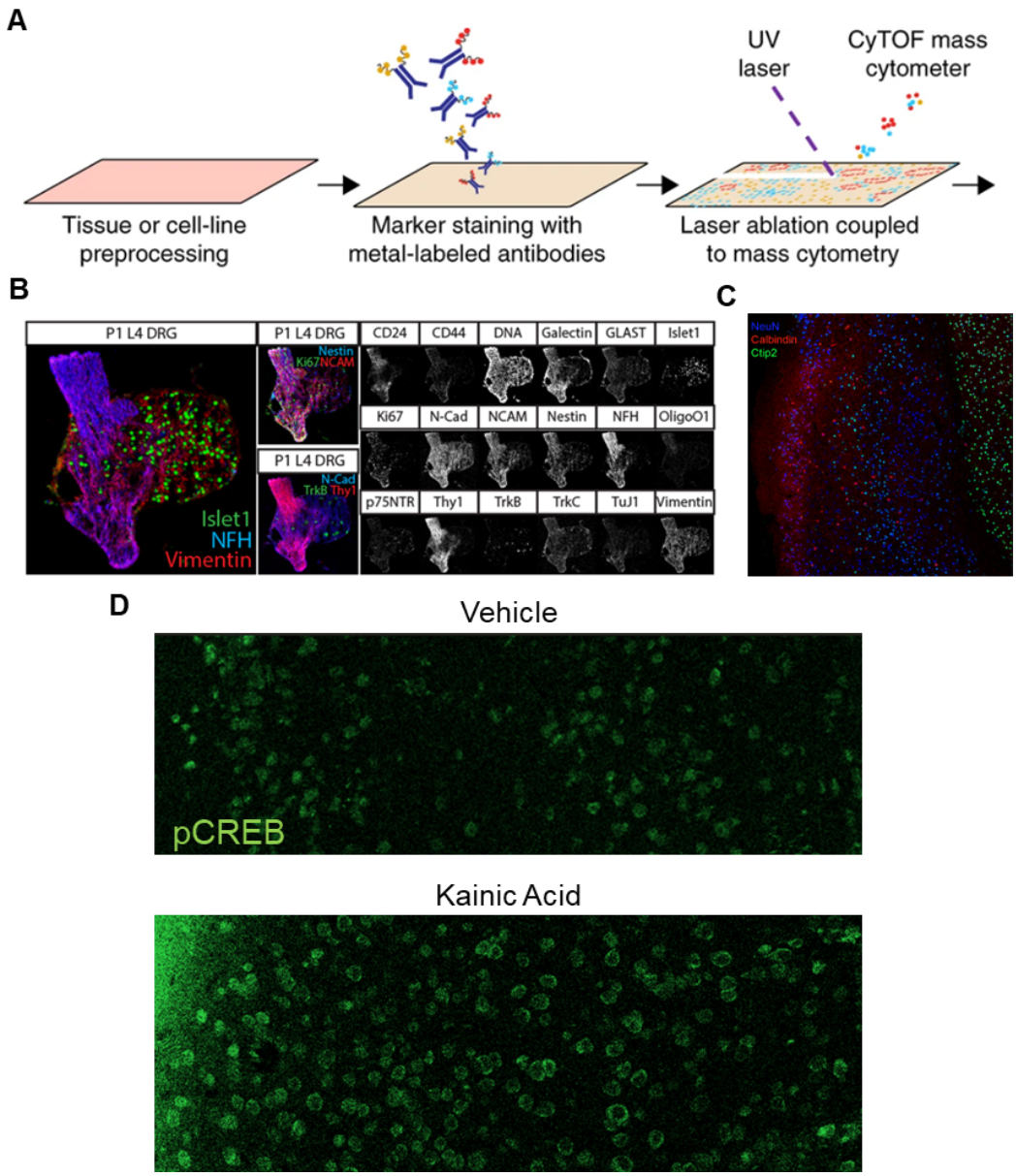

Figure 4.2. Using imaging mass cytometry to phenotype neural tissue. (**A**) Workflow for imaging mass cytometry (IMC). (**B**) IMC image of P1 L4 mouse DRG stained with various cell identity markers. (**C**) IMC image of mouse cortex stained with NeuN (neuronal marker), Calbindin (cortical interneuron marker), and Ctip2 (cortical layer 5/6 marker). (**D**) IMC images from mice treated with either vehicle or kainic acid then stained with pCREB. ROIs are from the cortex. Credit to Austin Keeler for images.

Despite significant research efforts, our cellular and molecular comprehension of AD remains incomplete. In this dissertation I have described my primary project as a graduate student in trying to better understand the roles of Caspase-8 and RIPK3 in AD. I have attempted

to position our findings within the larger picture of inflammation in AD, providing an introduction to AD along with critical cell death and inflammatory regulators, outlining how Caspase-8 and RIPK3 modulate AD progression, and addressing where there are still gaps in our knowledge. In summary, I hope that the findings put forth help to clarify our understanding of AD pathogenesis and present Caspase-8 as a novel mediator of disease progression.

Chapter 5. Materials and Methods

Mice

5xFAD mice were purchased from The Jackson Laboratory (catalog 34848) and were crossed with either *Ripk3* or *Caspase-8 Ripk3* (DKO) mice to generate 5xFAD-DKO mice (204, 206, 262). Animals were housed on a 12-hour light/12-hour dark cycle. Primers used for genotyping were 5xFAD (5′-CGGGCCTCTTCGCTATTAC-3′, 5′-TATACAACCTTGGGGGATGG-3′, 5′-ACCCCCATGTCAGAGTTCCT-3′), Caspase-8 (5′-GGATGTCCAGGAAAAGATTTGTGTC-3′, 5′-CCTTCCTGAGTACTGTCACCTGT-3′), and RIPK3 (5′-CGCTTTAGAAGCCTTCAGGTTGAC-3′, 5′-GCAGGCTCTGGTGACAAGATTCATGG-3′, 5′-CCAGAGGCCACTTGTGTAGCG-3′) (Integrated DNA Technologies). Non-5xFAD transgenic littermates were used as controls during the study. All mice used in experiments were male.

Cell Culture

Briefly, mixed glial cultures were prepared from the cortices of newborn mice (P0–P2). Meninges were carefully removed in ice-cold DMEM/F12 (Thermo Fisher Scientific) and cortices dissociated via trituration. Dissociated cortices were spun at 600*g* for 5 minutes. Cells from 2 brains (n = 4 cortices) were plated in a T-75 flask coated with poly-d-lysine (Sigma) in 15 mL of DMEM/F12 (Thermo Fisher Scientific) with 10% FBS (Gibco), 1% penicillin and streptomycin (Thermo Fisher Scientific), sodium pyruvate (Thermo Fisher Scientific), and MEM Non-Essential Amino Acids (Thermo Fisher Scientific). On day in vitro 7 (DIV7) and DIV9, 5 mL of L-929 cell–conditioned medium (LCM) was added to promote microglial growth. On DIV12, glial cultures were trypsinized and plated at 100,000 cells/well of a 24-well plate. Cells were treated on DIV2.

Cell Treatments

For IL-1β release studies, cells were primed with 500 ng/mL LPS (Sigma, catalog L4391) for 3 hours, then treated with oligomeric Aβ (oAβ) for 24 hours. Supernatants were collected and analyzed for IL-1β (Thermo Fisher Scientific, catalog 88-7013-22) according to manufacturer instructions.

Preparation of LCM

L-929 cells (ATCC) were cultured in a T-25 flask with 5 mL of DMEM (Thermo Fisher Scientific) with 10% FBS (heat-inactivated), 1% HEPES, 1% l-glutamine, and sodium pyruvate. Upon reaching confluence, cells were lifted with 1× Trypsin-EDTA (Thermo Fisher Scientific), resuspended in 15 mL of medium, transferred to a T-75 flask. After reaching confluence, cells were again lifted with Trypsin-EDTA and transferred to a T-175 flask in 50 mL of medium. After 7 days in culture, the supernatant was harvested and spun at 1,700*g* for 5 minutes, then filtered through a 0.45 μm filter before freezing at –80°C.

Preparation of oAβ

oAβ was prepared as described (263). We dissolved 1 mg of $A\beta_{1\text{-}42}$ peptides (Echelon Biosciences) in 250 μL of 1,1,1,3,3,3-hexafluoro-2-propanol (HFIP; Sigma-Aldrich) via room temperature incubation for 2–3 hours. Upon dissolution, Aβ peptide was aliquoted into Eppendorf tubes. HFIP was evaporated overnight in a biosafety cabinet, and the dried peptide was stored at –80°C. Before use, aliquots were kept at room temperature for 15 minutes. Films were dissolved in anhydrous DMSO (Sigma) to 5 mM. Cold phenol-free F-12 medium (Thomas Scientific, catalog C994K53) was added to yield a final concentration of 100 μM. The resulting solution was then vortexed for 15 seconds and left at 4°C for 24 hours with gentle rocking.

Tissue Preparation

Mice were euthanized via CO_2 inhalation and transcardially perfused with 50 mL of ice-cold PBS. Brains were removed from the skull. One hemisphere was fixed in 4% paraformaldehyde (PFA) for 24 hours while the other was micro-dissected into cortex and hippocampus and frozen in dry ice and then transferred to –80°C.

Immunohistochemistry

PFA-fixed hemispheres were washed with PBS (3 washes, 10 minutes per wash) then transferred to 30% sucrose/PBS for 48–72 hours. Brains were then frozen on dry ice after they sank. Free-floating, 30 μm thick serial coronal sections were collected on a cryostat and kept in 1× PBS plus 0.002% sodium azide at 4°C. Sections were washed 3 times for 5 minutes in PBS, blocked in 2% normal donkey serum plus 1% BSA plus 0.1% Triton plus 0.05% Tween-20 for 1 hour, incubated overnight at 4°C in blocking solution and primary Ab (Iba1, goat, 1:500, Abcam, catalog ab5076; GFAP, mouse, 1:500, EMD Millipore, catalog MAB360; D54D2, rabbit, 1:500, Cell Signaling Technology, catalog 8243S; CD68, rat, 1:800, BioRad, catalog MCA1957; ASC, rabbit, 1:300, Adipogen, catalog AL177; NeuN, rabbit, 1:1,000, Abcam, catalog ab177487; Dectin-1 (Clec7A), 1:30, InvivoGen, catalog mabg-mdect; and Ctip2, 1:400, Abcam, catalog ab240636), washed again, then incubated in blocking solution with the corresponding Alexa Fluor secondary Abs (1:500) — donkey anti-rabbit IgG (H+L) Alexa Fluor 568, A10042 (Thermo Fisher Scientific), donkey anti-mouse IgG (H+L) Alexa Fluor 568, A10037 (Thermo Fisher Scientific), donkey anti-goat IgG (H+L) Alexa Fluor 647, A-21447 (Thermo Fisher Scientific), and donkey anti-rat IgG (H&L) Alexa Fluor 647 preadsorbed, ab150155 (Abcam) — for 2 hours in darkness at room temperature, washed again, and then mounted in Fluoromount-G (SouthernBiotech, catalog 0100-01).

For ThioS staining, after secondary Ab–staining incubation and washes, sections were incubated in 1% ThioS in 80% ethanol for 15 minutes at room temperature. Sections were then

washed for 2 minutes in 80% ethanol, 70% ethanol, and deionized water 2 times, then mounted using Fluoromount G. TUNEL labeling was carried out using the In Situ Cell Death Detection Kit, Fluorescein (Roche), according to manufacturer's instructions, after Iba1 secondary staining and washes.

In situ Hybridization Assay by RNAscope

Brains were dissected from C57BL/6N and 5xFAD mice and fixed with 4% PFA in PBS for 24 hours at 4°C. Tissues were then incubated in 30% sucrose solution at 4°C overnight. Fixed tissues were then frozen on dry ice and stored at –80°C. Frozen tissues were cryosectioned at 20 μm thickness, collected onto positively charged slides (Shandon Superfrost Plus, Thermo Fisher Scientific, catalog 6776214), and air-dried overnight in the dark. The following day, slides were washed with PBS (2 washes for 2 minutes per wash) then incubated for 10 minutes in H_2O_2 (RNAscope H_2O_2 and Protease Reagents Kit, Advanced Cell Diagnostics, catalog 322381). Slides were then twice washed for 2 minutes with distilled water to remove H_2O_2 before incubation with protease IV solution (RNAscope H_2O_2 and Protease Reagents Kit, Advanced Cell Diagnostics, catalog 322381) for 30 minutes at 40°C in a HybEZ II oven (Advanced Cell Diagnostics, catalog 321710/321720) and 2 additional 2-minute washes in distilled water. Tissues were then incubated in Probe Master Mix for 2 hours at 40°C (Probe1: Mm-RipK3, catalog 462541; Probe2: Mm-Casp8-C2, catalog 468971-C2; Advanced Cell Diagnostics) and then washed twice in 1× wash buffer (RNAscope Wash Buffer Reagents, Advanced Cell Diagnostics, catalog 310091).

After amplification by sequential incubations with AMP1, 2, and 3 solutions (RNAscope Multiplex Fluorescent Detection Kit v2, Advanced Cell Diagnostics, catalog 323110) for 30 minutes at 40°C (separated with two 2-minute washes with wash buffer between solutions), slides were incubated for 15 minutes at 40°C with HRP-Channel 1 (RNAscope Multiplex

Fluorescent Detection Kit v2, Advanced Cell Diagnostics, catalog 323110), before an additional 2 washes for 2 minutes in wash buffer. Slides were then incubated in a fluorescent dye for 30 minutes at 40°C (1:750 dilution; Tyramide Signal Amplification [TSA] Cyanine 3, Akoya, catalog TS000202) before two 2-minute washes with wash buffer and blocking with HRP blocker for 15 minutes at 40°C. The same HRP steps were repeated for channel 2 by applying a second fluorescent dye (1:750 dilution; TSA Fluorescein, Akoya; catalog TS000200). Finally, 10–20 µL of DAPI was applied at room temperature to stain the nuclei (DAPI Fluoromount-G, SouthernBiotech, catalog 0100-20), and then slides were sealed with coverslips.

Image Analysis

Images were taken using a Zeiss 980 confocal laser-scanning microscope at either ×10/.45, ×20/0.8, or ×40/1.3 (oil) original magnification. Maximum intensity projections of *Z*-stacks were used for all analysis. For percentage area measurements and plaque counts, 8-bit images were exported to FIJI. To analyze D54D2 staining, regions of interest covering the RS or subiculum were drawn, and analysis was performed following background subtraction (rolling-ball radius, 50 pixels) and thresholding using the Intermodes function. ThioS$^+$ plaques were manually counted in both the RS and subiculum. For Iba1 and GFAP percent area measurements, 8–10 fields of view throughout the cortex were taken across 2 sections at ×40 original magnification. For Iba1 staining, analysis was performed after background subtraction (rolling-ball radius, 50 pixels), applying an unsharp mask filter (3.0, 0.6), despeckle, and thresholding (min intensity 32, max intensity 255). GFAP analysis was performed after background subtraction (rolling-ball radius, 50 pixels) and thresholding (min intensity 54, max intensity 255).

Images for both microglial periplaque and Sholl analyses were taken at ×40 original magnification. Local microgliosis was evaluated for ThioS$^+$ plaques spanning the cortex.

Plaques were excluded if they were within 15 μm of another plaque. Images were imported into Imaris 9.7.2 and plaques and were labeled using the Surfaces feature. For volume-fraction calculations, microglia were labeled using the Surfaces feature and the volume of Iba1 staining within 15 μm of each plaque was calculated. For Iba1$^+$ cell counts, microglia were labeled using the Spots feature, and microglia within 15 μm of each plaque were counted. In total, 46–51 microglia were analyzed per experimental group (*n* = 6 mice/group). Sholl analysis was performed using the filament tracer tool in Imaris 9.7.2. Microglial soma volumes were determined using the Surfaces feature in Imaris. Microglia were excluded if they were within 15 μm of a plaque and/or the entire microglia was not covered in the field of view. For each mouse, 10–15 cortical microglia were chosen for a total of 70–80 microglia/group (*n* = 6 mice/group).

For ASC speck quantification, images were taken at ×40 original magnification. Random plaque-containing fields of view were taken across the cortex. ASC specks were counted within 15 μm of plaques.

For NeuN analysis, images from cortical layer V were taken at ×20 original magnification, and NeuN$^+$ cells were counted in FIJI. Cells were counted using the Analyze Particles feature (greater than 12 μm^2) after thresholding (min intensity 116, max intensity 255) and watershed separation.

For RNAscope analysis, images from the subiculum, cortex, and thalamus were taken at ×40 original magnification. *Casp8*$^+$ and *Ripk3*$^+$ puncta were counted in FIJI using the Analyze Particles feature (greater than 0.8 μm^2) after thresholding.

ELISA Quantification of Aβ

Snap-frozen cortices were massed and homogenized initially in 1× RIPA buffer (25 mM Tris-HCl, pH 7.5, 150 mM NaCl, 1% NP-40, 0.5% sodium deoxycholate, 0.1% SDS)

supplemented with complete protease inhibitor (Roche) and PhosSTOP phosphatase inhibitor (Roche). Homogenates were spun at 16,000*g* for 20 minutes, and the supernatants were collected and saved at –80°C as the RIPA-soluble fraction. Pellets were further homogenized in ice-cold 5 M guanidine–HCl diluted in 50 mM Tris at pH 8.0. Homogenates were mixed on a shaker for 3–4 hours at room temperature, then stored in –80°C as the guanidine-soluble fraction. ELISAs for $A\beta_{1-42}$ were run using commercial kits (R&D Systems).

Real-time PCR

Total RNA was extracted from hippocampal tissue using Trizol (Thermo Fisher Scientific, catalog 15596026) combined with the RNeasy Mini Kit (Qiagen, catalog 74104). For cDNA synthesis, 500 ng of RNA was used (Thermo Fisher Scientific, catalog 18080051). Transcript levels of *Nlrp3* (Thermo Fisher Scientific, assay ID Mm00840904_m1), *Il1b* (Thermo Fisher Scientific, assay ID Mm00434228_m1), *Casp1* (Thermo Fisher Scientific, assay ID Mm00438023_m1), and *Pycard* (Thermo Fisher Scientific, assay ID Mm00445747_g1) were quantified by RT-PCR using a CFX96 Real-Time System. *Gapdh* (Thermo Fisher Scientific, assay ID Mm99999915_g1) expression was used for normalization, and results are presented as a fold change induction over levels in WT samples.

Western Blotting

Hippocampi were massed and homogenized in 1x RIPA buffer. 20 µg of hippocampal homogenate were boiled for 5 min in an equal volume of 2x laemmli buffer prior to loading onto a 4-15% Mini-PROTEAN TGX Precast Gel. Samples were then transferred onto PVDF membranes and blocked for 1 hr in 5 % milk (Fisher, catalog # NC9121673) in TBS + 0.05% Tween (TBST) at room temperature. Membranes were then probed overnight at 4 C with primary antibody in 5 % milk in TBST. Membranes were then washed in TBST then incubated

for 1 hr at RT with the corresponding HRP conjugated secondary antibody in 5 % milk in TBST. Membranes were then washed again in TBS and signals developed using the SuperSignal™ West Femto Maximum Sensitivity Substrate (Thermo Fisher Scientific; according to the manufacturer's protocol). The following antibodies were used: anti-NLRP3 (Adipogen, AG-20B-0014-C100, 1:1000), Phospho-NF-κB p65 (CST, 3033T, 1:1000), NF-κB p65 (CST, 8242T, 1:1000), β-actin (CST, 4967S, 1:10000), goat anti-rabbit HRP (Fisher, catalog # G21234, 1:5000), goat anti-mouse HRP (Fisher, catalog # G-21040, 1:5000) . In some cases membranes were stripped and reprobed using the Western BLoT Stripping Buffer (Takara, T7135A, according to manufacturer's protocol).

Ex vivo IL-1β release assay

Cortical suspensions were prepared as described previously (226), with some modifications. Briefly, cortices were minced and harvested in HBSS (with calcium and magnesium). HBSS was then aspirated and replaced with enzyme solution (2 mg/mL papain, 1 mg/mL DNase I in HBSS with calcium and magnesium). Cortices were passed through an 18G needle, then incubated for 45 minutes at 37°C for digestion. To aid in the dissociation, tissue was removed every 15 minutes and passed through an 18G needle. After incubation, tissue was passed through a 70 μm filter, then washed with complete RPMI (cRPMI) medium (10% FBS, 1% penicillin/streptomycin, 1% sodium pyruvate, 1% nonessential amino acids, and 0.1% 2-ME). Tissue was then resuspended in 10 mL of 40% percoll and spun at 650*g* for 25 minutes (no brake, 22°C). Supernatant was aspirated and the pellet resuspended in cRPMI and then spun at 650*g* for 5 minutes to remove residual percoll (full brake, 22°C). Pellet was resuspended in cRPMI and cells were plated at 100,000/ well of a 96-well plate. After 48 hours, supernatants were collected and evaluated by ELISA for IL-1β release.

Mass Cytometry Sample Dissociation

Mixed cultures were prepared as described above and microglia were isolated by shaking at 180 rpm for 1 hr. Microglia were then reseeded 250,000 cells/well of a 6 well plate and cultured for 2 days using identical media as in the mixed culture. After two days, microglia were treated with either LPS (500 ng/mL) or Poly(I:C) (10 μg/mL) for varying amounts of time. Following treatment, media was removed and then 1 mL of StemPro Accutase was added to the cells. Immediately upon Accutase addition cells were scraped off and added 1:1 to 4 % PFA. Cells were fixed for 10 min then spun at 500g for 5 minutes. Supernatant was discarded and cells were resuspended in 1 mL of 0.5 % BSA + 0.02 % sodium azide then stored in -80 C for later analysis.

Metal Conjugation and Antibody Validation

Antibodies were conjugated to specific metal isotopes as detailed in (247). Antibodies were then validated following metal conjugation as detailed in (247). In brief, antibodies were considered both specific and reliable if they produced a signal in DNA intercalator-positive cells as well as cells with positive, but not negative, counterstains. Optimal antibody concentrations for use in staining were determined by titration. Concentrations that resulted in the greatest dynamic range in signal while minimizing background were chosen for each antibody. Signaling antibodies were validated in a similar manner using known pharmacological triggers for a particular pathway on appropriate cell lines. Responses were compared to vehicle treated cells to determine optimal antibody concentration.

Mass Cytometry Sample Staining

Samples were stained and mass cytometry was performed as detailed in (247). Briefly, samples were barcoded by incubation with specific combinations of 1mM isothiocyanobenzyl EDTA-chelated palladium metals prior to being pooled into barcoded sets for staining. Cells were first stained for surface epitopes by incubation with primary antibodies against extracellular

proteins. Samples were next permeabilized with ice-cold 100% methanol prior to staining with primary antibodies against intracellular epitopes.

Mass Cytometry

Cells were analyzed on a Helios CyTOF 2 system (Fluidigm). Prior to analysis, cells were resuspended in water (approximately 1 ml per 1×10^6 cells) containing 1:20 EQ Four Element Calibration Beads (Fluidigm) and passed through a 40-μm nylon mesh filter. Cells were analyzed in multiple runs at a rate of 500 cells per second or less. Data were collected on a Helios CyTOF 2 using CyTOF Software version 6.7.1014.

High-Dimensional Analysis

Normalization, debarcoding, and isolation of quality, single-cell events were performed as detailed in (247). Leiden clustering was then employed to identify cell types defined by either 12 identity and activation markers or all 33 markers in our panel. UMAP dimensionality reduction was then utilized to visualize the data in two dimensions with parameters as follows: nearest neighbors = 15, metric = Euclidean, local connectivity = 1, components = 2, and epochs = 1,000. All scripts used are accessible via linked githubs in (247).

Statistics

Data in figures represent mean ± SEM. Each *n* represents an independent biological sample. Analysis was performed with GraphPad Prism, version 8.0, applying either a 1- or 2-way ANOVA with Tukey's post hoc test comparing all groups with each other. All Student's *t* tests were 2 tailed. Statistical significance is defined as $P < 0.05$.

Bibliography

1. Hippius H. The discovery of Alzheimer's disease. *Dialogues Clin Neurosci*. 2003; 5(1): 101-108.

2. Dahm R. Alzheimer’s discovery. *Cell Reports*. 2006; 21(7): R906-R910.

3. St. George-Hyslop PH, et al. The genetic defect causing familial Alzheimer’s disease maps on Chromosome. *Science*. 1987; 21(235): 885–890.

4. Sherrington R, et al. Cloning of a gene bearing missense mutations in early-onset familial Alzheimer's disease. *Nature*. 1995; 375(6534): 754-760.

5. Levy-Lahad E, et al. Candidate gene for the chromosome 1 familial Alzheimer’s disease locus. *Science*. 1995; 269(5226): 973–977.

6. Vassar R, et al. Beta-secretase cleavage of Alzheimer's amyloid precursor protein by the transmembrane aspartic protease BACE. *Science*. 1999; 286(5440): 735-741.

7. Hampel H, et al. The Amyloid-β Pathway in Alzheimer’s Disease. *Mol Psychiatry*. 2021; 26(10): 5481-5503.

8. Murphy MP and Levine H. Alzheimer’s Disease the β-Amyloid Peptide. *J Alzheimers Dis*. 2010; 19(1): 311.

9. Bentahir M, et al. Presenilin clinical mutations can affect γ‐secretase activity by different mechanisms. *J Neurochem*. 2006; 96(3): 732-42.

10. Walsh DM, et al. Naturally secreted oligomers of amyloid β protein potently inhibit hippocampal long-term potentiation *in vivo*. *Nature*. 2002; 416(6880): 535-539.

11. Willem M, et al. η-Secretase processing of APP inhibits neuronal activity in the hippocampus. *Nature*. 2015; 526(7573): 443-447.

12. Zhang Z, et al. Delta-secretase cleaves amyloid precursor protein and regulates the pathogenesis in Alzheimer’s disease. *Nat Commun*. 2015; 6(1): 8762.

13. Vassar R, et al. The β-Secretase Enzyme BACE in Health and Alzheimer's Disease: Regulation, Cell Biology, Function, and Therapeutic Potential. *J Neurosci*. 2009; 29(41): 12787-12794.

14. Sun X, He G, and Song W. BACE2, as a novel APP theta-secretase, is not responsible for the pathogenesis of Alzheimer's disease in Down syndrome. *FASEB J*. 2006; 20(9): 1369-1376.

15. Alić I, et al. Patient-specific Alzheimer-like pathology in trisomy 21 cerebral organoids reveals BACE2 as a gene dose-sensitive AD suppressor in human brain. *Mol Psychiatry*. 2021; 26(10): 5766-5788.

16. Mok KY, et al. Polymorphisms in BACE2 may affect the age of onset Alzheimer's dementia in Down syndrome. *Neurobiology of Aging*. 2014; 35(6): 1513.e1-1513.e5.

17. Hardy J and Selkoe DJ. The Amyloid Hypothesis of Alzheimer's Disease: Progress and Problems on the Road to Therapeutics. *Science*. 2002; 297(5580): 353-356.

18. Luna S, Cameron DJ, Ethell DW. Amyloid-β and APP deficiencies cause severe cerebrovascular defects: important work for an old villain. *PLoS One*. 2013; 8(9): e75052.

19. Soscia SJ, et al. The Alzheimer's Disease-Associated Amyloid β-Protein Is an Antimicrobial Peptide. *PLoS One*. 2010; 5(3): e9505.

20. Kumar D, et al. Amyloid-β Peptide Protects Against Microbial Infection In Mouse and Worm Models of Alzheimer’s Disease. *Sci Transl Med*. 2016; 8(340): 340ra72

21. Eimer WA, et al. Alzheimer’s Disease-Associated β-Amyloid Is Rapidly Seeded by Herpesviridae to Protect against Brain Infection. *Neuron*. 2018; 99(1): 56-63.

22. Dominy SS, et al. Porphyromonas gingivalis in Alzheimer's disease brains: Evidence for disease causation and treatment with small-molecule inhibitors. *Sci Adv*. 2019; 5(1).

23. Pisa D, et al. Different Brain Regions are Infected with Fungi in Alzheimer’s Disease. *Sci Rep*. 2015; 5(1): 15015.

24. Jamieson GA, et al. Latent herpes simplex virus type 1 in normal and Alzheimer's disease brains. *J Med Virol*. 1991; 33(4): 224-227.

25. Wozniak MA, Mee AP, Itzhaki RF. Herpes simplex virus type 1 DNA is located within Alzheimer's disease amyloid plaques. *J Pathol*. 2009; 217(1): 131-138.

26. Readhead B, et al. Multiscale Analysis of Independent Alzheimer's Cohorts Finds Disruption of Molecular, Genetic, and Clinical Networks by Human Herpesvirus. *Neuron*. 2018; 99(1): 64-82.

27. Senechal Y, Kelly PH, Dev KK. Amyloid precursor protein knockout mice show age-dependent deficits in passive avoidance learning. *Behav Brain Res*. 2008; 186(1): 126-132.

28. Ring S, et al. The Secreted β-Amyloid Precursor Protein Ectodomain APPsα Is Sufficient to Rescue the Anatomical, Behavioral, and Electrophysiological Abnormalities of APP-Deficient Mice. *J Neurosci*. 2007; 27(29): 7817-7826.

29. Martín MG, Pfrieger F, and Dotti CG. Cholesterol in brain disease: sometimes determinant and frequently implicated. *EMBO Rep*. 2014; 15(10): 1036-1052.

30. Holtzman DM, Herz J, Bu G. Apolipoprotein E and Apolipoprotein E Receptors: Normal Biology and Roles in Alzheimer Disease. *Cold Spring Harb Perspect Med*. 2012; 2(3): a006312.

31. Belloy ME, Napolioni V, Greicius MD. A Quarter Century of APOE and Alzheimer's Disease: Progress to Date and the Path Forward. *Neuron*. 2019; 101(5): 820-838.

32. Strittmatter WJ, et al. Binding of human apolipoprotein E to synthetic amyloid beta peptide: isoform-specific effects and implications for late-onset Alzheimer disease. *Proc Natl Acad Sci USA*. 1993; 90(17): 8098-8102.

33. Namba Y, et al. Apolipoprotein E immunoreactivity in cerebral amyloid deposits and neurofibrillary tangles in Alzheimer's disease and kuru plaque amyloid in Creutzfeldt-Jakob disease. *Brain Res*. 1991; 541(1): 163-166.

34. Verghese PB, et al. ApoE influences amyloid-β (Aβ) clearance despite minimal apoE/Aβ association in physiological conditions. *Proc Natl Acad Sci USA*. 2013; 110(19): E1807-1816.

35. Liu C-C, et al. ApoE4 accelerates early seeding of amyloid pathology. *Neuron*. 2017; 96(5): 1024-1032.

36. Bales KR, et al. Apolipoprotein E is essential for amyloid deposition in the APPV717F transgenic mouse model of Alzheimer's disease. *Proc Natl Acad Sci USA*. 1999; 96(26): 15233-15238.

37. Krasemann S, et al. The TREM2-APOE Pathway Drives the Transcriptional Phenotype of Dysfunctional Microglia in Neurodegenerative Diseases. *Immunity*. 2017; 47(3): 566-581.

38. Ulrich JD, et al. ApoE facilitates the microglial response to amyloid plaque pathology. *J Exp Med*. 2018; 215(4): 1047-1058.

39. Arnaud L, et al. APOE4 drives inflammation in human astrocytes via TAGLN3 repression and NF-κB activation. *Cell Rep*. 2022; 40(7): 111200.

40. Serrano-Pozo A, et al. Effect of APOE alleles on the glial transcriptome in normal aging and Alzheimer's disease. *Nat Aging*. 2021; 1(10): 919-931.

41. Marschallinger J, et al. Lipid droplet accumulating microglia represent a dysfunctional and pro-inflammatory state in the aging brain. *Nat Neurosci*. 2020; 23(2): 194-208.

42. Sienski G, et al. APOE4 disrupts intracellular lipid homeostasis in human iPSC-derived glia. *Sci Transl Med*. 2021; 13(583): eaaz4564.

43. Dixit R, et al. Differential Regulation of Dynein and Kinesin Motor Proteins by Tau. *Science*. 2008; 319(5866): 1086-1089.

44. Hanger DP, Anderton BH, Noble W. Tau phosphorylation: the therapeutic challenge for neurodegenerative disease. *Trends Mol Med*. 2009; 15(3): 112-119.

45. Rodríguez-Matellán A, Avila J, Hernández F. Overexpression of GSK-3β in Adult Tet-OFF GSK-3β Transgenic Mice, and Not During Embryonic or Postnatal Development, Induces Tau Phosphorylation, Neurodegeneration and Learning Deficits. *Front Mol Neurosci*. 2020; 13: 561470.

46. Lasagna-Reeves CA, et al. Tau oligomers impair memory and induce synaptic and mitochondrial dysfunction in wild-type mice. *Mol Neurodegener*. 2011; 6: 39.

47. Feuillette S, et al. Drosophila models of human tauopathies indicate that Tau protein toxicity in vivo is mediated by soluble cytosolic phosphorylated forms of the protein. *J Neurochem*. 2010; 113(4): 895-903.

48. Kuchibhotla KV, et al. Neurofibrillary tangle-bearing neurons are functionally integrated in cortical circuits in vivo. *Proc Natl Acad Sci USA*. 2014; 111(1): 510-514.

49. Long JM and Holtzman DM. Alzheimer Disease: An Update on Pathobiology and Treatment Strategies. *Cell*. 2019; 179(2): 312-339.

50. Jack CR, et al. The bivariate distribution of amyloid-β and tau: relationship with established neurocognitive clinical syndromes. *Brain*. 2019; 142(10): 3230-3242.

51. Zempel H, et al. Aβ Oligomers Cause Localized Ca2+ Elevation, Missorting of Endogenous Tau into Dendrites, Tau Phosphorylation, and Destruction of Microtubules and Spines. *J Neurosci*. 2010; 30(36): 11938-11950.

52. Götz J, et al. Formation of neurofibrillary tangles in P301l tau transgenic mice induced by Abeta 42 fibrils. *Science*. 2001; 293(5534): 1491-1495.

53. Leroy K, et al. Lack of tau proteins rescues neuronal cell death and decreases amyloidogenic processing of APP in APP/PS1 mice. *Am J Pathol*. 2012; 181(6): 1928-1940.

54. Mairet-Coello G, et al. The CAMKK2-AMPK kinase pathway mediates the synaptotoxic effects of Aβ oligomers through Tau phosphorylation. *Neuron*. 2013; 78(1): 94-108.

55. Tackenberg C, et al. NMDA receptor subunit composition determines beta-amyloid-induced neurodegeneration and synaptic loss. *Cell Death Dis*. 2013; 4(4): e608.

56. Um, JW, et al. Metabotropic glutamate receptor 5 is a coreceptor for Alzheimer aβ oligomer bound to cellular prion protein. *Neuron*. 2013; 79(5): 887-902.

57. Kitazawa M, et al. Lipopolysaccharide-induced inflammation exacerbates tau pathology by a cyclin-dependent kinase 5-mediated pathway in a transgenic model of Alzheimer's disease. *J Neurosci*. 2005; 25(39): 8843-8853.

58. Sy M, et al. Inflammation induced by infection potentiates tau pathological features in transgenic mice. *Am J Pathol*. 2011; 178(6): 2811-2822.

59. Aschenbrenner AJ, et al. Influence of tau PET, amyloid PET, and hippocampal volume on cognition in Alzheimer disease. *Neurology*. 2018; 91(9): e859-e866.

60. Mass E, et al. Specification of tissue-resident macrophages during organogenesis. *Science*. 2016; 353(6304).

61. Li Q, et al. Developmental Heterogeneity of Microglia and Brain Myeloid Cells Revealed by Deep Single-Cell RNA Sequencing. *Neuron*. 2019; 101(2): 207-223.e10.

62. Schafer DP, et al. Microglia Sculpt Postnatal Neural Circuits in an Activity and Complement-Dependent Manner. *Neuron*. 2012; 74(4): 691-705.

63. Wlodarczyk A, et al. A novel microglial subset plays a key role in myelinogenesis in developing brain. *EMBO J*. 2017; 36(22): 3292-3308.

64. Safaiyan S, et al. White matter aging drives microglial diversity. *Neuron*. 2021; 109(7): 1100-1117.

65. Stowell RD, et al. Cerebellar microglia are dynamically unique and survey Purkinje neurons in vivo. *Dev Neurobiol*. 2018; 78(6): 627-644.

66. Grabert K, et al. Microglial brain region-dependent diversity and selective regional sensitivities to ageing. *Nat Neurosci*. 2016; 19(3): 504-516.

67. Ginhoux F, et al. Origin and differentiation of microglia. *Front Cell Neurosci*. 2013; 7: 45.

68. Elmore MR, et al. Characterizing Newly Repopulated Microglia in the Adult Mouse: Impacts on Animal Behavior, Cell Morphology, and Neuroinflammation. *PLoS One*. 2015; 10(4): e0122912.

69. Uribe-Querol E and Rosales C. Phagocytosis: Our Current Understanding of a Universal Biological Process. *Front Immunol*. 2020; 11: 1066.

70. Ries M and Sastre M. Mechanisms of Aβ Clearance and Degradation by Glial Cells. *Front Aging Neurosci*. 2016; 8: 160.

71. Momtazmanesh S, Perry G, and Rezaei N. Toll-like receptors in Alzheimer's disease. *Journal of Neuroimmunology*. 2020; 348: 577362.

72. Reed-Geaghan E-G, et al. CD14 and toll-like receptors 2 and 4 are required for fibrillar A{beta}-stimulated microglial activation. *J Neurosci*. 2009; 29(38): 11982-11992.

73. Richard KL, et al. Toll-like receptor 2 acts as a natural innate immune receptor to clear amyloid beta 1-42 and delay the cognitive decline in a mouse model of Alzheimer's disease. *J Neurosci*. 2008; 28(22): 5784-5793.

74. Song M, et al. TLR4 mutation reduces microglial activation, increases Aβ deposits and exacerbates cognitive deficits in a mouse model of Alzheimer's disease. *J Neuroinflammation*. 2011; 8: 92.

75. Chung H, et al. Uptake of fibrillar beta-amyloid by microglia isolated from MSR-A (type I and type II) knockout mice. *Neuroreport*. 2001; 12(6): 1151-1154.

76. Stewart CR, et al. CD36 ligands promote sterile inflammation through assembly of a Toll-like receptor 4 and 6 heterodimer. *Nat Immunol*. 2010; 11(2): 155-161.

77. Dobri A-M, et al. CD36 in Alzheimer's Disease: An Overview of Molecular Mechanisms and Therapeutic Targeting. *Neuroscience*. 2021; 453: 301-311.

78. Delikkaya B, et al. Altered expression of insulin-degrading enzyme and regulator of calcineurin in the rat intracerebral streptozotocin model and human apolipoprotein E-ε4–associated Alzheimer's disease. *Alzheimers Dement (Amst)*. 2019; 11: 392-404.

79. Hellström-Lindahl E, Ravid R, Nordberg A. Age-dependent decline of neprilysin in Alzheimer's disease and normal brain: inverse correlation with A beta levels. *Neurobiol Aging*. 2008; 29(2): 210-221.

80. Farris W, et al. Insulin-degrading enzyme regulates the levels of insulin, amyloid β-protein, and the β-amyloid precursor protein intracellular domain in vivo. *Proc Natl Acad Sci U S A*. 2003; 100(7): 4162-4167.

81. Huang S-M, et al. Neprilysin-sensitive Synapse-associated Amyloid-β Peptide Oligomers Impair Neuronal Plasticity and Cognitive Function. *Journal of Biological Chemistry*. 2006; 281(26): 17941-17951.

82. Linebaugh BE, et al. Exocytosis of active cathepsin B enzyme activity at pH 7.0, inhibition and molecular mass. *Eur J Biochem*. 1999; 264(1): 100-109.

83. Mueller-Steiner S, et al. Antiamyloidogenic and neuroprotective functions of cathepsin B: implications for Alzheimer's disease. *Neuron*. 2006; 51(6): 703-714.

84. Sun L, et al. Microglial Cathepsin B Contributes to the Initiation of Peripheral Inflammation-Induced Chronic Pain. *J Neurosci*. 2012; 32(33): 11330-11342.

85. Galluzzi L, et al. Metabolic control of autophagy. *Cell*. 2014; 159(6): 1263-1276.

86. Pickford F, et al. The autophagy-related protein beclin 1 shows reduced expression in early Alzheimer disease and regulates amyloid β accumulation in mice. *J Clin Invest*. 2008; 118(6): 2190-2199.

87. Cho M-H, et al. Autophagy in microglia degrades extracellular β-amyloid fibrils and regulates the NLRP3 inflammasome. *Autophagy*. 2014; 10(10): 1761-1775.

88. Xu Y, et al. Autophagy deficiency modulates microglial lipid homeostasis and aggravates tau pathology and spreading. *Proc Natl Acad Sci U S A*. 2021; 118(27): e2023418118.

89. Schmukler E and Pinkas-Kramarski R. Autophagy induction in the treatment of Alzheimer's disease. *Drug Dev Res*. 2020; 81(2): 184-193.

90. Lemke G. How macrophages deal with death. *Nat Rev Immunol*. 2019; 19(9): 539-549.

91. Huang Y, et al. Microglia use TAM receptors to detect and engulf amyloid β plaques. *Nat Immunol*. 2021; 22(5): 586-594.

92. Colonna M and Butovsky O. Microglia Function in the Central Nervous System During Health and Neurodegeneration. *Annu Rev Immunol*. 2017; 35: 441-468.

93. Keren-Shaul H, et al. A unique microglia type associated with restricting development of Alzheimer’s disease. *Cell*. 2017;169(7):1276–1290.

94. Ennerfelt H, et al. SYK coordinates neuroprotective microglial responses in neurodegenerative disease. *Cell*. 2022; 185(22): 4135-4152.

95. Yuan P, et al. TREM2 Haplodeficiency in Mice and Humans Impairs the Microglia Barrier Function Leading to Decreased Amyloid Compaction and Severe Axonal Dystrophy. *Neuron*. 2016; 90(4): 724-739.

96. Srinivasan K, et al. Alzheimer's Patient Microglia Exhibit Enhanced Aging and Unique Transcriptional Activation. *Cell Rep*. 2020; 31(13): 107843.

97. Hasselmann J, et al. Development of a Chimeric Model to Study and Manipulate Human Microglia In Vivo. *Neuron*. 2019; 103(6): 1016-1033.

98. Guerreiro R, et al. TREM2 variants in Alzheimer's disease. *N Engl J Med*. 2013; 368(2): 117-127.

99. Ulland TK and Colonna M. TREM2 - a key player in microglial biology and Alzheimer disease. *Nat Rev Neurol*. 2018; 14(11): 667-675.

100. Wang Y, et al. TREM2 lipid sensing sustains the microglial response in an Alzheimer's disease model. *Cell*. 2015; 160(6): 1061-1071.

101. Wang Y, et al. TREM2-mediated early microglial response limits diffusion and toxicity of amyloid plaques. *J Exp Med*. 2016;213(5):667–675.

102. Ulland TK, et al. TREM2 maintains microglial metabolic fitness in Alzheimer’s disease. *Cell*. 2017; 170(4): 649-663.

103. Spangenberg EE, et al. Sustained microglial depletion with CSF1R inhibitor impairs parenchymal plaque development in an Alzheimer’s disease model. *Nat Commun*. 2019;10(1):3758.

104. Spangenberg EE, et al. Eliminating microglia in Alzheimer’s mice prevents neuronal loss without modulating amyloid-β pathology. *Brain*. 2016;139(4):1265–1281.

105. Molofsky AV and Deneen B. Astrocyte development: A Guide for the Perplexed. *Glia*. 2015; 63(8): 1320-29.

106. Sofroniew MV and Vinters HV. Astrocytes: biology and pathology. *Acta Neuropathol*. 2010; 119(1): 7-35.

107. Schneider J, et al. Astrogenesis in the murine dentate gyrus is a life-long and dynamic process. *EMBO J*. 2022; 41(11): e110409.

108. Köhler S, Winkler U, and Hirrlinger J. Heterogeneity of Astrocytes in Grey and White Matter. *Neurochem Res*. 2021; 46(1): 3-14.

109. Chai H, et al. Neural Circuit-Specialized Astrocytes: Transcriptomic, Proteomic, Morphological, and Functional Evidence. *Neuron*. 2017; 95(3): 531-549.e9.

110. Boisvert MM, et al. The Aging Astrocyte Transcriptome from Multiple Regions of the Mouse Brain. *Cell Rep*. 2018; 22(1): 269-285.

111. Mathys H, et al. Single-cell transcriptomic analysis of Alzheimer's disease. *Nature*. 2019;570(7761):332–337.

112. Wu T, et al. Complement C3 Is Activated in Human AD Brain and Is Required for Neurodegeneration in Mouse Models of Amyloidosis and Tauopathy. *Cell Rep*. 2019; 28(8): 2111-2123.e6.

113. Zamanian JL, et al. Genomic analysis of reactive astrogliosis. *J Neurosci*. 2012; 32(18): 6391-6410.

114. Liddelow SA, et al. Neurotoxic reactive astrocytes are induced by activated microglia. *Nature*. 2017; 541(7638): 481-487.

115. Jiwaji Z, et al. Reactive astrocytes acquire neuroprotective as well as deleterious signatures in response to Tau and Aß pathology. *Nat Commun*. 2022; 13(1): 135.

116. Lau S-F, et al. Single-nucleus transcriptome analysis reveals dysregulation of angiogenic endothelial cells and neuroprotective glia in Alzheimer's disease. *Proc Natl Acad Sci U S A*. 2020; 117(41): 25800-25809.

117. Habib N, et al. Disease-associated astrocytes in Alzheimer's disease and aging. *Nat Neurosci*. 2020; 23(6): 701-706.

118. Iliff JJ, et al. A Paravascular Pathway Facilitates CSF Flow Through the Brain Parenchyma and the Clearance of Interstitial Solutes, Including Amyloid β. *Sci Transl Med*. 2012; 4(147): 147ra111.

119. Aspelund A, et al. A dural lymphatic vascular system that drains brain interstitial fluid and macromolecules. *J Exp Med*. 2015; 212(7): 991-999.

120. Louveau A, et al. Structural and functional features of central nervous system lymphatic vessels. *Nature*. 2015; 523(7560): 337-341.

121. Wilcock DM, Vitek MP, and Colton CA. Vascular amyloid alters astrocytic water and potassium channels in mouse models and humans with Alzheimer's disease. *Neuroscience*. 2009; 159(3): 1055-1069.

122. Chandra A, et al. Aquaporin-4 polymorphisms predict amyloid burden and clinical outcome in the Alzheimer's disease spectrum. *Neurobiol Aging*. 2021; 97: 1-9.

123. Xu Z, et al. Deletion of aquaporin-4 in APP/PS1 mice exacerbates brain Aβ accumulation and memory deficits. *Mol Neurodegener*. 2015; 10: 58.

124. Johansson JU, et al. Prostaglandin signaling suppresses beneficial microglial function in Alzheimer's disease models. *J Clin Invest*. 2015; 125(1): 350-364.

125. Côté S, et al. Nonsteroidal anti-inflammatory drug use and the risk of cognitive impairment and Alzheimer's disease. *Alzheimers Dement*. 2012; 8(3): 219-226.

126. Vlad SC, et al. Protective effects of NSAIDs on the development of Alzheimer disease. *Neurology*. 2008; 70(19): 1672-1677.

127. Meyer P-F, et al. INTREPAD: A randomized trial of naproxen to slow progress of presymptomatic Alzheimer disease. *Neurology*. 2019; 92(18).e2070-e2080.

128. Imbimbo BP, Solfrizzi V, and Panza F. Are NSAIDs Useful to Treat Alzheimer's Disease or Mild Cognitive Impairment? *Front Aging Neurosci*. 2010; 2: 19.

129. Garwood CJ, et al. Anti-Inflammatory Impact of Minocycline in a Mouse Model of Tauopathy. *Front Psychiatry*. 2010; 1: 136.

130. Howard R, et al. Minocycline at 2 Different Dosages vs Placebo for Patients With Mild Alzheimer Disease: A Randomized Clinical Trial. *JAMA Neurol*. 2019; 77(2): 164-174.

131. Inmune Bio, Inc. A Phase 2, Randomized, Placebo-Controlled, Double-Blind Study of XPro1595 in Patients With Mild Cognitive Impairment (MCI) With Biomarkers of Inflammation. ClinicalTrials.gov identifier: NCT05321498.

132. Novartis Pharmaceuticals. Exploratory PLatform Trial on Anti-Inflammatory Agents in Alzheimer's Disease (EXPLAIN-AD): A Randomized, Placebo-controlled, Multicenter Platform Study to Evaluate the Efficacy, Safety, Tolerability and Pharmacokinetics of Various Anti-inflammatory Agents in Patients With Mild Cognitive Impairment Due to Alzheimer's Disease and Mild Alzheimer's Disease. ClinicalTrials.gov identifier: NCT04795466.

133. Wang S, et al. Anti-human TREM2 induces microglia proliferation and reduces pathology in an Alzheimer's disease model. *J Exp Med*. 2020; 217(9): e20200785.

134. Alector Inc. A Phase 2 Randomized, Double-Blind, Placebo-Controlled, Multicenter Study to Evaluate the Efficacy and Safety of AL002 in Participants With Early Alzheimer's Disease. ClinicalTrials.gov identifier: NCT04592874.

135. Griciuc A, et al. Alzheimer's disease risk gene CD33 inhibits microglial uptake of amyloid beta. *Neuron*. 2013; 78(4): 631-643.

136. Bradshaw EM, et al. CD33 Alzheimer's disease locus: Altered monocyte function and amyloid biology. *Nat Neurosci*. 2013; 16(7): 848-850.

137. Alector Inc. A Phase I Study Evaluating the Safety, Tolerability, Pharmacokinetics, Pharmacodynamics, and Immunogenicity of Single and Multiple Doses of AL003 in Healthy Participants and in Participants With Mild to Moderate Alzheimer's Disease. ClinicalTrials.gov identifier: NCT03822208.

138. Lockshin RA. Programmed cell death. Activation of lysis by a mechanism involving the synthesis of protein. *J Insect Physiol*. 1969; 15, 1505–1516.

139. Saunders JW Jr. (1966). Death in embryonic systems. *Science*. 1966; 154, 604–612.

140. Kerr JF, Wyllie AH, Currie AR. Apoptosis: a basic biological phenomenon with wide-ranging implications in tissue kinetics. *Br J Cancer*. 1972; 26, 239–257.

141. Ellis HM, and Horvitz HR. (1986). Genetic control of programmed cell death in the nematode C. elegans. *Cell*. 1986; 44, 817–829.

142. Oltvai Z, Milliman C and Korsmeyer S. Bcl-2 heterodimerizes *in vivo* with a conserved homolog, Bax, that accelerates programmed cell death. *Cell*. 1993; 74; 609–619.

143. Korsmeyer SJ, et al. Pro-apoptotic cascade activates BID, which oligomerizes BAK or BAX into pores that result in the release of cytochrome *c*. *Cell Death Differ.* 2000; 7; 1166–1173.

144. Cope TE, et al. Tau burden and the functional connectome in Alzheimer's disease and progressive supranuclear palsy. *Brain*. 2018; 141(2), 550–567.

145. Schmitz TW, et al. Basal forebrain degeneration precedes and predicts the cortical spread of Alzheimer's pathology. *Nature Communications*. 2016; 7: 13249.

146. Galluzzi L, et al. Necroptosis: Mechanisms and Relevance to Disease. *Annu Rev Pathol*. 2017; 12: 103-130.

147. Van Valen, L. A new evolutionary law. *Evol Theory*. 1973; 1, 1-30.

148. Kaiser WJ, Upton JW, Mocarski ES. Viral modulation of programmed necrosis. *Curr Opin Virol*. 2013; 3(3): 296-306.

149. Caccamo A, et al. Necroptosis activation in Alzheimer's disease. *Nat Neurosci*. 2017; 20(9):1236–1246.

150. Koper MJ, et al. Necrosome complex detected in granulovacuolar degeneration is associated with neuronal loss in Alzheimer's disease. *Acta Neuropathologica*. 2020; 139: 463-484.

151. Salvadores N, et al. Aβ oligomers trigger necroptosis-mediated neurodegeneration via microglia activation in Alzheimer's disease. *Acta Neuropathologica Communications*. 2022; 10(31).

152. Najjar M, et al. RIPK1 and RIPK3 kinases promote cell-death-independent inflammation by Toll-like receptor 4. *Immunity*. 2016; 45(1): 46–59.

153. Orozco SL, et al. RIPK3 activation leads to cytokine synthesis that continues after loss of cell membrane integrity. *Cell Rep*. 2019; 28(9): 2275–2287.

154. Heneka MT, et al. NLRP3 is activated in Alzheimer's disease and contributes to pathology in APP/PS1 mice. *Nature*. 2013; 493(7434): 674–678.

155. Huell M, et al. Interleukin-6 is present in early stages of plaque formation and is restricted to the brains of Alzheimer's disease patients. *Acta Neuropathol.* 1995; 89: 544–551.

156. Janelsins MC, et al. Early correlation of microglial activation with enhanced tumor necrosis factor-alpha and monocyte chemoattractant protein-1 expression specifically within the entorhinal cortex of triple transgenic Alzheimer's disease mice. *J Neuroinflammation*. 2005; 2.

157. Ofengeim D, et al. RIPK1 mediates a disease-associated microglial response in Alzheimer's disease. *Proc Natl Acad Sci U S A*. 2017; 114(41): E8788–E8797.

158. Julien O, et al. Quantitative MS-based enzymology of caspases reveals distinct protein substrate specificities, hierarchies, and cellular roles. *Proc Natl Acad Sci U S A*. 2016; 113(14), E2001-E2010.

159. Yamaguchi H, et al. Immunosuppression via adenosine receptor activation by adenosine monophosphate released from apoptotic cells. *eLife*. 2014; 3: e02172.

160. Ke FF, et al. Embryogenesis and Adult Life in the Absence of Intrinsic Apoptosis Effectors BAX, BAK, and BOK. *Cell*. 2018; 173(5): 1217-1230.

161. Kuida K, et al. Decreased apoptosis in the brain and premature lethality in CPP32-deficient mice. *Nature*. 1996; 384(6607): 368-72.

162. Yoshida H, et al. Apaf1 Is Required for Mitochondrial Pathways of Apoptosis and Brain Development. *Cell*. 1998; 94(6): 739-750.

163. Hu Y, et al. A DR6/p75(NTR) complex is responsible for β-amyloid-induced cortical neuron death. *Cell Death Dis*. 2013; 4(4): e579.

164. Xu Y, et al. Beta amyloid-induced upregulation of death receptor 6 accelerates the toxic effect of N-terminal fragment of amyloid precursor protein. *Neurobiol Aging*. 2015; 36(1): 157–168.

165. Su JH, et al. Activated caspase-3 expression in Alzheimer's and aged control brain: correlation with Alzheimer pathology. *Brain Res*. 2001; 898(2): 350–357.

166. Hoozemans JM, et al. The Unfolded Protein Response Is Activated in Pretangle Neurons in Alzheimer's Disease Hippocampus. *Am J Pathol*. 2009; 174(4): 1241-1251.

167. Salminen A, et al. ER stress in Alzheimer's disease: a novel neuronal trigger for inflammation and Alzheimer's pathology. *J Neuroinflammation*. 2009; 6(41).

168. Su JH, Deng G, Cotman CW. Bax protein expression is increased in Alzheimer's brain: correlations with DNA damage, Bcl-2 expression, and brain pathology. *J Neuropathol Exp Neurol*. 1997; 56(1): 86-93.

169. Tortosa A, López E, and Ferrer I. Bcl-2 and Bax protein expression in Alzheimer's disease. *Acta Neuropathol*. 1998; 95(4): 407-412.

170. Kudo W, et al. Inhibition of Bax protects neuronal cells from oligomeric A*β* neurotoxicity. *Cell Death Dis*. 2012; 3(5): e309.

171. Rohn TT, et al. Lack of Pathology in a Triple Transgenic Mouse Model of Alzheimer's Disease after Overexpression of the Anti-Apoptotic Protein Bcl-2. *J of Neurosci*. 2008; 28(12): 3051-3059.

172. Shanbhag N, et al. Early neuronal accumulation of DNA double strand breaks in Alzheimer's disease. *Acta Neuropathol Commun*. 2019; 7(77).

173. Thadathil N, et al. DNA Double-Strand Break Accumulation in Alzheimer's Disease: Evidence from Experimental Models and Postmortem Human Brains. *Mol Neurobiol*. 2021; 58(1): 118-131.

174. Misiak M, et al. DNA polymerase β decrement triggers death of olfactory bulb cells and impairs olfaction in a mouse model of Alzheimer's disease. *Aging Cell*. 2017; 16(1): 162-172.

175. Zhang L, et al. BAD-mediated neuronal apoptosis and neuroinflammation contribute to Alzheimer's disease pathology. *iScience*. 2021; 24(9): 102942.

176. Galluzzi L, et al. Molecular mechanisms of cell death: recommendations of the Nomenclature Committee on Cell Death 2018. *Cell Death Differ*. 2018; 25(3): 486-541.

177. Zychlinsky A, Prevost MC, and Sansonetti PJ. Shigella flexneri induces apoptosis in infected macrophages. *Nature*. 1992; 358: 167–169.

178. Broz P and Dixit VM. Inflammasomes: mechanism of assembly, regulation and signalling. *Nature Reviews Immunology*. 2016; 16: 407-420.

179. Tsuchiya K, et al. Caspase-1 initiates apoptosis in the absence of gasdermin D. *Nature Commun*. 2019; 10(2091).

180. Kayagaki N, et al. Non-canonical inflammasome activation targets caspase-11. *Nature*. 2011; 479: 117–121.

181. Kayagai N, et al. Noncanonical Inflammasome Activation by Intracellular LPS Independent of TLR4. *Science*. 2013; 341(6151): 1246-1249.

182. Shi J, et al. Inflammatory caspases are innate immune receptors for intracellular LPS. *Nature*. 2014; 514: 187-192.

183. Aachoui Y, et al. Caspase-11 protects against bacteria that escape the vacuole. *Science*. 2013; 339(6122): 975-978.

184. Ising C, et al. NLRP3 inflammasome activation drives tau pathology. *Nature*. 2019; 575(7784): 669–673.

185. Shippy DC, et al. β-Hydroxybutyrate inhibits inflammasome activation to attenuate Alzheimer's disease pathology. *J Neuroinflammation*. 2020; 17(1): 280.

186. Venegas C, et al. Microglia-derived ASC specks cross-seed amyloid-β in Alzheimer's disease. *Nature*. 2017; 552(7685): 355–361.

187. Yin J, et al. NLRP3 inflammasome inhibitor ameliorates amyloid pathology in a mouse model of Alzheimer's disease. *Mol Neurobiol*. 2018; 55(3): 1977–1987.

188. Flores J, et al. Caspase-1 inhibition alleviates cognitive impairment and neuropathology in an Alzheimer's disease mouse model. *Cell Death Dis.* 2022; 13(10): 864.

189. Tan MS, et al. Amyloid-b induces NLRP1-dependent neuronal pyroptosis in models of Alzheimer's disease. *Cell Death Dis*. 2014; 5(8): e1382.

190. Kashual V, et al. Neuronal NLRP1 inflammasome activation of Caspase-1 coordinately regulates inflammatory interleukin-1-beta production and axonal

degeneration-associated Caspase-6 activation. *Cell Death Dis*. 2015; 22(10): 1676–1686.

191. Dolma S, et al. Identification of genotype-selective antitumor agents using synthetic lethal chemical screening in engineered human tumor cells. *Cancer Cell*. 2003; 3(3): 285-296.

192. Yang WT and Stockwell BR. Synthetic Lethal Screening Identifies Compounds Activating Iron-Dependent, Nonapoptotic Cell Death in Oncogenic-RAS-Harboring Cancer Cells. *Chemistry & Biology*. 2008; 15(3): 234-245.

193. Stockwell BR, et al. Ferroptosis: a regulated cell death nexus linking metabolism, redox biology, and disease. *Cell*. 2017; 171(2): 273-285.

194. Roberts BR, et al. The role of metallobiology and amyloid-β peptides in Alzheimer's disease. *Journal of Neurochemistry*. 2012; 120: 149-166.

195. Chen L, et al. Enhanced defense against ferroptosis ameliorates cognitive impairment and reduces neurodegeneration in 5xFAD mice. *Free Radical Biology and Medicine*. 2022; 180(20): 1-12.

196. Van der Jeugd A, et al. Reversal of memory and neuropsychiatric symptoms and reduced tau pathology by selenium in 3xTg-AD mice. *Sci Rep*. 2018; 8(1): 6431.

197. Heneka MT, et al. Neuroinflammation in Alzheimer's disease. *Lancet Neurol*. 2015; 14(4): 388–405.

198. Luo B, et al. Phagocyte respiratory burst activates macrophage erythropoietin signalling to promote acute inflammation resolution. *Nat Commun*. 2016; 7(1): 12177.

199. Paresce DM, Ghosh RN, Maxfield FR. Microglial Cells Internalize Aggregates of the Alzheimer's Disease Amyloid β-Protein Via a Scavenger Receptor. *Neuron*. 1996; 17(3): 553-565.

200. Ennerfelt HE, Lukens JR. The role of innate immunity in Alzheimer's disease. *Immunol Rev*. 2020; 297(1): 225-246.

201. Tummers B, Green DR. Caspase-8; regulating life and death. *Immunol Rev*. 2017; 277(1): 76-89.

202. Rohn TT, et al. Activation of caspase-8 in the Alzheimer's disease brain. *Neurobiol Dis*. 2001; 8(6): 1006-1016.

203. Dillon CP, et al. RIPK1 blocks early postnatal lethality mediated by caspase-8 and RIPK3. *Cell*. 2014; 157(5): 1189-1202.

204. Kaiser WJ, et al. RIP3 mediates the embryonic lethality of caspase-8-deficient mice. *Nature*. 2011; 471(7338): 368-372.

205. Oberst A, et al. Catalytic activity of the caspase-8-FLIPL complex inhibits RIPK3-dependent necrosis. *Nature*. 2011; 471(7338): 363-367.

206. Newton K, Sun X, Dixit VM. Kinase RIP3 is dispensable for normal NF-kappa Bs, signaling by the B-cell and T-cell receptors, tumor necrosis factor receptor 1, and Toll-like receptors 2 and 4. *Mol Cell Biol*. 2004; 24(4): 1464-1469.

207. Feltham R, Vince JE, Lawlor KE. Caspase-8: not so silently deadly. *Clinical & Translational Immunology*. 2017; 6(1): e124.

208. Feng Y, et al. Caspase-8 restricts antiviral CD8 T cell hyperaccumulation. *PNAS*. 2019; 116(30): 15170-15177.

209. Gurung P, Burton A, Kanneganti TD. NLRP3 inflammasome plays a redundant role with caspase 8 to promote IL-1β–mediated osteomyelitis. *Proc Natl Acad Sci U S A*. 2016; 113(16): 4452-4457.

210. Henry CM, Martin SJ. Caspase-8 Acts in a Non-enzymatic Role as a Scaffold for Assembly of a Pro-inflammatory "FADDosome" Complex upon TRAIL Stimulation. *Mol Cell*. 2017; 65(4): 715-729. e5.

211. Monie TP, Bryant CE. Caspase-8 functions as a key mediator of inflammation and pro-IL-1β processing via both canonical and non-canonical pathways. *Immunol Rev*. 2015; 265(1): 181-193.

212. Gurung P, et al. FADD and caspase-8 mediate priming and activation of the canonical and non-canonical Nlrp3 inflammasomes. *J Immunol*. 2014; 192(4): 1835-1846.

213. Pereira LMN, et al. Caspase-8 mediates inflammation and disease in rodent malaria. *Nat Commun*. 2020; 11(1): 4596.

214. Zhang X, Dowling JP, Zhang J. RIPK1 can mediate apoptosis in addition to necroptosis during embryonic development. *Cell Death Dis*. 2019; 10(3): 1-11.

215. Forner S, et al. Systematic phenotyping and characterization of the 5xFAD mouse model of Alzheimer's disease. *Sci Data*. 2021; 8(270).

216. Chun H, et al. Elucidating the Interactive Roles of Glia in Alzheimer's Disease Using Established and Newly Developed Experimental Models. *Front Neurol*. 2018;0. doi:10.3389/fneur.2018.00797

217. Condello C, et al. Microglia constitute a barrier that prevents neurotoxic protofibrillar Aβ42 hotspots around plaques. *Nat Commun*. 2015; 6(1): 6176.

218. Leyns CEG, et al. TREM2 deficiency attenuates neuroinflammation and protects against neurodegeneration in a mouse model of tauopathy. *Proc Natl Acad Sci U S A*. 2017; 114(43): 11524-11529.

219. Eimer WA, Vassar R. Neuron loss in the 5XFAD mouse model of Alzheimer's disease correlates with intraneuronal Aβ42 accumulation and Caspase-3 activation. *Molecular Neurodegeneration*. 2013;8(1):2.

220. Griciuc A, et al. TREM2 Acts Downstream of CD33 in Modulating Microglial Pathology in Alzheimer's Disease. *Neuron*. 2019;103(5):820-835.e7.

221. Zhang CJ, et al. TLR-stimulated IRAKM activates caspase-8 inflammasome in microglia and promotes neuroinflammation. *J Clin Invest*. 2018; 128(12): 5399-5412.

222. Parajuli B, et al. Oligomeric amyloid β induces IL-1β processing via production of ROS: implication in Alzheimer's disease. *Cell Death Dis*. 2013; 4(12): e975.

223. Fang R, et al. ASC and NLRP3 maintain innate immune homeostasis in the airway through an inflammasome-independent mechanism. *Mucosal Immunol*. 2019; 12(5): 1092-1103.

224. Franklin BS, et al. ASC has extracellular and prionoid activities that propagate inflammation. *Nat Immunol*. 2014;15(8):727-737.

225. Friker LL, et al. β-Amyloid Clustering around ASC Fibrils Boosts Its Toxicity in Microglia. *Cell Reports*. 2020;30(11):3743-3754.e6.

226. Batista SJ, et al. Gasdermin-D-dependent IL-1α release from microglia promotes protective immunity during chronic Toxoplasma gondii infection. *Nat Commun*. 2020; 11(1): 3687.

227. Burgold S, et al. In vivo imaging reveals sigmoidal growth kinetic of β-amyloid plaques. *Acta Neuropathol Commun*. 2014; 2(1): 30.

228. Yan P, et al. Characterizing the appearance and growth of amyloid plaques in APP/PS1 mice. *J Neurosci*. 2009; 29(34): 10706–10714.

229. Tummers B, et al. Caspase-8-dependent inflammatory responses are controlled by its adaptor, FADD, and necroptosis. *Immunity*. 2020; 53(6): 994–1006.

230. Meng H, et al. Death-domain dimerization-mediated activation of RIPK1 controls necroptosis and RIPK1-dependent apoptosis. *Proc Natl Acad Sci U S A*. 2018; 115(9): E2001–E2009.

231. Xu D, et al. TBK1 Suppresses RIPK1-Driven Apoptosis and Inflammation during Development and in Aging. *Cell*. 2018; 174(6): 1477-1491. e19.

232. Zelic M, et al. RIPK1 activation mediates neuroinflammation and disease progression in multiple sclerosis. *Cell Rep*. 2021; 35(6): 109112.

233. Zhang X, et al. Oligodendroglial glycolytic stress triggers inflammasome activation and neuropathology in Alzheimer's disease. *Sci Adv*. 2020; 6(49).

234. Tible M, et al. PKR knockout in the 5xFAD model of Alzheimer's disease reveals beneficial effects on spatial memory and brain lesions. *Aging Cell*. 2019; 18(3): e12887.

235. Braak H, Braak E. Neuropathological stageing of Alzheimer-related changes. *Acta Neuropathol*. 1991; 82(4): 239–259.

236. Vogel JW, et al. Spread of pathological tau proteins through communicating neurons in human Alzheimer's disease. *Nat Commun*. 2020; 11(1): 2612.

237. Kane MD, et al. Evidence for seeding of beta -amyloid by intracerebral infusion of Alzheimer brain extracts in beta -amyloid precursor protein-transgenic mice. *J Neurosci*. 2000; 20(10): 3606–3611.

238. Clavaguera F, et al. Brain homogenates from human tauopathies induce tau inclusions in mouse brain. *Proc Natl Acad Sci U S A*. 2013;110(23):9535–9540.

239. Asai H, et al. Depletion of microglia and inhibition of exosome synthesis halt tau propagation. *Nat Neurosci*. 2015; 18(11): 1584–1593.

240. Pignataro A, Middei S. Trans-synaptic spread of amyloid-β in Alzheimer's disease: paths to β-amyloidosis. *Neural Plast*. 2017; 2017: 5281829.

241. Roos TT, et al. Neuronal spreading and plaque induction of intracellular Aβ and its disruption of Aβ homeostasis. *Acta Neuropathol*. 2021; 142(4): 669–687.

242. Freeman L, et al. NLR members NLRC4 and NLRP3 mediate sterile inflammasome activation in microglia and astrocytes. *J Exp Med*. 2017; 214(5): 1351–1370.

243. Song L, et al. NLRP3 inflammasome in neurological diseases, from functions to therapies. *Front Cell Neurosci*. 2017; 11: 63.

244. Rivera-Escalera F, et al. IL-1β-driven amyloid plaque clearance is associated with an expansion of transcriptionally reprogrammed microglia. *J Neuroinflammation*. 2019; 16(1): 261.

245. Nagar A, et al. The ASC speck and NLRP3 inflammasome function are spatially and temporally distinct. *Front Immunol*. 2021; 12: 752482.

246. Lopatin U, et al. Increases in circulating and lymphoid tissue interleukin-10 in autoimmune lymphoproliferative syndrome are associated with disease expression. *Blood*. 2001; 97(10): 3161-3170.

247. Keeler AB, et al. A developmental atlas of somatosensory diversification and maturation in the dorsal root ganglia by single-cell mass cytometry. *Nat Neurosci*. 2022; 25(11): 1543-1558.

248. Vogel C and Marcotte EM. Insights into the regulation of protein abundance from proteomic and transcriptomic analyses. *Nat Rev Genet*. 2012; 13(4): 227-232.

249. Mrdjen D, et al. High-Dimensional Single-Cell Mapping of Central Nervous System Immune Cells Reveals Distinct Myeloid Subsets in Health, Aging, and Disease. *Immunity*. 2018; 48(2): 380-395.

250. Phongpreecha T, et al. Single-cell peripheral immunoprofiling of Alzheimer's and Parkinson's diseases. *Sci Adv*. 2020; 6(48).

251. Phongpreecha T, et al. Single-synapse analyses of Alzheimer’s disease implicate pathologic tau, DJ1, CD47, and ApoE. *Sci Adv*. 2021; 7(51).

252. He Y, et al. Mouse primary microglia respond differently to LPS and poly(I:C) in vitro. *Sci Rep*. 2021; 11(1): 10447.

253. Das A, et al. Transcriptome sequencing of microglial cells stimulated with TLR3 and TLR4 ligands. *BMC Genomics*. 2015; 16(1): 517.

254. Yoon S, et al. MLKL, the Protein that Mediates Necroptosis, Also Regulates Endosomal Trafficking and Extracellular Vesicle Generation. *Immunity*. 2017; 47(1): 51-65.

255. Nicoll JAR, et al. Association of Interleukin-1 Gene Polymorphisms with Alzheimer’s Disease. *Ann Neurol*. 2000; 47(3): 365-368.

256. Kitazawa M, et al. Blocking IL-1 signaling rescues cognition, attenuates tau pathology, and restores neuronal β-catenin pathway function in an Alzheimer's disease model. *J Immunol*. 2011; 187(12): 6539-6549.

257. Barroeta-Espar I, et al. Distinct cytokine profiles in human brains resilient to Alzheimer's pathology. *Neurobiology of Disease*. 2018; 121: 327-337.

258. Gibbons TD, et al. Fasting for 20 h does not affect exercise-induced increases in circulating BDNF in humans. *J Physiol*. 2023.

259. Jiao SS, et al. Brain-derived neurotrophic factor protects against tau-related neurodegeneration of Alzheimer's disease. *Transl Psychiatry*. 2016; 6(10): e907.

260. Krishnaswamy S, et al. Conditional Density-based Analysis of T cell Signaling in Single Cell Data. *Science*. 2014; 346(6213): 1250689.

261. Giesen C, et al. Highly multiplexed imaging of tumor tissues with subcellular resolution by mass cytometry. *Nat Methods*. 2014; 11(4): 417-422.

262. Oakley H, et al. Intraneuronal beta-amyloid aggregates, neurodegeneration, and neuron loss in transgenic mice with five familial Alzheimer’s disease mutations: potential factors in amyloid plaque formation. *J Neurosci*. 2006; 26(40): 10129–10140.

263. Stine WB, et al. Preparing synthetic Aβ in different aggregation states. *Methods Mol Biol*. 2011; 670: 13–32.

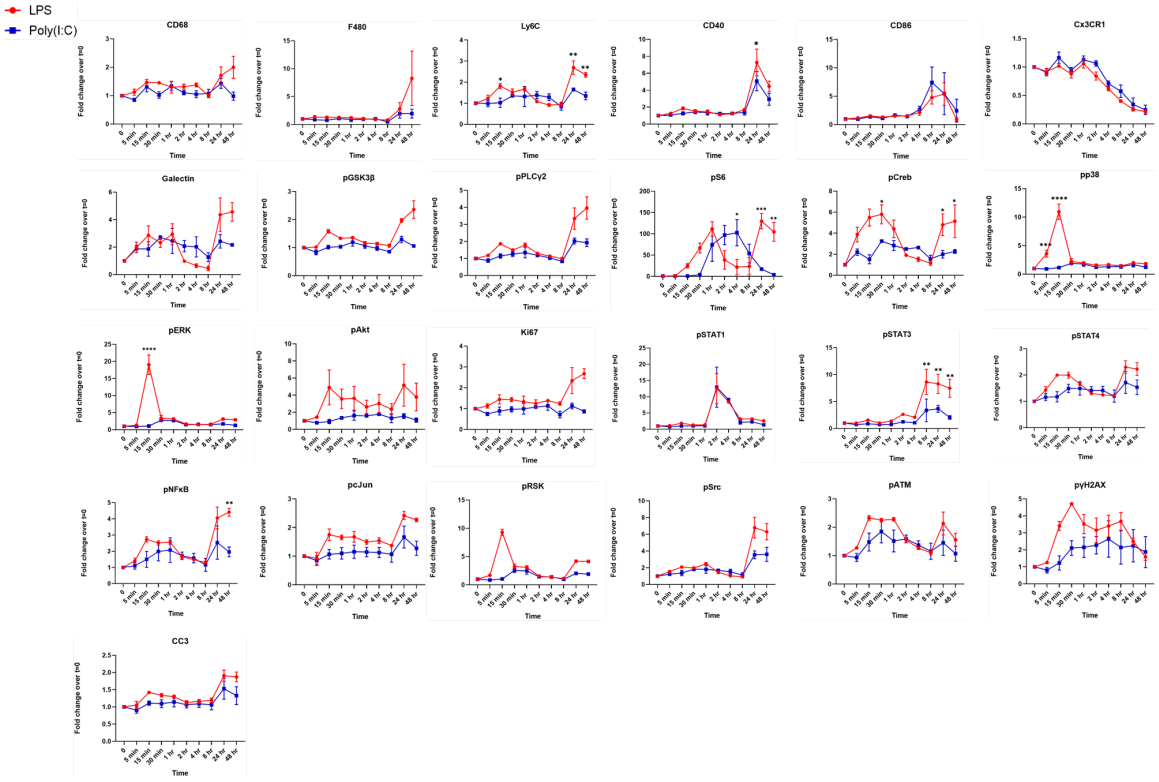

Appendix I. LPS and Poly(I:C) signaling dynamics in pure microglia culture. Line plots of time course data derived from heatmap presented in Figure 3.3.

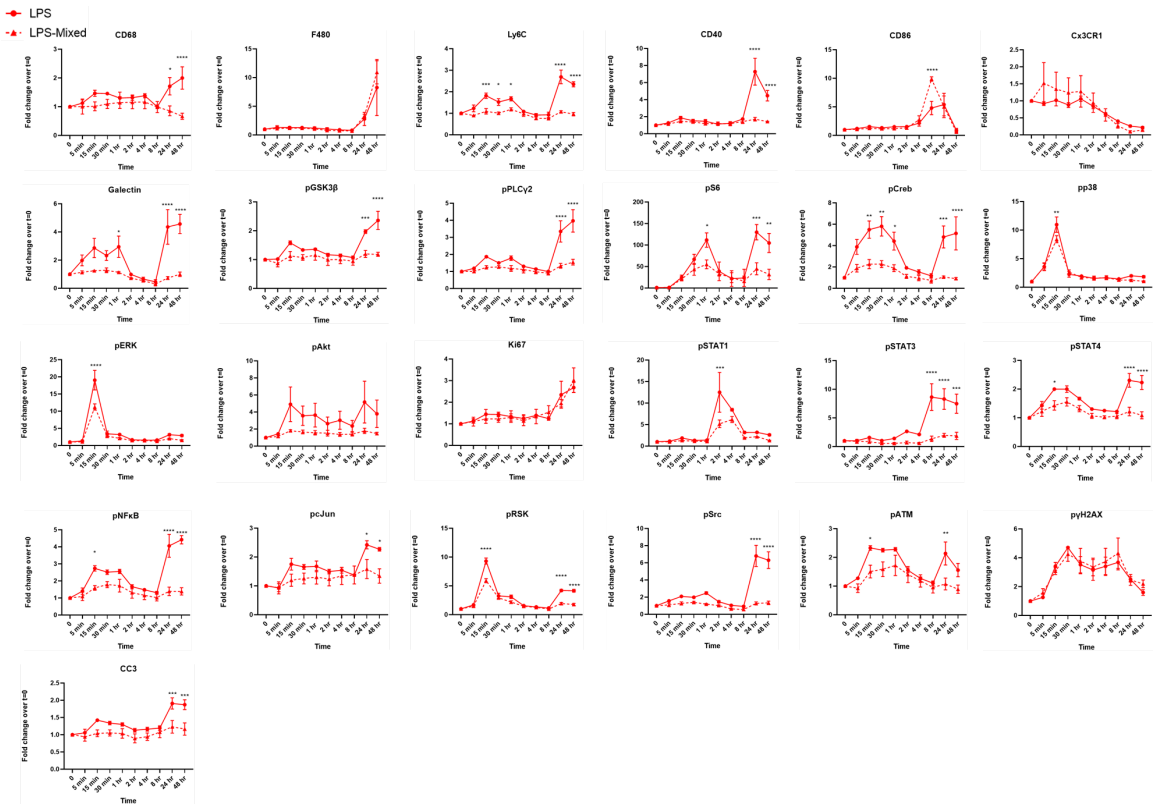

Appendix II. LPS signaling dynamics between pure microglia and mixed cultures. Line plots of time course data derived from heatmap presented in Figure 3.5.

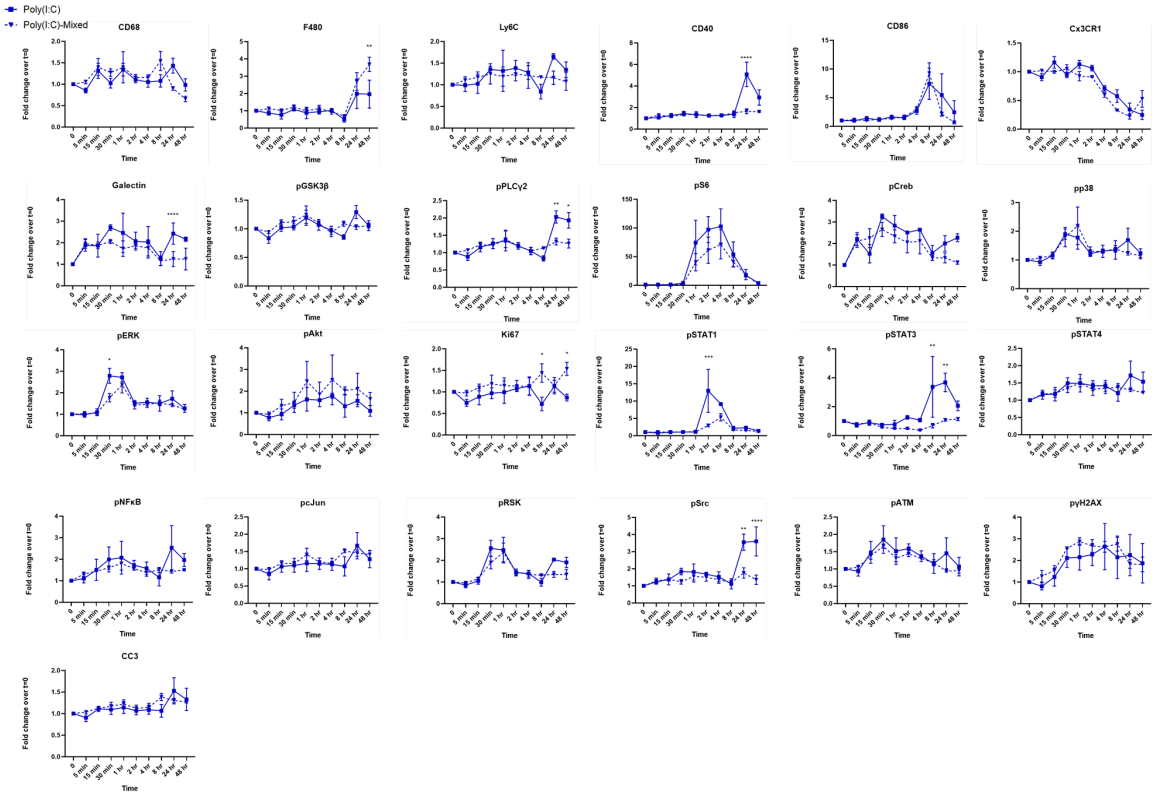

Appendix III. Poly(I:C) signaling dynamics between pure microglia and mixed cultures. Line plots of time course data derived from heatmap presented in Figure 3.5.